An Air Breathing Lithium-Oxygen Battery

BY

BAHARAK SAYAHPOUR

B.S., University of Tehran, 2014

THESIS

Submitted as partial fulfillment of the requirements for the degree of

Master of Science in Mechanical Engineering

in the Graduate College of the

University of Illinois at Chicago

2017

Chicago, Illinois

Defense Committee:

Dr. Amin Salehi-Khojin, Chair and Advisor

Dr. Constantine M. Megaridis

Dr. Robert Klie, Physics

To My Wonderful Parents, Mahrang and Dariush

To My Only Brother, Bardia

To My Best Friend, Pedram

For always believing in me, inspiring me, and encourage me.

ACKNOWLEDGEMENT

First, I would like to thank my advisor, Dr. Amin Salehi-Khojin, who gave me this opportunity to work in his laboratory and provided me support and assistance during the two years.

My deepest gratitude goes to my parents, Mahrang Ghamkhar and Dariush Sayahpour, for their love and lifetime supports and giving me this opportunity to come to the US to pursue my dreams.

I would also like to thank my collaborators, Dr. Larry A. Curtiss from Argonne National Laboratory, Dr. Robert F. Klie from the University of Illinois at Chicago (UIC), Physics department, and Dr. Fatemeh Khalili-Araghi from the University of Illinois at Chicago (UIC), Physics department.

Finally, I would like to thank all my lab mates and friends, including Dr. Mohammad Asadi, Pedram Abbasi, Venkata Aditya Addepalli, Marc Gerard, Poya Yasaei, and Amirhossein Behranginia for friendship and all their supports.

AUTHORS CONTRIBUTIONS

The results and discussions in this thesis are copied from my work which is submitted and under review process. Below, the contributions of all the co-authors are listed:

Amin Salehi-Khojin, Baharak Sayahpour, Pedram Abbasi, and Mohammad Asadi conceived the idea. Baharak Sayahpour, Pedram Abbasi, and Mohammad Asadi, and Marc Gerald performed the electrochemical experiments. Baharak Sayahpour synthesized the MoS_2 nanoflakes and prepared the materials. Baharak Sayahpour, Pedram Abbasi, Mohammad Asadi, and Poya Yasaei carried out the characterizations. Badri Narayanan, Kah Chun Lau, Rajeev S. Assary and Larry A. Curtiss carried out computational studies of electrolytes. Cong Liu and Anh Ngo performed computational studies of surfaces and the Li_2CO_3 coating. Jacob R. Jokisaari, Xuan Hu, and Robert F. Klie carried out STEM and EELS experiments. Klas Karis and Fatemeh Khalili-Araghi performed classical MD simulation.

TABLE OF CONTENTS

LIST OF TABLES

LIST OF FIGURES

LIST OF ABBREVIATIONS

1-ethyl-3-methylimidazolium tetrafluoroborate	EMIM-BF_4
Aluminum	Al
Ampere	A
Ampere-hour	Ah
Ampere-hour per gram	Ah/g
Argon	Ar
Calcium	Ca
Carbon dioxide	CO_2
Carbon nanotubes	CNT
Chemical vapor deposition	CVD
Chemical vapor transfer	CVT
Cyclic voltammetry	CV
Density Functional Theory	DFT
Deuterated tetrahydrofuran	THF-d_8
Differential electrochemical mass spectrometry	DEMS
Dimethyl carbonate	DMC
Dimethyl sulfoxide	DMSO
Donor number	DN
Dynamic light scattering	DLS
Electrochemical impedance spectroscopy	EIS
Electron energy loss spectroscopy	EELS
Energy Dispersive Spectroscopy	EDS

Ethylene carbonate	EC
Gas diffusion layer	GDL
Gas diffusion layer	GDL
Gold nano particles	Au NPs
Graphene nanosheets	GNS
Hexagonal Boron-Nitride	h-BN
Humidity	H_2O
Hydrogen	H_2
Ionic Liquid	IL
Iron	Fe
Isopropyl Alcohol	IPA
Li-ion batteries	LIBs
Lithium	Li
Lithium-Oxygen battery	Li-O_2 battery
Lithium bicarbonate	$LiHCO_3$
Lithium Bis (Trifluoromethanesulfonyl) Imide	LiTFSI
Lithium carbonate	Li_2CO_3
Lithium hydroxide	LiOH
Lithium iodine	LiI
Lithium peroxide	Li_2O_2
Magnesium	Mg
Moisture	H_2O
Moisture	H_2O

Molybdenum disulfide	MoS_2
Molybdenum disulfide nanoflakes	MoS_2 NFs
Nanometer	nm
Nitrogen	N_2
Nuclear Magnetic Resonance	NMR
Open-circuit voltage	OCV
Oxygen	O_2
Oxygen evolution reaction	OER
Oxygen reduction reaction	ORR
Platinum nano particles	Pt NPs
Potassium	K
Propylene carbonate	PC
Reduced graphene oxide	rGO
Relative humidity	RH
Rotating disk electrode	RDE
Scanning Electron Microscopy	SEM
Scanning transmission electron microscope	STEM
Secondary Electron Multiplier Mode	SEM mode
Signal to noise ratio	S/N
Sodium	Na
Solid electrolyte interface	SEI
Tetraethylene glycol dimethyl ether	TEGDME
Transition Electron Microscopy	TEM

Transition metal carbides	TMCs
Transition metal carbonitrides	TMCNs
Transition metal dichalcogenides	TMDCs
Transition metal hydroxides	TMH
Transition metal nitrates	TMNs
Transition metal oxide	TMO
Two-dimensional	2D
Ultra-high purity	UHP
Volt	V
Watt per kilogram	W/kg
Watt per liter	W/L
Watt-hour per kilogram	Wh/kg
Watt-hour per liter	Wh/L
X-Ray Diffraction	XRD
X-ray Photoelectron Spectroscopy	XPS
Zinc	Zn

SUMMARY

Given that the current Li-ion battery technology is approaching theoretical specific capacity and specific energy values that are still not enough for powering satisfactorily electric vehicles or providing enough grid level storage capacities, interest in other electrochemical energy conversion and storage devices have emerged. Although systems based on multi-valent cations (Mg^{2+}, Zn^{2+}, etc.) are also been studied, metal air batteries have shown the highest theoretical capacity and energy densities of any other battery chemistries. However, some fundamental challenges have hampered the applications of this class of batteries as the alternative for metal-ion batteries.

In brief, the major challenges holding the metal air system from large scale applications are: (i) absence of an effective air electrode which easily transfer oxygen to the heterogenous reaction interphase for oxygen reduction and evolution reactions. (ii) electrolyte instability in large voltage windows which usually occurs because of high charge overpotentials. (iii) anode poisoning and corrosion due to oxidation or reaction with air species such as CO_2 and moisture. Given such obstacles, development of novel materials is needed to overcome these challenges in metal air batteries.

In this thesis, a system comprised of a protected anode based on lithium carbonate, molybdenum disulfide cathode, and ionic liquid/dimethyl sulfoxide electrolyte is studied that work together, in presence of air components, such as Nitrogen, Carbon dioxide, and humidity, as a real Li-air battery with high cyclability performance up to 700 cycles. The combination of experimental and computational studies are used to provide insight into how this system operates in air and revealed that the long-life performance of this system is due to (i) a suppression of side reactions on the cathode side, which prevent the formation of by-products such as Li_2CO_3 and LiOH, and (ii) an effective protected anode covered with a Li_2CO_3 coating that effectively blocks the diffusion of the actual air components e.g., N_2, CO_2, and H_2O and allowing only for Li ion transport. The Li-air battery developed in this work, which for the first time successfully operates in a realistic atmosphere with high cycle-life, is a promising step toward engineering the next generation of Li batteries with much higher specific energy density than Li-ion batteries.

1. INTRODUCTION

1.1. On Batteries

Energy storage has become a global concern due to ever-growing demand for reliable, large-scale and safe energy resources. Current constraints of traditional energy resources specifically fossil fuels and environmental concerns have led to increasing need to clean energy resources. The capability of batteries to possess higher energy conversion efficiency, compared to combustion or heat engines, makes them a promising technology to work on.

A cell, a device which converts the chemical energy into electrical energy through an electrochemical oxidation and reduction reactions. The active materials in a cell are used integrated to provide the required chemical energy. One or several cells create a battery, in which the number and arrangement of cells provide the desired voltage and capacity of a battery.

An electrochemical cell is consisted of a positive electrode, a negative electrode, and an electrolyte with salt. The chemical reactions happening at both electrodes will result in releasing and taking electrons.

1.2. Primary Batteries

The primary or un-rechargeable batteries have been used for more than 100 years. The primary batteries are the ones which are not rechargeable. It means they are going to be discarded after delivery of all their electrical energy.

Through the time, different materials have been used as the positive or negative electrodes in this type of batteries. Carbon, Silver, Aluminum, Magnesium, Zinc, Lithium, Vanadium, metal oxides, and sulfur dioxide were the most popular materials reported in literature. However, based on the good electrochemical properties, compatibility, availability and cost, Zinc (Zn) have been known as the most common anode material in primary batteries. They have been used for several years and still are using in some applications. However, the need to improve the battery application to have it rechargeable moves this technology forward.

1.3. Secondary Batteries

Secondary batteries are the batteries which are rechargeable and can be used for multiple times charging and re-using. During the past few decades, significant improvements have been done on secondary batteries development. The most well-known secondary batteries are lead-acid batteries, nickel-cadmium batteries, nickel-metal hydrate battery, metal-ion batteries, metal-sulfur batteries, and metal-air batteries [1].

In this thesis will be focused on one type of metal-air batteries, lithium-air batteries. The principles, characteristics, and operation of this type of batteries will be discussed in more details.

1.3.1. Metal Air Batteries

Metal-air batteries are considered a possible alternative to metal-ion batteries as the energy storage systems of the future due to their high specific energy [2]–[5]. Li-ion batteries have been very attractive for years due to their high-energy density and capacity [4]. However, by emerging the electric vehicle (EVs) technologies, these batteries fall behind the requirements for this application, limiting the driving range of EVs [6]–[8]. Among different systems studied as the alternative for Li-ion, metal air batteries have shown the highest theoretical capacity and energy densities of any other battery chemistries. Moreover, they are light weight, compact and cost-effective which makes them more feasible candidates for mobile applications [2], [5], [9], [10].

Different metals are considered as a candidate in metal-air batteries, such as lithium (Li), sodium (Na), potassium (K), magnesium (Mg), calcium (Ca), aluminum (Al), zinc (Zn), and iron (Fe). Despite a lot of studies on different metal-air systems, there are still much challenges to have to be solved to reach a practical system [11]–[16].

1.3.2. Lithium Air Batteries

After the very first demonstration of rechargeable Li-O_2 system by Abraham on 1996 [17], there have been a great attention on this system and numerous efforts to improve the life cycle and performance of Li-O_2 batteries. The different chemistry of Li-O_2 batteries compared to previous Li-ion batteries (LIBs) results in much higher theoretical specific energy of 11,430 Wh/kg (based on the mass of lithium metal) which can easily compete

with internal combustion engines [4], [18]. In more details, gasoline possesses around 13,000 Wh/kg theoretical specific energy in internal combustion engines with less than 13% conversion energy that leads the practical specific energy of gasoline to 1700 Wh/kg. So, Li-O_2 batteries need to deliver 33% of its theoretical specific energy to compete with gasoline in a cheaper, cleaner and more environmentally friendly operation.

This high specific energy density in Li-O_2 battery is coming from high-energy Li metal as negative and oxygen as positive electrode materials. However, in general, there are four different types of electrolyte using in Li-O_2 battery systems [16]; aqueous electrolyte, non-aqueous electrolyte, dual aqueous and non-aqueous electrolyte, and solid-state electrolyte; as it is shown in Figure 1.

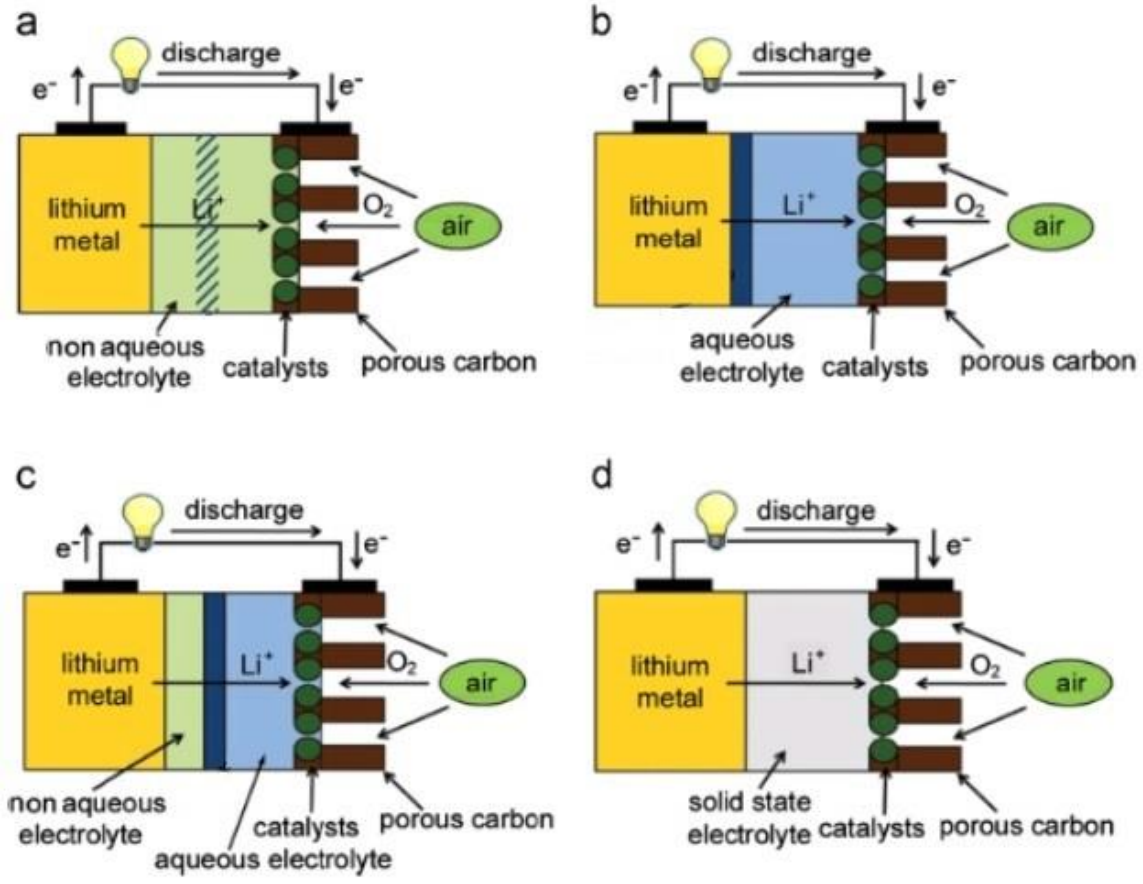

Figure 1. Schematic illustration of cell configurations for the typical Li-air batteries. **(a)** Non-aqueous electrolytes, **(b)** Aqueous electrolytes, **(c)** Dual aqueous and non-aqueous, and **(d)** Solid state electrolyte. Adapted from Reference [12].

Aprotic electrolyte means a non-aqueous solvent that does not contain any reactive protons, though it may contain hydrogen atoms in the molecule. The systems using non-aqueous electrolytes are investigated more than other systems [19], due to the fact that lithium metal can be resist more and be stable to form a possible solid electrolyte interface (SEI). There are different proposed reaction pathways for this system [20], however as it will be discussed more in Mechanism section (2.3), the more possible happening reactions' pathway will be as follow [21]:

$$\text{Negative electrode: } 2\,Li \rightarrow 2\,Li^{+} + 2\,e^{-} \qquad \text{(Eq. 1)}$$

$$\text{Positive electrode: } O_2 + 2\,e^{-} \rightarrow O_2^{2-} \qquad \text{(Eq. 2)}$$

$$\text{Overall: } 2\,Li + O_2 \rightarrow Li_2O_2 \qquad \text{(Eq. 3)}$$

The main product in non-aqueous or aprotic media is lithium peroxide (Li_2O_2) which is an electrically insulator and insoluble material in electrolyte. On the other hand, in the systems using aqueous or protic electrolytes the reactions will be going through following half-reactions [22]:

Negative electrode:	*Aprotic*	$2\,Li \rightarrow 2\,Li^{+} + 2\,e^{-}$	(Eq. 4)
Positive electrode:	*Basic*	$\frac{1}{2}\,O_2 + H_2O + 2\,e^{-} \rightarrow 2\,OH^{-}$	(Eq. 5)
	Acidic	$\frac{1}{2}\,O_2 + 2\,H^{+} + 2e^{-} \rightarrow H_2O$	(Eq. 6)
Overall:	*Basic*	$2\,Li + \frac{1}{2}\,O_2 + H_2O \rightarrow 2\,Li^{+} + 2\,OH^{-}$	(Eq. 7)
	Acidic	$2\,Li + H_2O \rightarrow 2\,Li^{+} + H_2O$	(Eq. 8)

In this case, the main product is lithium hydroxide (LiOH) which is a soluble compound in the protic electrolyte and makes the clogging of the cathode less possible. However, the main challenge in utilizing the aqueous electrolytes is poisoning and instability of the anode and necessity of membrane usage to protect the anode.

In studies using the dual aqueous and non-aqueous electrolytes, they utilize the advantages in each case, by keep the anode in aprotic media and let the cathode to be in protic media with an interface separation method.

One other possible configuration is using solid state electrolyte in which the electrolyte is replaced by a solid-state one. Safety, durability, and wide operational temperature make this type of batteries a good candidate to be investigated. They also prevent the system from dendrite growth and create a barrier against moisture and ambient gas diffusions. However, the main drawback of this system is low ion conductivity of Li^+ which is a key factor in performance of the battery. Inflexibility in volumetric changes and low electrolyte and electrodes contact also can be mentioned as the other challenges in this type of Li-O_2 system.

2. NON-AQUEOUS LITHIUM AIR BATTERY

Here, the system with non-aqueous electrolyte will be studied.

2.1. Theoretical Definitions and Properties

There are several terms which are well-known defined and widely used in battery community. Following are a brief overview on some more common terms [23].

2.1.1. Electrochemical Principles

Electrochemical cell can be defined as a cell which exchange the electrochemical reactions into electrical energy or vice versa. In a secondary battery, both cases are happening. If only one of the changes happening, it is not called rechargeable battery. In the case with only exchange of the electrochemical reactions into the electricity, it is called galvanic cell, and in the other case with only exchange of the electricity into the electrochemical reactions is named electrolysis cell.

Two main terms in electrochemical storage systems are discharge and charge processes. Discharge is the conversion of chemical energy to electrical energy in a cell. This electrical energy can be stored, used, or applied in a load. While charge is the conversion of electrical energy into chemical energy in a cell. This conversion needs an external energy source to be given to the system.

One other general term is current density which means the current in the unit of Ampere (A) per unit of surface area of the cathode which is the active surface participates in the reactions.

2.1.2. Standard Electrode Potential

Standard electrode potential is an equilibrium value of an electrode potential which all the conditions related to electrode reaction are in the standard state. This value is measured with the reference to Hydrogen (H_2). This value for Li in half reaction of $Li^+_{(aq)} + e^- \rightarrow Li_{(s)}$ is -3.04 V which the lowest one in the standard table. There is another term which is called open-circuit voltage (OCV) means the voltage between the two electrodes without load on the system.

2.1.3. Cycle and Cycle Life

A cycle in a battery means a discharge process followed by a charge process, that in ideal case, bring back the cell to its initial condition. On the other hand, the cycle life in a battery means the number of cycles under specific conditions which a battery can be run rechargeable. The failure point is defined by a specific criteria of battery performance, such as cut-off voltage, potential gap, capacity, or time.

2.1.4. Capacity

Capacity in a battery is defined as the electrical charge which can be taken from a battery in unit of Ampere-hour (Ah). In the other hand, when a battery is run under the constant current, the longer the cell works, the higher capacity delivers. The battery design and the applied current effect the capacity of a battery.

To compare different systems in a more realistic way, the capacity is usually defined as a function of the catalyst weight in unit of Ah/g.

2.1.5. Energy and Power Density

Energy density and specific energy of a cell are the ratio of the available energy of a cell to its volume and its weight with the unit of Wh/L and Wh/kg, respectively.

Power density and specific power of a cell are the ratio of the available power of a cell to its volume and its weight with the unit of W/L and W/kg, respectively.

2.1.6. C-rate

C-rate of a battery is the discharge current which is normalized based on the capacity of a battery. Therefore, the C-rate is the rate in which the battery is discharged in according to its capacity. For example, in the case of a battery with the capacity of 1 Ah, the following table have shown the time which is needed in each C-rate to discharge the entire battery.

Table 1. The relation between C-rate and time in case of 1 Ah capacity.

C-rate	Time
5C	12 min
2C	30 min
1C	1 hr
C/2	2 hrs
C/5	5 hrs
C/10	10 hrs

2.1.7. Efficiency

In general, efficiency is defined as the ratio of the output over the input. In a battery, efficiency can be defined as the output of the cell over the input required to convert the system to its initial state.

In more specific, energy efficiency and voltage efficiency are defined and used to describe a system. Energy efficiency in a battery is defined as the ratio of Watt-hours gained during discharging over the Watt-hour required to bring back the cell to its initial conditions before discharging. Voltage efficiency means the ratio of discharge voltage average over charge voltage average in that specific conditions which the battery is run.

2.2. Battery Components

A Li-O_2 battery is consisted of three main components; cathode, anode, and electrolyte. In this study, these components are assembled in a Swagelok cell which is presented in Figure 2. As it is shown, there are two sections as inlet and outlet to let the air comes in and goes out with this capability to measure the inside pressure. From top to down, in the cathode part, the catalyst is coated on a porous substrate which is a gas diffusion layer (GDL). A glass fiber separator is used between the cathode and the anode to avoid the direct contact of them to prevent the short-circuit. The separator is wet with the electrolyte

and a specific desired amount of the salt solved in the electrolyte. Pure lithium chip is used as the anode. Aluminum mesh is utilized to make a better connection and electron flow in the system.

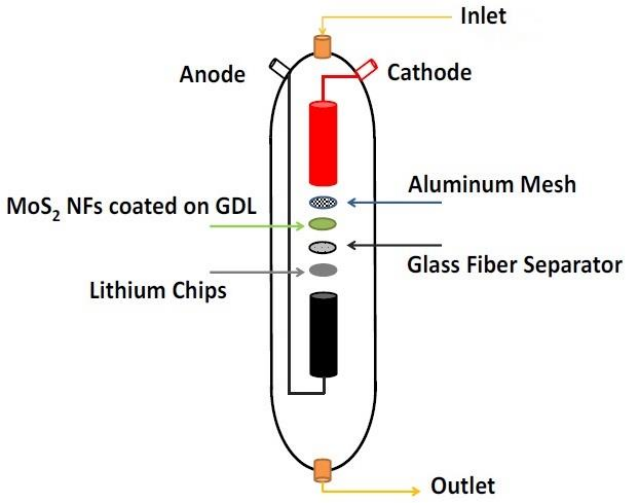

Figure 2. The schematic of the cell component and assembly.

Following is a more discussion on each of these components. It should be taken into account that these terms are defined differently in various systems.

2.2.1. Cathode

Cathode, which is also called as positive electrode during discharge, is the electrode where reduction takes place in the cell. The oxygen from air is assumed as the active material in the electrode. However, an air electrode needs to be a porous material to let the oxygen goes into the system. In general, the porous structure is responsible for oxygen transition, product formation and decomposition, and product storage [23], [24]. To select an appropriate porous structure following parameters should be taken into account; pore size distribution, pore volume, and thickness. On the other hand, chemical stability, conductivity, price, and surface to volume ratio are also important parameters and affect the performance [15].

2.2.2. Anode

Anode, which is also called as negative electrode during discharge, is the electrode where oxidation takes place in the cell.

Among all the metals, lithium metal with the symbol of Li is the first alkali metal with atomic number of 3 means the lightest metal and in general the lightest element in solid phase. It is very soft and easily formable metal with bright silver/beige color. Lithium has the most negative electrochemical potential which is -3.04 V versus standard hydrogen electrode and lowest molar mass which is 6.941 g/mol. These properties result in 11,430 Wh/kg theoretical specific energy for lithium metal used as the negative electrode [4].

Safety is a critical issue to be considered in anode side due to high reactivity and flammability of the alkaline metals with oxygen and moisture.

2.2.3. Electrolyte

Electrolyte is the media which provides the ion transport mechanism between cathode and anode. The key role of electrolyte in Li-O_2 battery is to enable the system to form and decompose the discharge product which means facilitates the oxygen reduction (ORR) and evolution reactions (OER). On the other hand, the stability of the electrolyte during a long cycle life of a battery is very important and still challenging in studies [19].

There are a wide range of electrolytes family which are used in different conformations of Li-O_2 battery systems [19]. Among them, there are a few most popular electrolytes that are studied more which are described as follow.

2.2.3.1. Carbonate Based Electrolytes

This family of electrolytes are mainly made of ethylene carbonate (EC), propylene carbonate (PC), and dimethyl carbonate (DMC) or a combination of them. Despite their wide usage and stability in Li-ion batteries, they are shown unstable and having tendency to reaction with discharge products in Li-O_2 batteries [2], [25], [26]. Therefore, although carbonate based electrolytes have low volatility as an important factor in choosing electrolyte, but causing side reactions makes them inappropriate candidate in Li-O_2 systems.

2.2.3.2. Ether Based Electrolytes

Ether based electrolytes have shown an intermediate donor number (DN). Otherwise, the ether-based electrolytes have low volatility and shown better stability in Li-O_2 systems

[27], [28], recent studies have revealed that this type of electrolyte can be decomposed and react with Li_2O_2 as the main product during the discharge process in the cell [29]. In more details, they are capable of forming lithium carbonate, lithium alkyl carbonates, and polyethers while producing CO_2 and H_2O, which leads the system to side reactions, undesired products, higher charge potential, and in fact, low energy efficiency.

2.2.3.3. DMSO Based Electrolytes

Dimethyl sulfoxide-based electrolytes can be considered as one promising candidate. Dimethyl sulfoxide (DMSO) has the highest donor number compared to other more well-known electrolytes. The DN for this solvent is around 30 [30]. The low volatility, low viscosity, high oxygen diffusion coefficient, and high conductivity can also be mentioned as the advantages of this family. They have shown an acceptable stability with non-carbon based electrodes [31], [32] while demonstrated initiating side reactions with carbon-based electrodes [33].

2.2.3.4. Ionic Liquids

Their main characteristics such as very low vapor pressure and volatility, high ionic conductivity, wide potential window, stability, and hydrophobicity [2], [34] make them a promising candidate for being used in Li-O_2 battery systems. One limiting factor for ILs to be used as the electrolyte for all Li-O_2 systems is that most of the ILs have shown low Li^+ solubility which may cause in restrictions in choosing Li salt in the system.

2.2.4. Salt

Salts are a critical part in the electrolyte for batteries. They play a key role in electrolyte stability. Salt dissolution and stability of the salt in the electrolyte and under applied potential are an important parameters, since it can be decomposed and react with discharge products and results in battery failure [35]–[38].

2.2.5. Catalyst

To facilitate the reactions on cathode side, catalyst is employed. Catalyst is a type of materials which do not participate in the reactions, but facile the reactions toward.

In Li-O_2 batteries systems, different types of catalysts were investigated to evaluate the effect of them on the battery performance. However, the lack of advanced air electrode design and efficient catalysts for oxygen reduction and evolution reactions have been remained one of the main challenges in this system.

The catalyst can be categories in different lists. However, one way of studying these materials is to divide them based on their shape and structure. In which these materials can be in any forms of 0D, 1D, 2D, and bulk format. Here, the attention was focused on 2D materials and their application in Li-O_2 batteries.

2.2.5.1. Two Dimensional Materials

Among different class of materials, two-dimensional (2D) nano-materials have attracted more interests due to their relatively large surface area and short diffusion path lengths, which enables faster reaction rates, compared to the bulk [39]. Moreover, it is well known that nanomaterials have different thermodynamic, electronic, and mechanical properties.

2.2.5.1.1. Synthesis

There are various methods of preparation of two dimensional materials, generally they can be categorized in two major methods, the top-down approach and bottom-up approach.

Top down method: Two dimensional materials mostly share one property with each other which is very fragile out of plan van der Waals bonds and strong in plane covalent forces. The electronic and mechanical properties of this class of materials is proven to vary significantly from bulk to two dimensional structures [39]. This unique property has been the inspiring point of the research on two dimensional materials and exploring the top-down strategy. In this method two dimensional sheets are synthesized from bulk layered crystals by applying different external forces (e.g. mechanical cleavage, liquid exfoliation, or selective etching) [40]. Such forces break the interlayer van der Waals bonds leading to formation of one to few layers two dimensional materials.

Bottom-up approach: This method is usually based on direct synthesize of two dimensional materials in an appropriate precursor and environment. This method consists of two main synthesis strategies, chemical vapor deposition (CVD) and wet chemical

synthesis. In CVD method, a chemical precursor reacts in high temperature and vacuum pressure, and deposits on the substrate, and forms the two-dimensional structure [41].

CVD method is one of the most used methods for synthesizing two dimensional materials mainly due to its various advantages compared to other techniques such as scalability, ability to tune the electronic property and thickness, and high yield.

In wet chemical synthesis method, the two-dimensional materials are usually synthesized from a hydrothermal or solvothermal methods from a chemical reaction of a precursor in a solution. This method has many benefits compared to other techniques such as low cost and scalability. However, this method has some limitations such as challenges in synthesizing few or mono layer two dimensional materials [42].

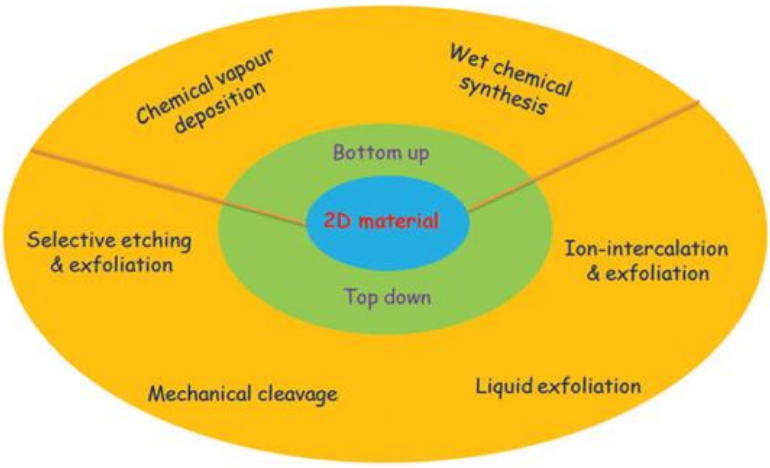

Figure 3. Different synthetic approaches for the preparation of 2D materials. Adapted from reference [3].

2.2.5.1.2. Categories

Two dimensional materials can be categories in different cases. One category can be in the way to do in carbon-based and non-carbon based 2D materials. Carbon based material can be listed as graphene, graphene oxide, reduced graphene oxide (rGO), and dopped/alloyed graphene based materials. Non-carbon based materials can be compressed in MXene, hexagonal Boron-Nitride (h-BN), transition metal oxide and hydroxides

(TMO/TMH), transition metal chalcogenides (TMDs), and transition metal dichalcogenides (TMDCs).

Graphene has been used in various metal air systems due to its superior electronic and morphological properties such as high electrical and thermal conductivity as well as very high surface to volume ratio. Reduced graphene oxide also has recently captured an increasing attention in the field of electrocatalysis due to its interesting properties such as very high electric conductivity even compared to graphene and relatively simple method of preparation [43].

MXene: A new class of two-dimensional inorganic materials, called MXenes including transition metal carbides (TMCs), transition metal nitrates (TMNs), and transition metal carbonitrides (TMCNs), have been investigated recently in energy storage applications due to their low metal diffusion barrier on the surface [44]–[46]. They are shown as $M_{n+1}AX_n$ (n=1,2,3) in which M,A, and X represent a transition metal, an atom from group III or IV, and carbon and/or nitrogen, respectively [47], [48]. Both properties of metallic conductivity and hydrophilicity along with their high melting point and chemical stability, make these materials a promising candidate as the electrode in metal batteries [49]–[57].

Hexagonal Boron-Nitride (h-BN): Hexagonal boron-nitrate, a member of "Boron Nitrates" families with layered structure. Hexagonal boron-nitrate also called as "White Graphene" is a two-dimensional material with an indirect bandgap and high thermal conductivity. Strong covalent bonds between boron and nitrogen atoms in layers and weak van der Waals forces between layers make this material a highly thermally and chemically stable [58].

Transition Metal Oxides/Hydroxides: Two dimensional transition metal oxide and hydroxides (TMO and TMH) are also classified as another electrode material due to their higher specific capacitance and catalytic activity compared to carbonaceous materials. They cannot participate in electrochemical reactions with their whole structure. But the best approach is to synthesize these materials in 0D, 1D, and 2D format to increase the exposed active surfaces [59]–[68].

Transition Metal Dichalcogenides: Another class of two dimensional materials with has gained interests for metal air systems is transition metal dichalcogenides (TMDCs). This class of materials can be shown as MX_2 in which M stands to one transition metal atom and X demonstrates the chalcogen atom (S, Se, Te). These layered materials owning strong in-plane bonding and weak out-of-plane interactions possess a large surface area in interlayer spaces and unique physical and chemical properties [69]–[73]. These features are comparable with single layer graphene regarding the electrochemical activity and show promises for these family to be used in the energy storage application[74]–[95].

2.3.Mechanism

Metal-air batteries are conceptually different from basic metal-ion batteries in that metal ions (e.g., Li) react with oxygen molecules at the cathode side and form covalent bonding (i.e., Li_2O_2) rather than being physically stored at the cathode [16], [96], [97]. Since the energy is stored in covalent bonds, metal-air batteries can store much higher amounts of energy compared to other energy storage systems. For example, the theoretical energy density of Li-air batteries (3500 Wh/kg based on the Li_2O_2 product) is about one order of magnitude higher than that of commonly used Li-ion batteries (380 Wh/kg) [4], [98].

2.3.1. Lithium Oxygen Battery

Fundamentally, the specific energy and rechargeability of metal-air batteries are governed by the oxygen reduction reaction (ORR) and oxygen evolution reaction (OER) rates at the cathode and their corresponding overpotentials. For instance, in lithium oxygen system the main discharge product is usually Li_2O_2 and the efficiency of the battery is mainly determined by the following reactions during discharging and charging processes:

$$\text{Discharging (ORR)} \quad 2Li^+ + 2e^- + O_2 \rightarrow Li_2O_2 \quad \text{(Eq. 9)}$$

$$\text{Charging (OER)} \quad Li_2O_2 \rightarrow 2Li^+ + 2e^- + O_2 \quad \text{(Eq. 10)}$$

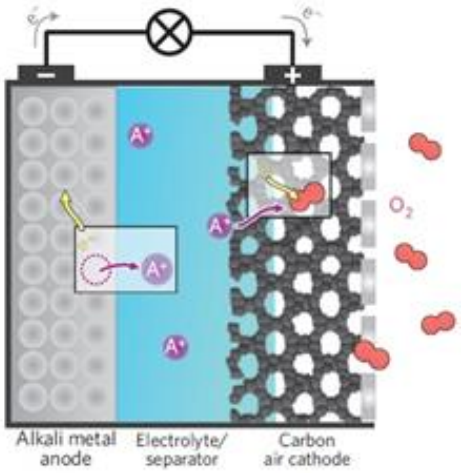

Figure 4. Schematic of a metal-oxygen system during discharge reaction.

However, it has been shown that the above reactions are usually hampered by slow kinetics of ORR and OER reactions giving rise to low efficiency of the cell due to high charge overpotential and partial irreversibility [99]–[101].

2.3.2. Lithium Air Battery

Despite the slow kinetics of ORR and OER reactions as the governing reactions in metal air system, there are some other challenges facing metal air batteries chemistry. In air environment, the presence of nitrogen (N_2), moisture (H_2O), and carbon dioxide (CO_2) can lead the reactions as following possible ones [102]:

$$2\ Li + O_2 \rightarrow Li_2O_2 \quad \text{(Eq. 11)}$$

$$4\ Li + O_2 \rightarrow 2\ Li_2O \quad \text{(Eq. 12)}$$

$$4\ Li + 2\ H_2O + O_2 \rightarrow 4\ LiOH \quad \text{(Eq. 13)}$$

$$2\ Li + 2\ H_2O \rightarrow 2\ LiOH + H_2 \quad \text{(Eq. 14)}$$

$$LiOH + H_2O \rightarrow LiOH + H_2O \quad \text{(Eq. 15)}$$

$$2\ Li_2O_2 + 2\ H_2O \rightarrow 4\ LiOH + O_2 \quad \text{(Eq. 16)}$$

$$4\ Li + O_2 + 2\ CO_2 \rightarrow 2\ Li_2CO_3 \quad \text{(Eq. 17)}$$

$$2\ Li_2O_2 + 2\ CO_2 \rightarrow O_2 + 2\ Li_2CO_3 \quad \text{(Eq. 18)}$$

$$2\ LiOH + CO_2 \rightarrow Li_2CO_3 + H_2O \quad \text{(Eq. 19)}$$

$$6\ Li + N_2 \rightarrow 2\ Li_3N \quad \text{(Eq. 20)}$$

$$Li_3N + 3\ H_2O \rightarrow 3\ LiOH + NH_3 \quad \text{(Eq. 21)}$$

As it has been shown in equations 11-21, the main byproducts in air environment will be LiOH and Li_2CO_3. The reactivity of Li with N_2 is negligible due to the very high Gibbs free energies for these reactions. To achieve an operational Li-air battery, the system needs to decompose the formed products during the discharge and make the system reversible. Any irreversibility in the system will cause in change of voltage, capacity loss, and finally failure of the system.

3. LITERATURE REVIEW

3.1. Non-Aqueous Lithium Oxygen Batteries

Since the very first successful demonstration of a metal oxygen battery based on carbon electrode by Abraham et al. [17] in 1996, many efforts have been placed on advancement of carbon based cathode materials as it was shown that decreasing carbon surface area decreases the specific capacity of the cell [15], [96]. A further study revealed that despite the active surface area of carbon electrode, mesopore volume (2-50 nm) of carbon catalysts used in their air electrodes also plays a vital role in specific capacity of metal air systems [103]. Different research groups have demonstrated some progress in engineering the morphology and surface properties of carbon based air electrodes by either increasing the active surface area and mesopore volumes such as carbon nanotubes (CNT), super P and Ketjen black [104] or improving its catalytic properties by physical and chemical synthesis methods which led to carbon electrodes such as acetalyne black or graphene [105].

Among different two-dimensional carbon-based air electrodes, graphene has been used in various metal air systems due to its superior electronic and morphological properties such as high electrical and thermal conductivity as well as very high surface to volume ratio.

Yoo et al. were the first group that examined the performance of graphene nanosheets (GNS) as air-electrodes in a hybrid Li-oxygen cell consist of an aqueous electrolyte on cathode side and an organic electrolyte in anode side [105]. This unique cell configuration with the use of GNS as the air electrode significantly reduced the charge overepotential compared to previous results with super P or acetaylene black. They have shown that the presence of dangling bonds (i.e., sp3 hybridized carbon atoms) in the graphene structure makes the performance of graphene sheets as the cathode to be very close to the performance of 20 wt% Pt/CB cathode as the benchmark air cathode. The cycling result of this system up to 50 cycles showed promises for possible potential of graphene as an alternative air cathode for noble metal based system and amorphous carbon structures.

The implementation of graphene as the air electrode has been later investigated by other groups in different metal air batteries [106], [107]. For instance, Xiao et.al reported the significant improvement in achievable discharge capacity of li-air as high as 15000 mAh/g

by using hierarchical arrangement of functionalized graphene sheets. They attributed this performance to the unique bimodal porous structure of the electrode which consists of microporous channels facilitating rapid O_2 diffusion [108].

Later other groups have put many efforts to increase the activity of carbon nanostructures for enhanced catalytic activity and active surface area for Li-air systems. Li et al. studied the effect of nitrogen doping on the electro catalytic performance of graphene toward oxygen reduction and evolution reaction [109]. They have shown that nitrogen doping can improve the performance of Li-O_2 by increasing its specific capacity from 8530 mAh g^{-1} to 11660 mAh g^{-1} under the current density of 75 mA gr^{-1}. In a similar study, Wu et al. showed an improved performance of nitrogen doped graphene sheets derived from polyaniline and Co precursors using MWNTs for lithium oxygen system [110].

More recently, Sun et al. studied the sulfur-doped graphene nanosheets as cathode materials for lithium–oxygen batteries [111]. They showed that morphology of discharge product has been modified as a result of sulfur doping. In particular, the Lithium peroxide formed with sulfur doped cathode had a rode shape structure compared to particle-like structure of products on the pristine graphene sheets.

Reduced graphene oxide has recently captured an increasing attention in the field of electrocatalysis due to its interesting properties such as very high electric conductivity even compared to graphene and relatively simple method of preparation [43]. In a study by Liu et al.; rGO has been used as the air electrode with a DMSO based electrolyte containing LiI as additive [112]. In this report, reversible formation of Lithium hydroxide was reported for the first time in opposite to the previous reports based on lithium oxide products (e.g lithium peroxide or lithium superoxide). The use of microporous rGO as a light, conductive and high porous media has been shown to lead to a significantly high specific capacity compared to graphene nanosheets or graphene oxide structures. The Li-O_2 cell based on r-GO and LiI mediator exhibits no capacity decay polarization after 2000, 300, and 100 cycles studied under different specific capacities of to 1000, 5000, and 8000 mAh/g, respectively. This system is also capable to perform under different C-rates. The role of additive in this report was remarkable since addition of LiI as the reactive agent to the electrolyte has led to a discharge plateau of 2.95 V which is significantly lower than similar

results of systems based on super P or Vulcan 32 [113]. The role of additive can be summarized as a redox mediator which guides the charge voltage and thus affects the cycling stability of the cell. Second, tailoring the morphology of the product (LiOH) by affecting the growth of large LiOH crystals that efficiently take up the pore volume of macroporous rGO electrodes. Finally, by facilitating decomposition of LiOH as a stable product that leads to low charge overpotential. The proposed reaction mechanism for reversible LiOH formation with LiI mediator is shown below:

Discharge Reactions:

$$\text{Electrochemical:}\quad 4Li^{+} + 4O_2 + 4e^{-} \rightarrow 4LiO_2 \qquad (Eq.\,22)$$

$$\text{Chemical}:\ 4LiO_2 + 2H_2O \rightarrow 4LiOH + 3O_2 \qquad (Eq.\,23)$$

Charge Reactions:

$$\text{Electrochemical}:\ 6I^{-} \rightarrow 2I_3^{-} + 4e^{-} \qquad (Eq.\,24)$$

$$\text{Chemical:}\quad 4LiOH + 2I_3^{-} \rightarrow 4Li^{+} + :\ 6I^{-} + 2H_2O + O_2 \qquad (Eq.\,25)$$

However, this mechanism has later been argued by Shen et.al [114], [115] by showing that LiOH cannot be oxidized by triiodide (I^{3-}) to evolve the oxygen during charge reaction. In the other word, the charge capacity is a result of iodine rather than lithium hydroxide.

In a similar study based on r-GO, Lu et al. [116] have successfully reported the possibility of a one-electron discharge process that forms only lithium superoxide (LiO_2) in a Li-oxygen environment this finding, in particular is different than the previous studies [117]–[121] that reported the formation of lithium peroxide (Li_2O_2) as the main discharge product despite the structure of nature of cathode materials. The authors have extensively studied the reaction mechanism of lithium superoxide formation by various in-situ and ex-situ studies. The Ir–rGO charge platue increases by only 0.3 V from 3.2 V to 3.5 V over 40 cycles exhibiting more than 85% efficiency in this system. This is about 0.7 V lower than that of rGO cathode under identical condition. The Lithium superoxide formed in this system exhibits needle or rod-like morphology evidenced by TEM and SEM images. Their differential electrochemical mass spectrometry (DEMS) as well as XRD and Raman results confirm the formation of a stable LiO_2 phase rather than Li_2O_2. These results have been

further confirmed by the density functional theory and TEM findings in which a templating growth mechanism based on Ir nanoparticles was proved to be responsible for lithium superoxide growth.

On the other hand as the first study of MXene materials in metal-air batteries, Liu et al. [50] have used tungsten carbide in lithium-oxygen batteries as the catalyst in a gas diffusion electrode. They have shown the improvement in conductivity and dispensability of tungsten carbide catalyst in the presence of amorphous carbon.

Bi-transition-metals (Fe- and Mo-) carbide supported on nitrogen-doped graphene (FeMo-NG) was synthesized by dispersion of $Fe(NO_3)_3.9H_2O$ and $(NH_4)_6Mo_7O_{24}.4H_2O$ in distilled water (DI water) and pretreating with ultrasonication. Graphene oxide (GO) was also synthesized through a modified Hummers method from natural flake graphite powder. The urea was added as the precursor to mediate the nucleation of metal species onto the functional group and the source of nitrogen into the first solution followed by adding the second solution. The obtained mixture was freeze-dried and collected for pyrolysis to enable the crystallization of metal carbide nanoparticles, N-doping and reduction of GO. They evaluated the synthesized materials by SEM, TEM, HR-TEM, XPS, and XRD to prove the accuracy of the synthesis.

Samples with different atomic ratios of Fe and Mo (4:0, 0:4, 1:3, 1:1, and 3:1) were tested by cyclic voltammetry and rotating disk electrode (RDE) measurements to evaluate the oxygen reduction reaction activity. The -0.09 V onset potential (vs. saturated KCl Ag/AgCl), 3.5 $mAcm^{-2}$ at -0.8 V current density (vs. Ag/AgCl) with nearly four electron transfer number was reported. The cycling stability, toxic tolerance for ORR in alkaline electrolyte, and in general, electrocatalytic activity were shown in this paper which are due to the synergic effect between well-dispersed carbide species and nitrogen-doped graphene.

Later works also reported that the oxygen reduction reaction activity of carbide materials with adding tungsten carbides to a graphene based material decorated with platinum and combination of tungsten carbide with different content of carbon [49], [50].

Another class of two dimensional materials which has been used for metal air batteries are metal sulfides which are also named as transition metal chalcogenides. Their high

theoretical capacity and higher intrinsic electrical conductivity, electrochemical activity and their low cost make them a promising candidate to be applied as the electrode material in metal air batteries and supercapacitors [122]–[130].

Ma et al. [131] have recently shown the performance of Nickel sulfides (NiS) with two different morphologies in lithium-oxygen batteries. They have synthesized two morphologies of the flower-like and rod-like nickel sulfides by a hydrothermal method with and without the assistant of cetyltrimethyl ammonium bromide (CTAB), respectively.

In particular, $Ni(NO_3)_2 \cdot 6H_2O$ and NaSCN have been used as the precursors to synthesize these materials. Both materials showed promising catalytic activities owned to proper formation and decomposition of Li_2O_2 as the main product during cycling. They have improved specific capacity and cycling performance and decreased overpotential compared to Super P based electrodes. Although both structures demonstrated satisfactory results, but the importance of the morphology was highlighted in this reported in which the system with flower-like NiS was a more favorable morphology rather than the rod-like one.

They have reported 30 cycles performance under 75 and 150 mAg^{-1} current densities resulting in different overpotentials. The capacity of 6733 mAh g^{-1} under 75 mA g^{-1} is presented in this work which mean a very good stability performance up to around 90 hrs.

Yan et al. [132] have shown a new designed electrode, a two-dimensional atomic crystal layer of hexagonal boron nitrate on Cu metal current collector. This coated layer overcomes the lithium dendrite growth and protect it from direct contact with electrolyte to avoid the possible side reactions. They also examined it in the air (containing oxygen and moisture) for 15 minutes and showed resistance against lithium oxidation compared to one without this coating layer which turned black. The main h-BN properties, which make this material a suitable candidate, are as follow: strong mechanical strength in its single atomic layer while being highly flexible in its ultrathin thickness, chemically inert and stable material against most chemicals, and relatively low-size diameter in hexagonal rings (1.2 °A) which is smaller than ions and atoms in battery environment. But existence of defects (points and lines) in 2D layer make it possible for ions to penetrate the layer. Considering the most important feature of SEI layer, ionic conductive and electrically insolating, h-BN can be a promising candidate for being used as anode protection layer in metal-air batteries.

For the first time in metal-air batteries, Liao et al. [133] have used Ruthenium oxide (RuO_2) based catalyst for lithium-air batteries. They have synthesized two-dimensional RuO_2 nanosheets with thickness of about 2 nm with a two-step process involving exfoliation and heat treatment. The lamellar morphology of the precursor on a large scale was observed and shown by SEM and TEM images. They have employed the catalyst in a lithium-oxygen system under different current densities. The cycling performance was limited to 50-cycles c under 200 mA g^{-1} current density was reported with up to 900 mAh g^{-1} charge and discharge capacity. The performance improvement is attributed to the good conductivity, large surface to mass ratio, and better catalytic activity of the synthesized material.

In another research, Tong et al. [134] have shown mesoporous NiO with a single crystalline structure utilized as a metal free catalyst for non-aqueous lithium-oxygen batteries. Mesoporous NiO nanosheets with a single-crystalline structure were synthesized by a facile alcohol-thermal method from $Ni(NO_3)_2.6H_2O$ and NaOH with ethanol as the dispersant. They synthesized material was investigated as an oxygen electrode catalyst in a Li-O_2 system and shown 40 cycles in 500 mAh g^{-1} limited capacity. Studying the reaction mechanism revealed Li_2O_2 and Li_2CO_3 were formed and decomposed during discharge and charge processes. They have shown that NiO nanosheet has the capability to facilitate the decomposition of the products.

Also, Shen et al. [135] have reported a Cobalt metal based free-standing cathode material for lithium-oxygen batteries with improved electrochemical performance. By replacing the metal-oxide catalysts with cobalt metal, the conductivity of the electrode was improved. On the other hand, the oxide layer on the surface of metal particles could still act as an effective catalyst during cell operations. A facile electrochemical deposition process followed by heat treatment in a reduction atmosphere was used to prepare the electrodes. The employment of this material in the system is reported up to 11042 mAh g^{-1} specific dishcarge capacity under 100 mA g^{-1} current density and 1416 mAh g^{-1} specific dishcarge capacity under 500 mA g^{-1} current density.

As the first report of TMDC materials in metal-air batteries, Zhang et al. [136] have shown molybdenum disulfide nanosheets decorated with gold nanoparticles

(MoS_2/AuNPs) as air cathode in the Li-air system to improve specific capacity and performance efficiency for rechargeable lithium-oxygen batteries. They synthesized MoS_2/AuNPs by a one-step hydrothermal synthesis, adding hydrazine to reduce $(NH_4)_2MoS_4$ and $HAuCl_4$ in an aqueous solution at 200ºC. The $HAuCl_4$ precursor was reduced to AuNPs, which are attached onto the MoS_2 nanosheets produced by the synchronous reduction of the $(NH_4)_2MoS_4$ precursor with the S–Au bond. The potential gap and specific capacity of 1.07 V and 4336 mAh g^{-1} have been shown, respectively, as the performance of the cell with new synthesized material. The pure Li metal foil and a 1.0 M solution of $LiCF_3SO_3$ in TEGDME were selected as the anode and electrolyte in the system and Li_2O_2 is confirmed as the major discharge product during cycling. A 0.09 and 0.05 V in discharge voltage, 0.2 and 0.03 V in charge voltage, and 1576 and 1329 mAh g^{-1} in specific capacity are shown as an improvement compared to pristine Super P and MoS_2 nanoflowers, respectively.

Later Asadi et al. [137] have shown the performance of molybdenum disulfide (MoS_2) nanoflakes (MoS_2 NFs) as a member of TMDC family combined with an ionic liquid works as a co-catalyst system with a bi-functional performance in lithium-oxygen batteries. The MoS_2 was synthesized by chemical vapor transfer (CVT) method, then exfoliated in Isopropyl Alcohol (IPA) solution for 20 hr followed by 1 hr centrifuging at 2000 rpm to produce MoS_2 nanoflakes (MoS_2 NFs). Comparison between oxygen reduction and evolution reactions (ORR and OER) of the system with different purged gases, electrolytes, and cathodes have been done to show the best performance of the system with MoS_2 NFs and an ionic liquid as the cathode and electrolyte, respectively. A 85% round trip efficiency in 50 continuous cycles was reported to prove the essential need of an ionic liquid existence to prevent the MoS_2 edges from poisoning compared to another case with dimethyl sulfoxide (DMSO) as a common electrolyte. Their reaction steps following oxygen reduction were based on a through solution mechanism which enables the system to work reversible. The formation and fully decomposition of the products were shown by Raman, XRD, and differential electrochemical mass spectrometry after discharge and charge of the cell.

To utilize the benefits of graphene, Li et al. [73] have developed a system based on a graphene aerogel decorated with MoS_x nanosheets (MoS_x/HRG) with a three-dimensional porous framework. The MoS_x/HRG aerogel functionalizes electrolyte and facilitate oxygen diffusion by providing hierarchical mesopores and micropores. It means there is more room for reaction products to form and decompose and oxygen molecules to diffuse. They have investigated different ratios of MoS_x to HRG (1:2, 1:1, and 2:1) under different current densities (0.05, 0.1, 0.2, and 0.5 $mAcm^{-2}$). The 6678.4 mAh g^{-1} discharge capacity is reported at 0.05 mA cm^{-2} current density for MoS_x/HRG (2:1) as the best result. It was shown that the system with MoS_x/HRG (2:1) aerogel cathode had better performance compared to a system with HRG aerogel cathode in which the life cycle is improved from 15 to 30 cycles with a cut-off capacity of 500 mAh g^{-1} at 0.1 $mAcm^{-2}$ current density. In brief, this material has shown promoted performance because of the ORR activity which is attributed to MoS_x. However, there was some limitation on catalytic performance in high current rates.

3.2. Non-Aqueous Lithium Air Batteries

After the very first demonstration of Li-O_2 system by Abraham on 1996 [17], there have been numerous efforts to improve the life cycle and performance of Li-O_2 batteries by either tailoring the air electrode structure a or manipulating electrolyte/salt combinations.

However, most of these systems suffer from low cycle life, mostly because of anode degradation. In previous section, these types of batteries were discussed extensively. Recently, there have been also a few reports in which some groups have studied the role of moisture and CO_2 addition on the performance of Li-O_2 system [138]. However, in most of these reports the performance of the system was severely affected by the addition of moisture. There are also some limited number of reports in which the performance of Li-O_2 battery is studied in simulated ambient air condition [15], [16], [19], [20], [139], [140]. In which the cycle performance of the Li-O_2 battery was not more than 50 cycles. The failure cause in most of these batteries was still the lack of an advanced protection on the li-anode to protect it from degradation, and also, high charge overpotentials because of formation of side products such as LiOH, Li_2CO_3 and $LiOH.H_2O$.

The studies on Li-air batteries are limited to two categories [141]. In which in one them, only the system with presence of H_2O is investigated. And in other one, the effect of the CO_2 on the performance of the system is studied [142]–[144].

4. METHODS AND MATERIALS

In this section, the experimental and electrochemical techniques and characterization methods used in this thesis is explained. It goes through a general overview of preparation and operation methods in different part of the system and a brief discussion of their outcomes.

4.1. Experimental Methods

As the main experimental part of this work, in this section, the materials preparation, cell assembly, and battery operation will be discussed.

4.1.1. Materials Preparation

As the main components of a battery, the preparation of cathode, electrolyte, and anode will be discussed in this section. The methods explained here are used before battery assembly.

4.1.1.1. Cathode

The MoS_2 NFs were synthesized using a liquid exfoliation method in which 300 mg of MoS_2 powder (99%) was dispersed in 60 mL isopropyl alcohol (IPA) (>99.5%). The solution was exfoliated for 20 hours and centrifuged for 1 hour to extract the supernatant (top two third of the centrifuged solution). MoS_2 NFs were then coated on a conductive substrate of the gas diffusion layer (GDL) (0.2 mm thickness, 80% porosity) to reach the catalyst loading of 0.1 mg/cm^2. Prepared cathodes were dried in a vacuum oven for 24 hours at 80°C to stabilize the cathode and remove impurities [137].

4.1.1.2. Electrolyte

To select an appropriate electrolyte, oxygen reduction and oxygen evolution reactions were performed in a three-electrode electrochemical cell using different volume ratios of IL/DMSO electrolytes. The cell was composed of lithium chips (>99.9%) as the reference and anode electrodes, and MoS_2 NFs coated on the gas diffusion layer as the cathode. The cathode, anode and reference electrodes were placed in different volume ratios of the 1-ethyl-3-methylimidazolium tetrafluoroborate (EMIM-BF_4) (HPLC grade, >99.0%) and dimethyl sulfoxide (DMSO) with 0.1 M Lithium Bis (Trifluoromethanesulfonyl) Imide

(LiTFSI) (>99.0%) as a lithium salt. The electrochemical results shown in Figure 5 indicate that 25:75 vol% of the IL/DMSO electrolyte exhibit the highest ORR and OER.

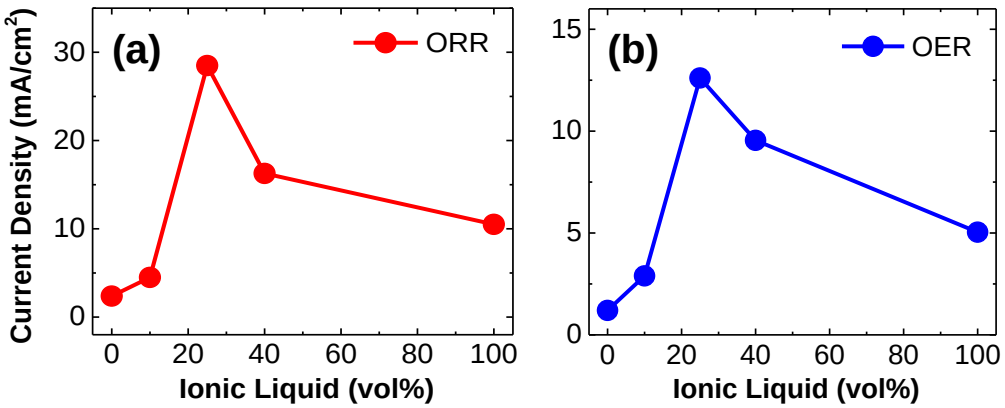

Figure 5. (a) ORR current density (mA/cm^2) and **(b)** OER current density (mA/cm^2) at different IL volume percentage in DMSO.

The comparison of this system performance with literature [137], [145]–[154] is presented in Figure 6. Interestingly, the obtained current densities in both ORR and OER show the bi-functional performance of MoS_2 NFs in IL/DMSO.

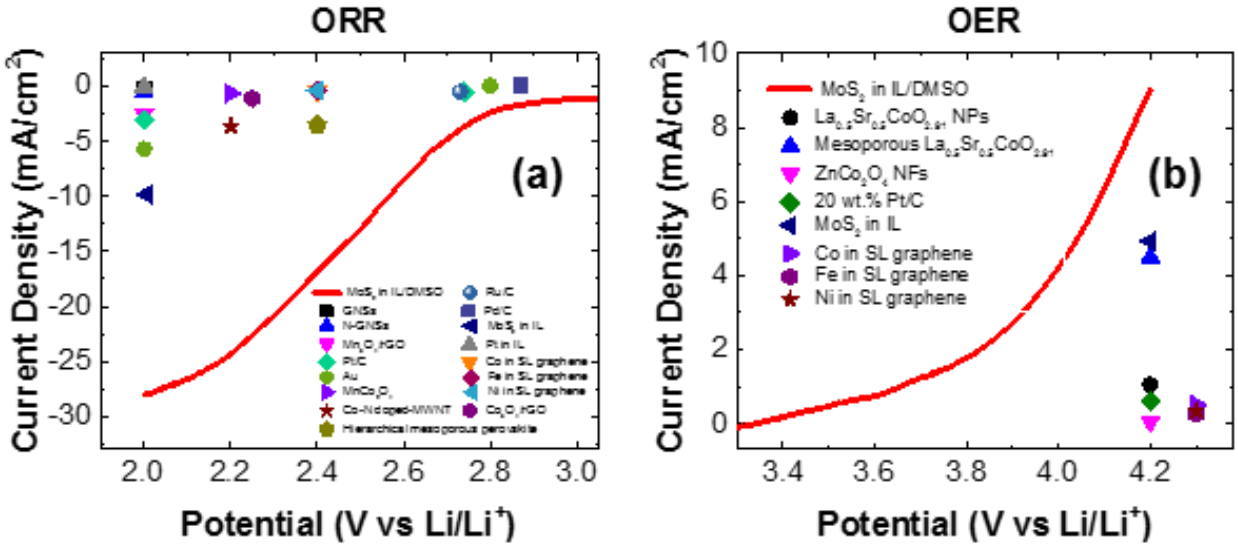

Figure 6. Performance comparison of MoS_2 NFs in IL/DMSO mixture electrolyte for **(a)** Oxygen reduction reaction (ORR), and **(b)** Oxygen evolution reaction (OER) with other reported systems in aprotic media.

4.1.1.3. Anode

For the anode protection, the battery cell was assembled using commercial pure lithium chips (>99.9%) with a thickness of 0.25 mm as the anode and MoS_2 nanoflakes coated on a gas diffusion layer as the cathode. The electrolyte of the cell was also composed of 25 %volume EMIM-BF_4 (HPLC grade, >99.0%) and 75 %volume DMSO with 0.1 M LiTFSI (>99.0%) as a lithium salt. The cell was run for 10 continuous cycles, each cycle consisting of a one-hour charge process followed by a one-hour discharge process, in pure CO_2 environment.

The assembled battery cell was first purged with pure CO_2 (99.99%) in order to remove gas impurities and parasitic reactions. The CO_2 filled battery was then connected to a potentiostat for cycling experiments with an applied current density of 500 mA/g for 10 continuous cycles. Results are shown in Figure 7.

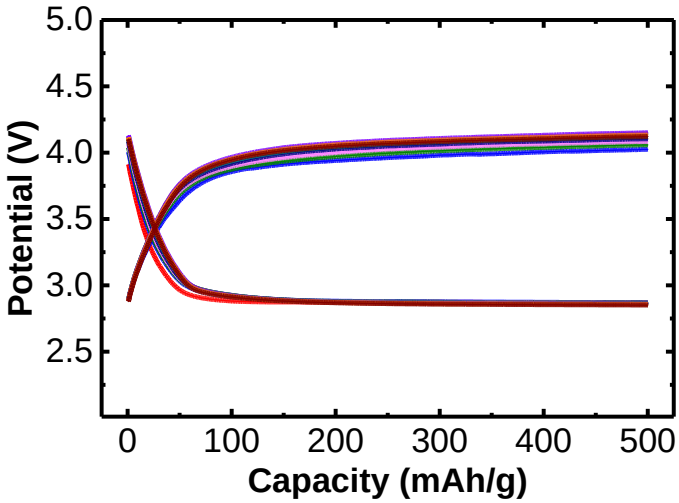

Figure 7. Charging and discharging profile of Li-CO_2 battery after 10 cycles.

The possible reaction between Li metal and CO_2 gas is as follow:

$$4\,Li(s) + 3\,CO_2(g) \rightarrow 2\,Li_2CO_3(s) + C(s) \qquad (Eq.\,26)$$

The presence of Li_2CO_3 and C products are confirmed by distinguishable peaks of C 1s at 289.5 and 284.8 eV in XPS measurements and also in Raman spectra (Section 4.3.3 and 4.3.4).

To address the possibility of the reaction between the Li_2CO_3 and water, it is important to take into account that the Li_2CO_3 is an insoluble compound in water with high anhydrous properties. However, the presence of CO_2 is crucial to forward this reaction toward the formation of lithium bicarbonate ($LiHCO_3$) through the following reaction:

$$Li_2CO_3\,(s) + CO_2\,(g) + H_2O\,(g) \rightarrow 2\,LiHCO_3\,(s) \qquad \text{(Eq. 27)}$$

There are two main points against the formation of lithium bicarbonate in this system. First, the concentration of CO_2 in the air mixture is relatively low compared to other species (500 ppm compared to 10,000 ppm of water and 21% of O_2) hindering the CO_2 interaction with protective anode. Second, from the thermodynamic point of view, the required conditions for conversion of Li_2CO_3 to bicarbonate is quite far from the ambient conditions used here. DFT results show three stability curves for $LiHCO_3$ and Li_2CO_3 as a function of temperature and CO_2 pressure, each at different fixed values of H_2O pressures [155]. For instance, $LiHCO_3$ can be formed from the reaction of Li_2CO_3 with CO_2 and water at the temperature of 300 K when the pressure of CO_2 is about 1000 bar and the pressure of water is at least 0.01 bar. In our case, considering a room temperature of 300 K and H_2O partial pressure of 10^{-2} bar (10,000 ppm), the required pressure of CO_2 for this reaction is more than 10^4 bar, much greater than in our system. These results clearly indicate that the reaction of water with Li_2CO_3 in ambient air conditions is very unlikely.

4.1.2. Cell Assembly

All battery systems were assembled using a custom-made Swagelok battery set-up in Argon (Ar) filled glove-box (Section 2.2). This setup was composed of the MoS_2 nanoflakes (NFs) cathode, the protected anode, and ~35 µL of the electrolyte (Section 4.1.1.2). A glass microfiber filter as a separator was used to prevent direct contact between the cathode and the anode.

4.1.3. Input Air

To saturate the air stream with a desired ratio of humidity, the stream was connected to a custom-made chamber and then purged to the battery cell. The relative humidity (RH) and temperature were monitored by a sensor (Silicon Laboratories-Si7005, Figure 8) to keep the RH at ~45% (±3%) and the temperature at ~25°C (±0.5℃) (room temperature).

The sensor was connected to the lab computer and recorded the RH and temperature versus time through Si700x Evaluation software continuously. The air-filled batteries were then sealed and connected to a potentiostat for cycling measurements. Figure 8 shows a typical monitoring data for relative humidity and temperature.

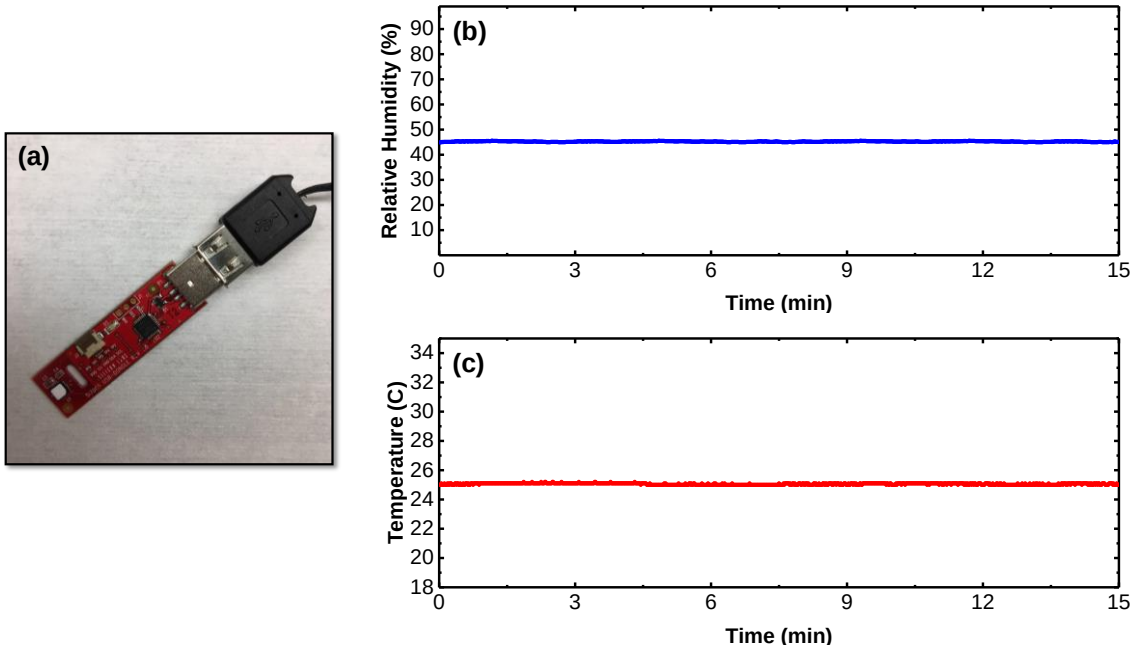

Figure 8. Humidity and Temperature Recording system. **(a)** an image of humidity sensor, **(b)** the relative humidity and **(c)** temperature profiles during the purging of the humidity saturated air into the cell.

4.1.4. Battery Operation

The batteries after purging the air inside and keep them at positive pressure were connected to a potensiostat. Constant current (500 mA/g) for specific time (1 hr) was applied on it to record the output voltage and potential changed as a function of time.

The performance of Li-Air battery up to 700 cycles is shown in Figure 9. The cell was run under 500 mA/g current density for 1 hour discharge followed by 1 hour charge process. The discharge capacity retention was 100% up to 550 cycles and was decreased to ~24% at 700 cycles considering the cut-off potential of 2.5V.

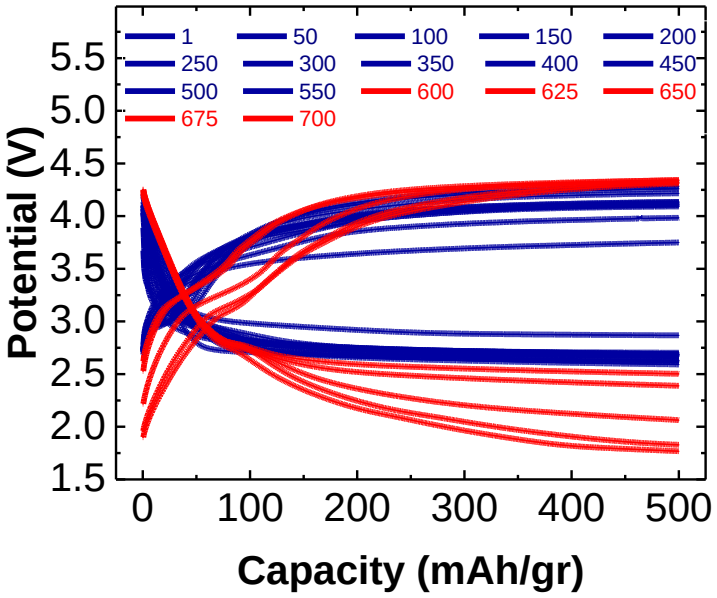

Figure 9. Performance of Li-Air battery system after 700 cycles.

The performance of the Li-O_2 battery in an identical condition as the Li-air system was also tested. Figure 10 presents the voltage profile as a function of capacity (mAh/g). The results show that the trend of the polarization gap is similar to the Li-air system as a function of the number of cycles up to 550 cycles.

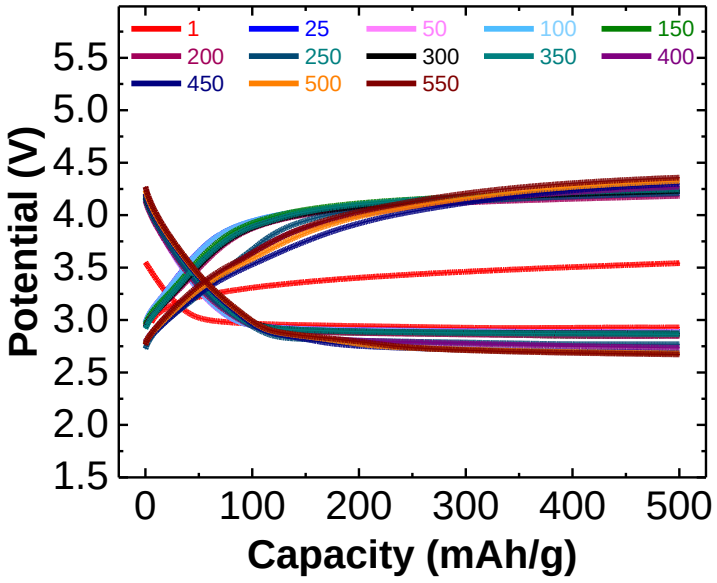

Figure 10. Performance of Lithium-Oxygen battery using a cathode based on MoS_2 NFs and an electrolyte of DMSO/IL saturated with 0.1 M LiTFSI as the Li salt.

Moreover, the performance of the Li-Air battery at the capacity of 1000 mAh/g is shown in Figure 11. This result shows the discharge and charge voltage profiles of the cell for 100 cycles in which the applied current density was 500 mA/g running for a two-hour charge process followed by a two-hour discharge process.

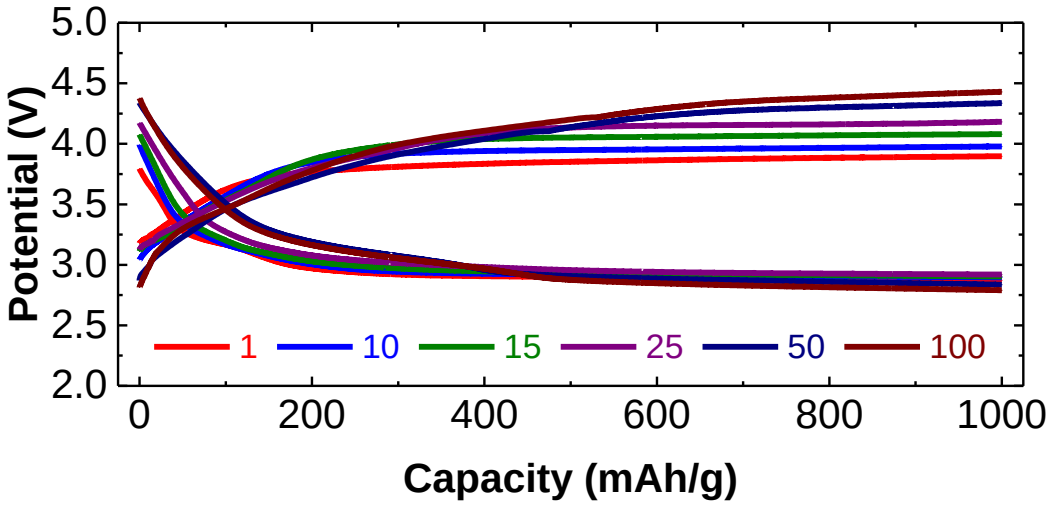

Figure 11. Discharging and charging voltage profile of the Lithium-Air battery using carbon free MoS_2 NFs and hybrid electrolyte (IL/DMSO) saturated with 0.1 M LiTFSI as the Li salt with protected lithium anode. It has been run in discharge capacity of 1000 mAh/g under the current rate of 500 mA/g.

4.2. Electrochemical Methods

There are different techniques which are utilized in electrochemical processes to study the electrochemical parameters in order to more investigate and improve the systems. To study the Li-air battery system, three main electrochemical characterizations were performed on the different parts of the system; cyclic voltammetry (CV), electrochemical impedance spectroscopy (EIS), and lithium swipe efficiency.

4.2.1. Cyclic Voltammetry (CV)

The cyclic voltammetry is a flexible, relatively sensitive, and multi-purpose technique to study the battery systems. This technique is used to identify the reversibility of the species in the system which is a desirable phenomenon in secondary type batteries.

Under the constant applied voltage, it evaluates the current rate as a criterion for activity in the system. Here, CV experiments are presented to evaluate, first in the Figure 12, the activity of the MoS_2 NFs as the cathode coupled with pure IL electrolyte, and, second in the Figure 13, the activity of the MoS_2 NFs in different ratio of DMSO and IL in the mixture electrolyte to improve the system.

Previously, it has been shown in our group that the MoS_2 NFs and IL electrolyte system works as an effective co-catalyst to enhance the performance of the Li-O_2 batteries [137]. They have shown that the activity of the MoS_2 NFs in IL coming from the synergic effect between the MoS_2 NFs and IL. In Figure 12, different cases to study this system are shown. As it can be seen by saturating the electrolyte with other gases like Argon (Ar), the activity of the system is extremely affected which shows that this activity in O_2 saturated electrolyte is governed by oxygen reduction and evolution reactions and is not coming from decomposition of salt or electrolyte as it is reported in other systems [156]. In another experiment, it was examined in which this activity is dependent on IL electrolyte or not. By changing the IL electrolyte to pure DMSO and pure TEGDME electrolytes as two common electrolytes in Li-O_2 batteries, the CV results have shown relatively no activity for them in case of using the MoS_2 NFs as the cathode.

In Figure 12 c-d, the performance of the MoS_2 NFs in pure IL electrolyte for both oxygen reduction and oxygen evolution is shown. These results, compared to performance of pristine substrate, Au NPs, and Pt NPs in the same system, have shown a very promising performance of the MoS_2 NFs in IL. The more important point in this system is that this system has shown a bi-functional performance in both ORR and OER part.

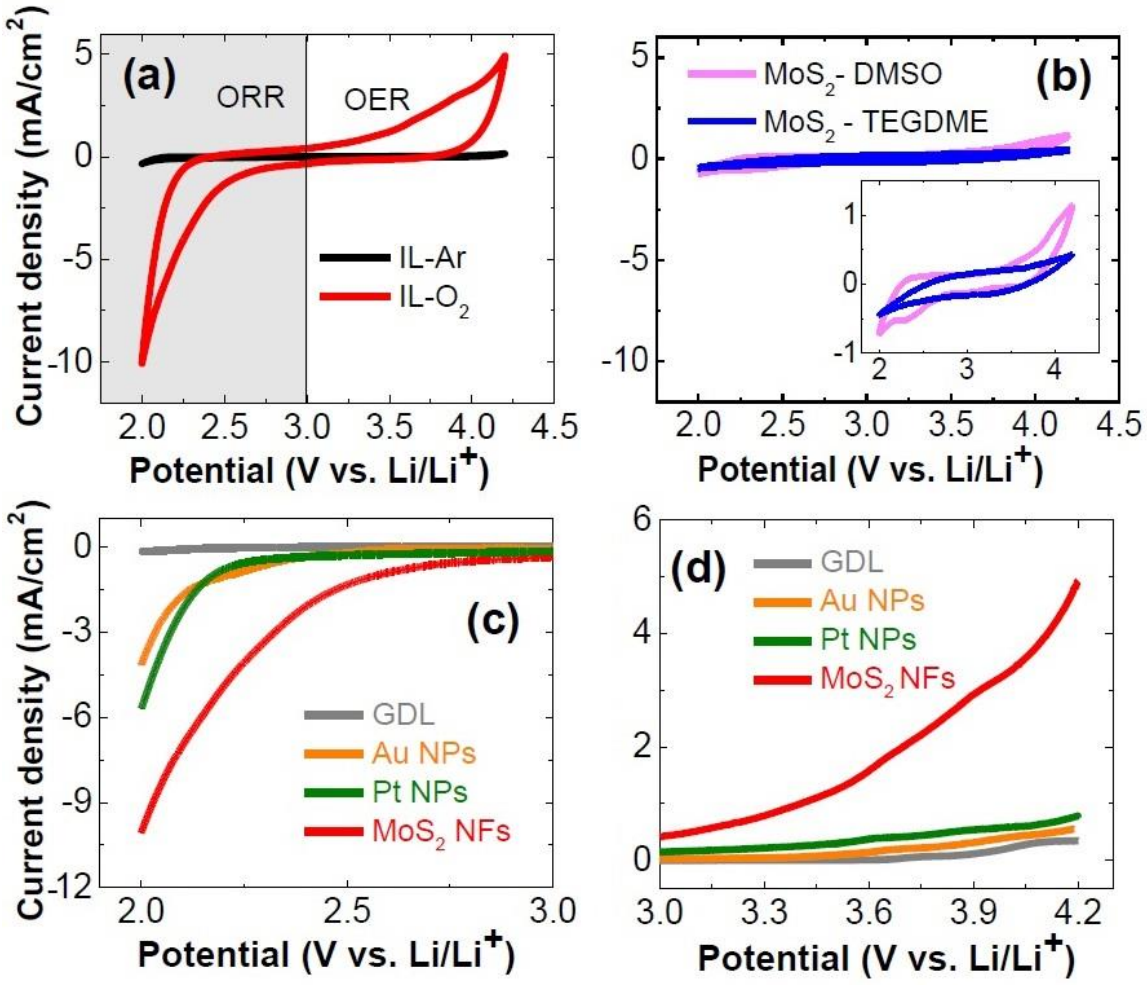

Figure 12. Cyclic voltammetry experiments indifferent controlled experiments. **(a)** MoS_2 NFs in O_2 and Ar saturated pure IL electrolyte, **(b)** MoS_2 NFs in O_2 saturated pure DMSO and pure TEGDME electrolytes, **(c)** comparison of MoS_2 NFs performance in O_2 saturated pure IL electrolyte for ORR, and **(d)** comparison of MoS_2 NFs performance in O_2 saturated pure IL electrolyte for OER.

To improve the performance of our system, there were tried to enhance the activity the system by modifying the electrolyte. In Figure 13, the performance of the system using the MoS_2 NFs with changing the electrolyte is reported. Different volumetric ratio of DMSO added in IL were used as the electrolyte with the MoS_2 NFs. The initial potential was 3.0 V. The voltage was swept between 2 V to 4.2 V with the scan rate of 20 mV/s. As it is shown, at 25 %vol IL in 75 %vol DMSO, the both ORR and OER performance of the

system were enhanced by around three times compared to the case with pure IL. This ratio is selected for all further experiments in this thesis.

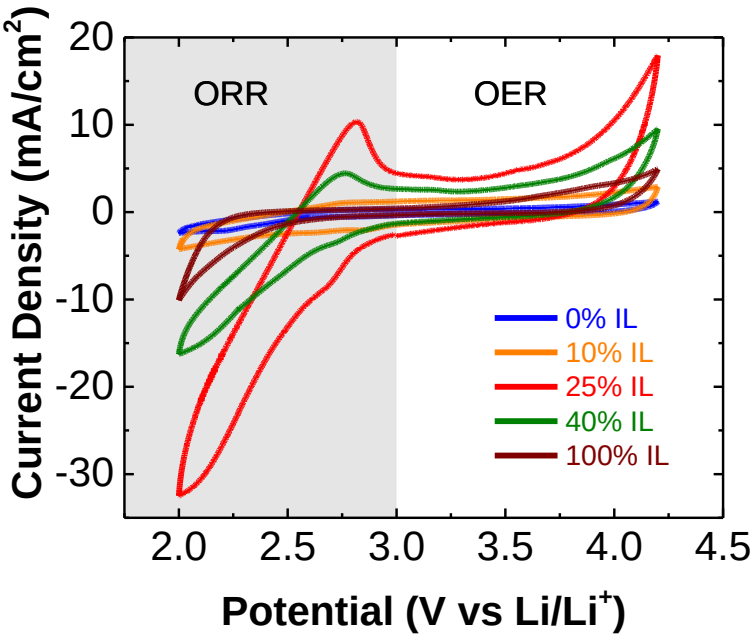

Figure 13. Cyclic voltammetry experiments for MoS_2 NFs in oxygen saturated electrolyte with different %vol IL in DMSO in both ORR and OER regions.

4.2.2. Electrochemical Impedance Spectroscopy (EIS)

Electrochemical impedance spectroscopy (EIS) is a direct technique to study the electrode processes by investigating the changes in the electrical impedance of an electrode. This technique by representing the dynamic characteristics of the electrode-electrolyte interface correlate the impedance of this interface to electrochemical parameter.

To perform the EIS, overpotential and a frequency range should be defined for the system. The typical shape of a EIS diagram is a semicircle which represents the interdependence of the capacity and charge transfer resistance of the components.

In here, all EIS experiments were performed using coin cells under identical experimental conditions of 700 mV overpotential and frequency range of 10 Hz to 100 kHz and the same concentration, size, and weight for all parts of the cell.

Different protected anodes were prepared by performing different numbers of charging and discharging processes in CO_2 environment. For discharge-charge experiments,

Swagelok battery set-up consisting of MoS_2 NFs as the cathode, 0.1M LiTFSI as the Li salt in 25:75% volume EMIM-BF_4:DMSO as the electrolyte, and protected Li as the anode was operated with a constant applied current density of 500 mA/g. The results are presented in Figure 14.

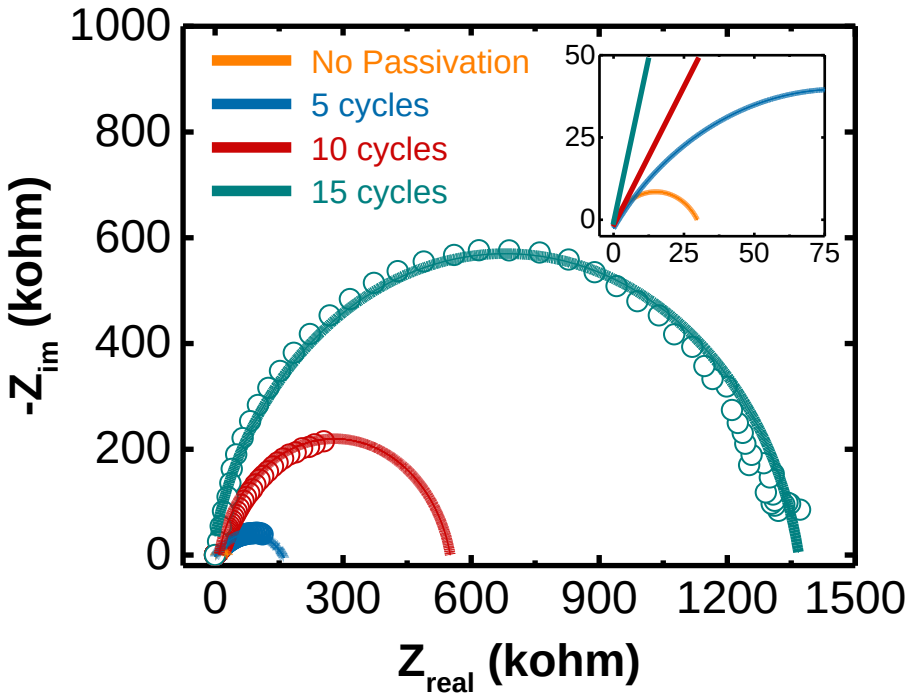

Figure 14. Electrochemical Impedance Spectroscopy of protected anodes after 5, 10, and 15 cycles of exposing to pure CO_2 environment compared to the anode without protection.

4.2.3. Lithium Retention and Lithium Loss

The lithium loss during the operation of the cell in the air is measured to get an insight into the efficiency of ion transfer for the protected anode inside the Li-air battery. A protected anode is prepared and then was assembled in the Li-air cell and run up to the 51 cycles with the current rate of 0.05 mA/cm^2 (Figure 15). The anode was then subjected to stripping experiment with the rate of 0.5 mA/cm^2 (Figure 16). The capacity loss of protected anode after 51 cycles of operation in the actual air environment was then calculated based on the difference of the initial capacity of the anode and its capacity after the striping test. This new finding show that the protected anode possesses an average of

99.97% lithium retention. This value results in ~14% loss of lithium after 550 cycles of operation and is in accord with the findings after long term cycling experiments.

The details of calculations are presented below:

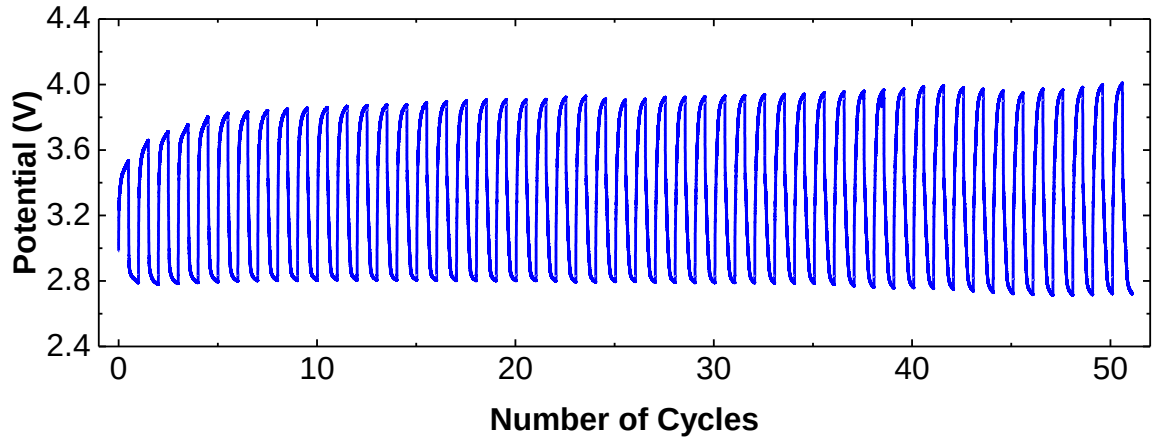

Figure 15. Performance cycling of the Li-Air system under the current rate of 500 mA/g in 51 cycles.

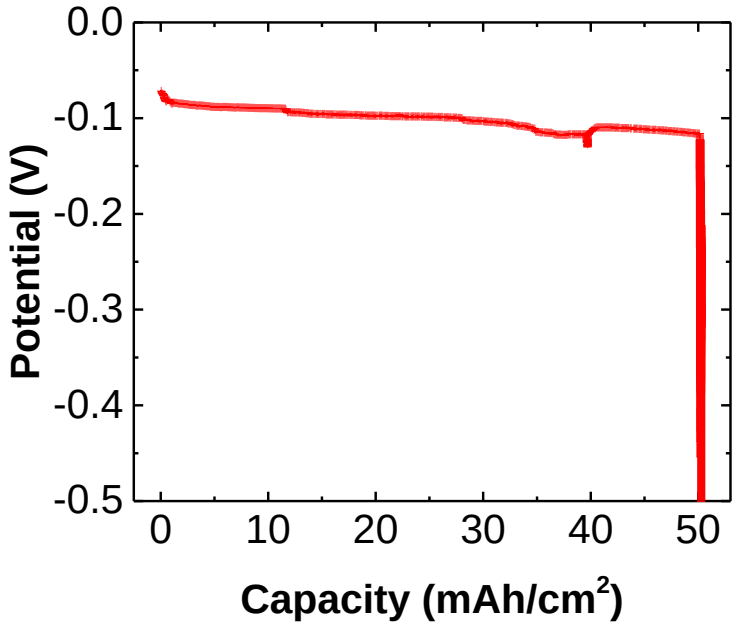

Figure 16. Exhaustive stripping of lithium anode after 51 cycles working in air environment using the current density of 0.5 mA/cm^2.

To calculate the lithium loss, the following procedure have been pursued:

Table 2. The initial and final capacity of a protected anode.

Initial Capacity	51 mAh/cm^2
Final Capacity after Stripping	50.283 mAh/cm^2

Total loss for 51 cycles:

$$\frac{51\ \text{mAh}/cm^2 - 50.283\ \text{mAh}/cm^2}{51\ \text{mAh}/cm^2} = 0.01406$$

Average loss:

$$\frac{0.01406}{51} = 0.00028/cycle$$

Average efficiency:

$$1 - 0.00028 = 0.99972/cycle$$

$$(1 - 0.00028) \times 100 = 99.972\ \%$$

Total loss for 550 cycles:

$$1 - 0.99972^{550} = 0.1407$$

$$(1 - 0.99972^{550}) \times 100 = 14.07\ \%$$

4.3. Characterization

To investigate the system and get a better insight into it, different in-situ and ex-situ characterization methods were utilized to study the cathode, anode, or electrolyte. In this section, these techniques are explained. A short discussion on obtained results are also discussed.

4.3.1. Dynamic Light Scattering (DLS)

To evaluate the particles size in our catalyst solution, dynamic light scattering (DLS) has been performed before coating the MoS_2 NFs from the IPA solution on GDL.

The DLS results have shown a uniform size distribution of MoS_2 nanoflakes in the solution. They have indicated a range size of 110 to 160 nm with average value of 135 nm. One of the obtained results in shown in Figure 17.

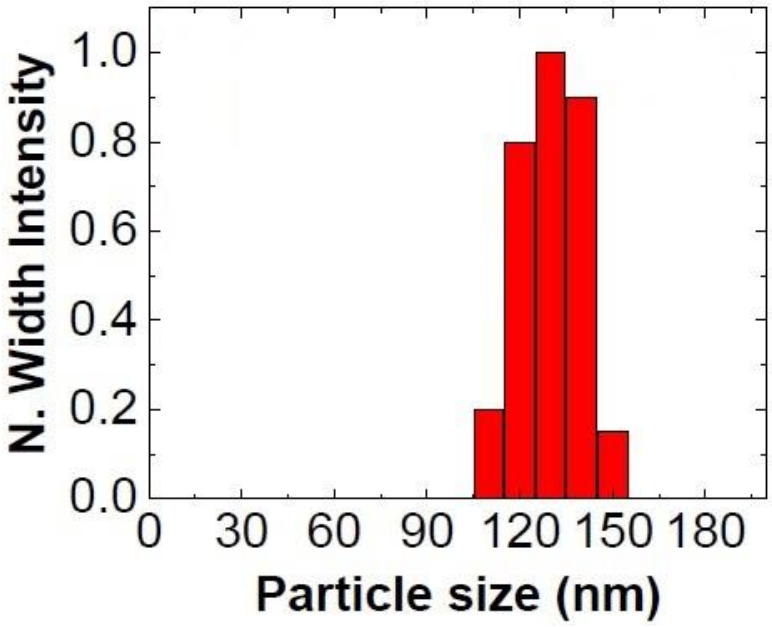

Figure 17. Dynamic light scattering results for MoS_2 nanoflakes in IPA.

4.3.2. Scanning Electron Microscopy (SEM)

The SEM instrument used for characterizing the cathode and anode surfaces was integrated in a Raith e-LiNE plus ultra-high resolution electron beam lithography system.

4.3.2.1. Cathode Surface

Surface structure and morphology of the samples were investigated by performing SEM of the cathode surfaces. The SEM images were performed by an acceleration voltage (EHT) of 10 kV in lens magnification of 5 kX, 15 kX, and 20 kX. Cathode samples were

collected from the battery cells after the discharge and charge processes of the 1, 100, and 250 cycles.

The samples were sealed in Ar filled vials and transferred to SEM instrument. The same method was also done for pristine cathode and the cathode after continuous running for 700 cycles. All procedures were done in Ar filled glove box with less than 1 ppm oxygen and moisture. Figures 18-20 shows the SEM images of the pristine cathode, discharged and charged cathode surface after 1, 100 and 250 cycles, and the discharged cathode after 700 cycles, respectively.

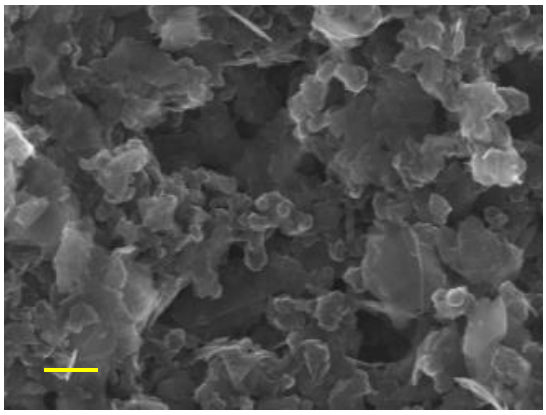

Figure 18. SEM image of the pristine cathode (the scale bar: 200 nm).

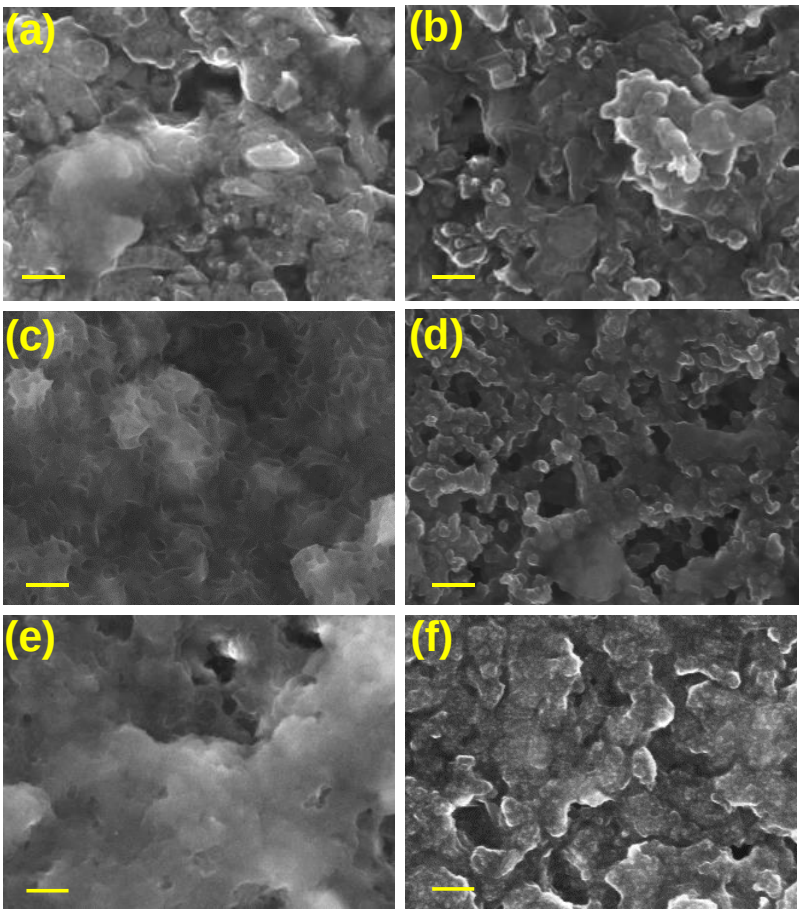

Figure 19. SEM images of the Li-air battery cathode surface after **(a)** the 1st discharge, **(b)** the 1st charge, **(c)** the 100th discharge, **(d)** the 100th charge, **(e)** the 250th discharge, **(f)** the 250th charge. The scale bars represent 200 nm.

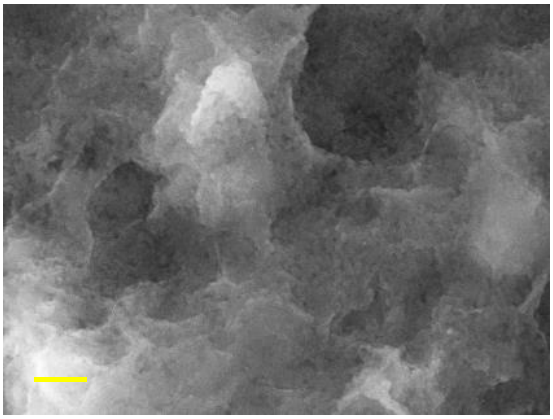

Figure 20. SEM image of the cathode after 700th discharge (the scale bar: 200 nm).

4.3.2.2. Anode Surface

The SEM images for the anode surface were performed by an acceleration voltage (EHT) of 10 kV in lens magnification of 15 kX and 25 kX. The prepared protected Li anode was first sealed in the Argon filled vial and then transferred to SEM chamber in Ar environment. Figure 21 shows the SEM images of the protected anode.

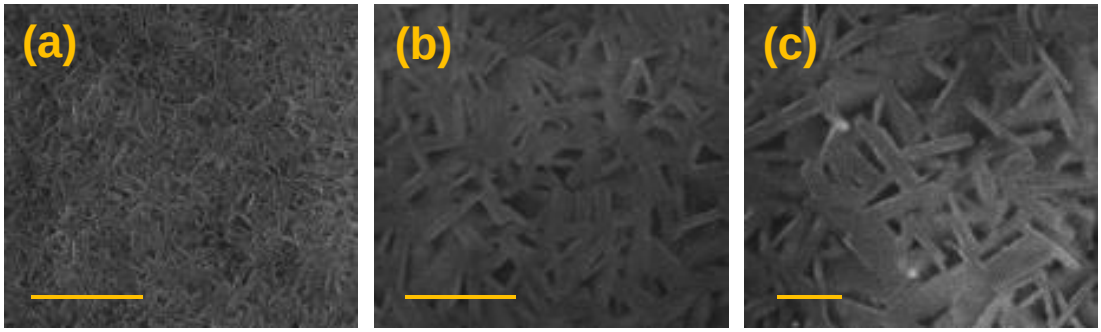

Figure 21. SEM images of the protected anode. The scale bars are **(a)** 1 µm. **(b)** 500 nm and **(c)** 200 nm.

4.3.3. Raman Spectroscopy

Raman spectroscopy experiments were performed using a HORIBA LabRAM HR Evolution confocal Raman microscope. The samples were sealed between two transparent glasses in the Argon filled glove box. The instrument was configured with a 785 nm laser source, 1200 g/mm grating, a Horiba Andor detector, and a LCD objective with a modifiable optical ring which allows aberration correction according to glass thickness.

4.3.3.1. Cathode Surface

To avoid any oxidation or unwanted species on the cathode surfaces, samples were carefully sealed between two transparent glasses in an argon filled glove box for Raman characterizations. The data were obtained with a HORIBA LabRAM HR Evolution confocal Raman microscope. The instrument was configured with a 785 nm laser source, 1200 g/mm grating, a Horiba Andor detector, and a LCD objective with a modifiable optical ring which allows aberration correction according to glass thickness. Laser powers at the sample were between 1-15 mW. Acquisition time, averaging parameters, and ND filters were optimized for the best signal to noise ratio (S/N). The intensity of the peaks

obtained in Raman spectroscopy experiments were normalized with C peak at 450 cm^{-1}. Figure 22 shows the results from different samples after discharge and charge processes in different cycles.

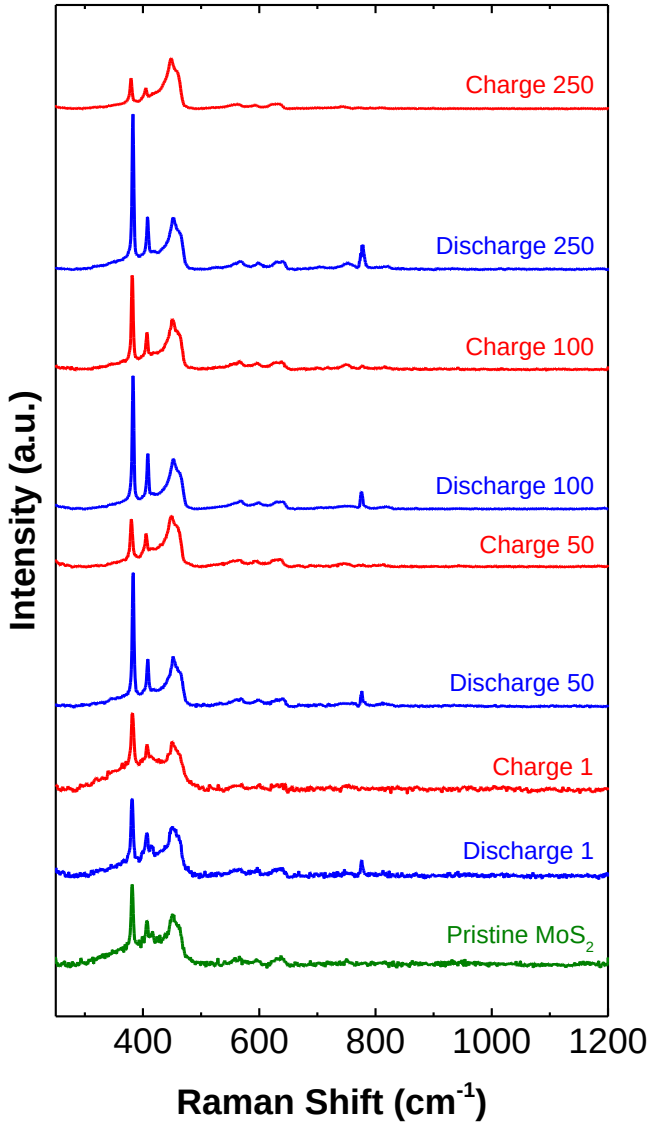

Figure 22. Raman shift of Li-Air battery cathode samples.

4.3.3.2. Anode Surface

The Raman spectroscopy experiments were performed to identify the protected coating of the anode surface. To avoid any oxidation or unwanted species on the anode surfaces, samples were carefully sealed between two transparent glasses in the Argon filled glove box.

Laser powers at the sample were between 1-15 mW. Acquisition time, averaging parameters and ND filters were optimized for the best signal to noise ratio.

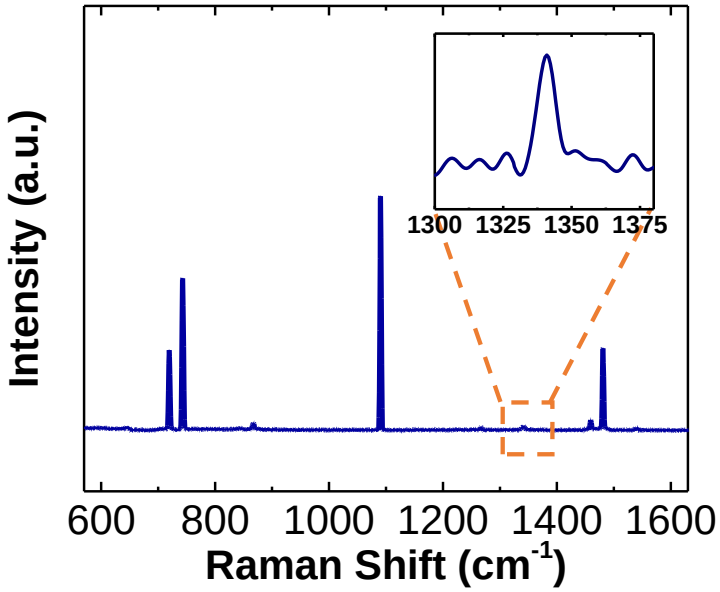

Figure 23. Raman spectra of protected anode surface.

Figure 23 represents the Raman spectra of protected anode surface. The inset shows the presence of C peak in the spectrum due to the presence of carbon in the coating in addition to Li_2CO_3.

4.3.4. X-ray Photoelectron Spectroscopy (XPS)

X-ray Photoelectron Spectroscopy (XPS) experiments were carried out using Thermo Scientific ESCALAB 250Xi instrument. The instrument was equipped with an electron flood and scanning ion gun. To prevent the samples from oxidation and any contamination, a mobile glove box filled with Ar was used for transfering the samples into the loading chamber of instrument.

4.3.4.1. Cathode Surface

The XPS experiments on the cathode were similar to the anode. The discharged cathodes after 1 and 100 cycles were dried with Argon flow before charactrizations. Figure 24 shows the XPS spectra of the discharged cathodes for the 1st and 100th cycles.

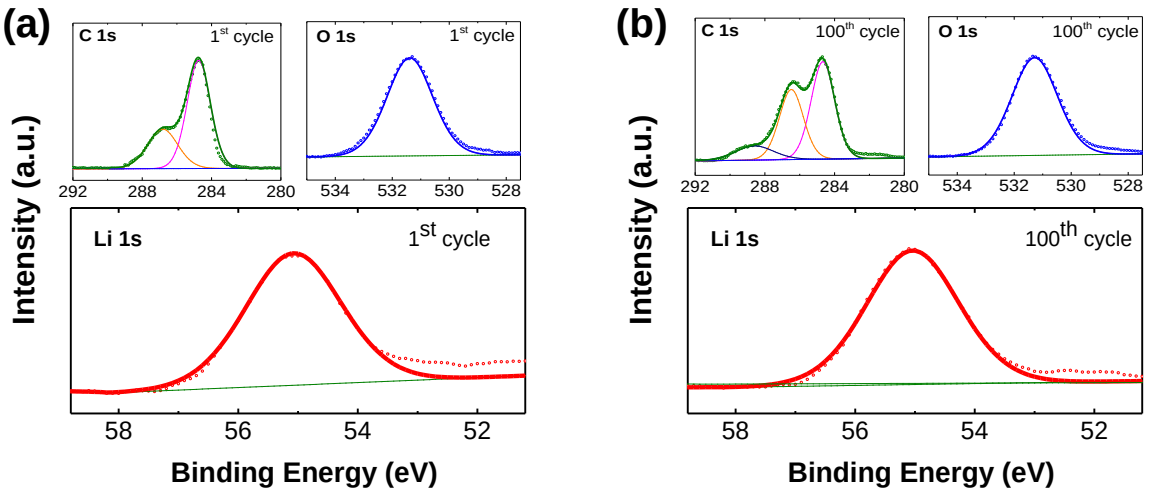

Figure 24. XPS results of the discharged cathode after 1 and 100 cycles.

4.3.4.2. Anode Surface

All spectra were calibrated to the C 1s binding energy at 284.8 eV. To quantify the atomic concenteration of each element, all data have been processed by Thermo Avantage software based on scofield sensitivity factors. Background singnal has also been removed by shierly method.

The XPS results of protected anode surface are shown in Figure 25. The corresponding peaks of the Li 1s, C 1s, and O 1s at 55.15, 289.5, and 531.5eV, respectively, confirm the existence of the Li_2CO_3 as a protected layer. The peak recorded at 284.8 eV for C 1s corresponds to the identical C-C bound used as a standard peak to calibrate the XPS spectra.

There is no evidence for other products such as Li_2O, Li_2O_2, and LiOH. The obtained spectra clearly illustrate that the binding energies are in good accordance with standard binding energies of Li_2CO_3.

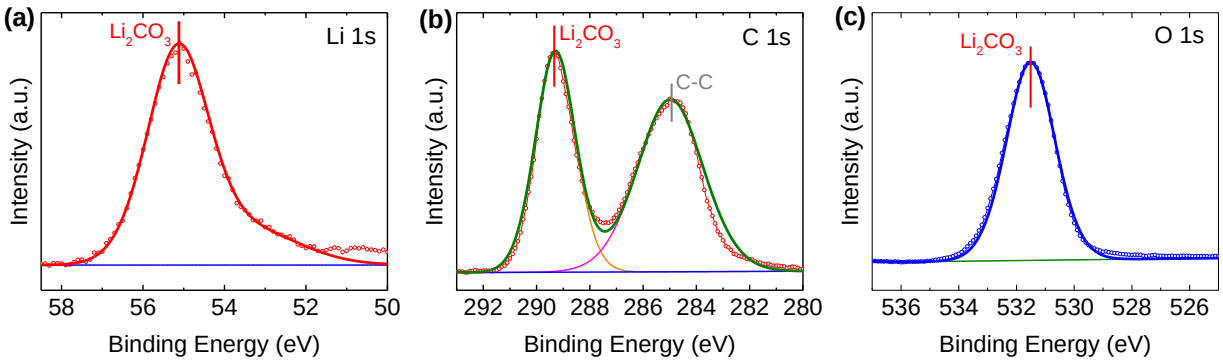

Figure 25. XPS spectra of the anode surface in **(a)** Li 1s, **(b)** C 1s, and **(c)** O 1s regions.

4.3.5. X-ray Powder Diffraction (XRD)

To determine the crystalline structure of Li_2O_2 on the cathode surface, the X-Ray Diffraction (XRD) method was utilized using a Rigaku ATX-G thin-film diffraction workstation. The discharged cathode after 550 cycles was dried in vacuum oven for 12 hrs at 85℃. Before scanning the sample, the calibration and sample alignment scans were carefully performed to maximize the signal to noise ratio. The 2-Theta scan was applied between 30 to 60 degree using a 0.005 width and 6 degree/min scan rate.

As shown in Figure 26, the peaks for Li_2O_2 were detected at 32° and 34° which correspond to the (100) and (101) crystal facets of Li_2O_2, respectively [137], [157]. The two peaks at 38° and 44° were from the substrate (GDL) and the catalyst (MoS_2) [158].

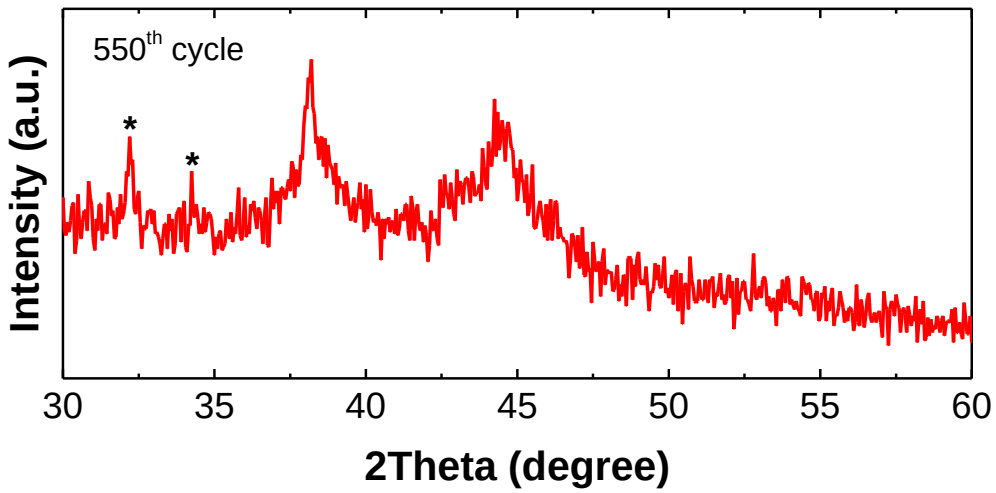

Figure 26. XRD spectra of discharged cathode after 550 cycles.

4.3.6. Differential Electrochemical Mass Spectrometry (DEMS)

The differential electrochemical mass spectrometry (DEMS) experiment was carried out in a custom-made Swagelok battery set-up. Experimental setup was consisted of a potentiostat and a mass spectrometer working under ultra-high vacuum pressure. The DEMS was calibrated by injecting standard samples of pure O_2 (99.99%) in research grade Argon (99.99%) with known concentrations to the mass spectrometer and measuring corresponding partial pressures of O_2.

The DEMS experiment was carried out in a custom-made Swagelok battery set-up. The cell consists of a gas diffusion layer coated with MoS_2 NFs as the cathode, 0.5 mm stainless steel spacer, 0.25 mm thick lithium chip, a 0.26 mm thick glassy fiber separator, and 0.1 M LiTFSI in $EMIMBF_4$-DMSO mixture electrolyte. This configuration creates a 1 mm thick headspace inside the Swagelok cell with the volume of ~0.11 mL. The current density of 500 mA/g was applied to the cell for 1 hr to achieve the 500 mAh/g capacity. The calibration curve is presented in Figure 27. The head space volume measurement and calibration procedure were similar to stablished DEMS calibration procedure by our group [137]. In particular the assembled cell without electrolyte was calibrated with standard volume loops (e.g. 100, 250, 500 μL) filled with ultra-high purity (UHP) Argon (99.99%) at known pressure [156].

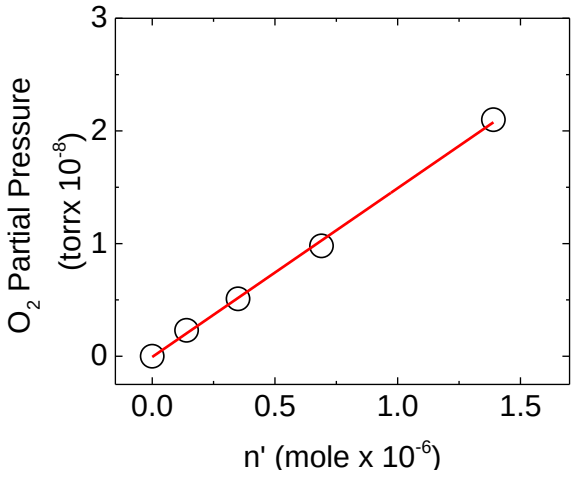

Figure 27. DEMS calibration points and corresponding fitted line based on different O_2 concentrations.

4.3.6.1. During Discharging Process

For discharge reaction, the cell and DEMS capillary were first purged with Argon to remove any impurities. The cell was then purged with pure O_2 (99.99%, research grade) for 15 minutes to saturate the electrolyte with O_2. The head space of the cell was then filled with 1.5 bar pure oxygen (99.99% research grade) and directly injected to the DEMS. The same experiment was performed after an hour discharge process. The calibration curve was then used to calculate the number of O_2 molefcules based on the variation of oxygen partial pressure before and after discharge process. To calculate the electron to O_2 ratio, Eq. 28 was used:

$$\frac{e^-}{O_2} = \frac{Mole\ of\ electrones}{Mole\ of\ consumed\ O_2} = \frac{\frac{0.05\times10^{-3}A\times60\text{min}\times60\text{sec/min}}{96485\ C/mol\ (faraday\ constant)}}{9.1\times10^{-7}\ \text{mole}} = 2.04 \quad \text{(Eq. 28)}$$

Table 3. Mole quantities of the consumed O_2 before and after discharge experiment.

Mole of O_2 before discharge	Mole of O_2 after discharge	Consumed moles of O_2	e^-/O_2 ratio
1.47×10^{-6}	0.56×10^{-6}	9.1×10^{-7}	2.04

4.3.6.2. During Charging Process

The charge reaction was also studied by in-situ monitoring of evolved gasses during the first cycle using DEMS. At first, the Swaglock cell was purged with pure Argon for 15 minutes, the cell was then connected to DEMS until the O_2 partial pressure signal was reached the steady state condition. The experiment was performed with the current density of 2,500 mA/gr for more accurate measurements of evolved gasses. In-situ measurements of O_2, CO_2, and H_2O signal were performed by Secondary Electron Multiplier (SEM) mode during the term of charging reaction. The results indicate an average O_2 evolution rate of 1.24×10^{-9} mol/s which results in 2.07 e^-/O_2 ratio during charging reaction.

The DEMS results for both discharging and charging processes will be discussed in results and discussion (section 5).

4.3.7. Nuclear Magnetic Resonance (NMR)

Nuclear Magnetic Resonance (NMR) spectra were collected on a 400 MHz Agilent MR-400 DD2 system equipped with autoX probe. The samples were prepared from the fresh and used electrolytes in deuterated tetrahydrofuran (THF-d8). The fresh electrolyte was consisted of 25% EMIM-BF_4 and 75% DMSO with 0.1M LiTFSI as the Li salt and the used electrolyte was obtained from the fiber after continuous running for 550 cycles. The samples were prepared and sealed in NMR tubes in Ar-filled glove box with less than 1 ppm oxygen and moisture. The ^{1}H-NMR spectra were tested for 128 scans in the whole region of ^{1}H, 14 to -2 ppm. And the ^{13}C-NMR spectra were tested for 256 scans in the whole region of ^{13}C, 234 to -14 ppm.

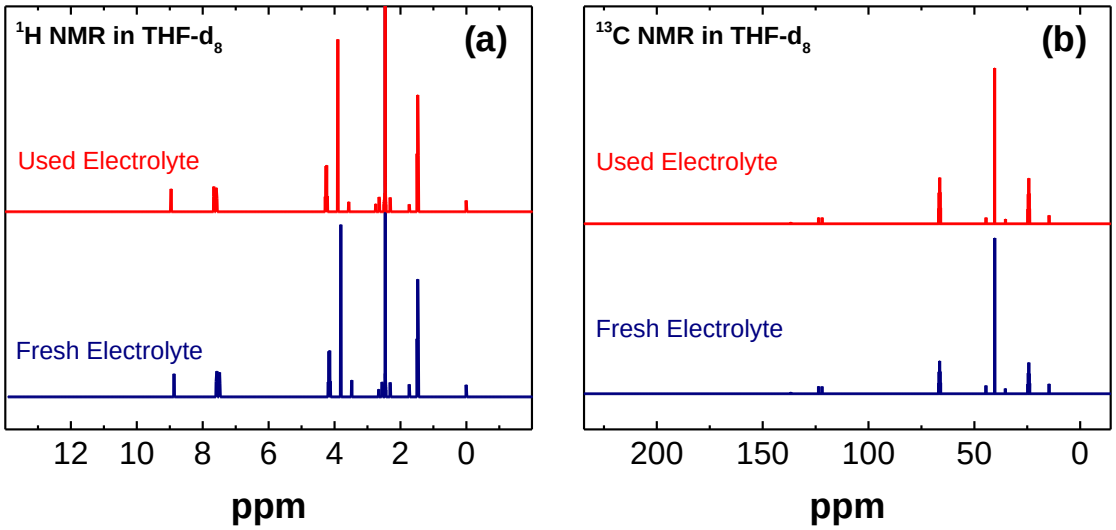

Figure 28. Nuclear Magnetic Resonance (NMR) results of fresh and used electrolytes at **(a)** ^{1}H NMR and **(b)** ^{13}C NMR in THF-d_8.

4.3.8. Transition Electron Microscopy (TEM)

In collaboration with Dr. klie's group at Physics department, UIC, scanning transmission electron microscope (STEM), electron energy loss spectroscopy (EELS), energy dispersive spectroscopy (EDS), and diffraction paterns were studied on cathode and anode samples. They results which are presented as follow are in a good accordance to other characterization methods performed previously.

STEM measurements were carried out on an aberration-corrected JOEL JEM-ARM200CF equipped with a cold field emission electron source and a post-column Gatan Enfina EELS spectrometer. An acceleration voltage of 80 kV was used for both imaging and EELS to reduce beam induced damage and contamination.

EELS signals were collected from particles suspended over vacuum to exclude any signals from the support films. EELS results for the anode, including accompanying standard data, are shown in Figure 29. Lithium, carbon, and oxygen *K*-edges were all collected from the same area, confirming the presence of lithium carbonate in the anode. In particular, the strong splitting of the carbon peak, panel (b) labeled (ii) and (iii), and the strong oxygen pre-edge, panel (c) labeled (i), is indicative of the double bonds in the carbonate ion.

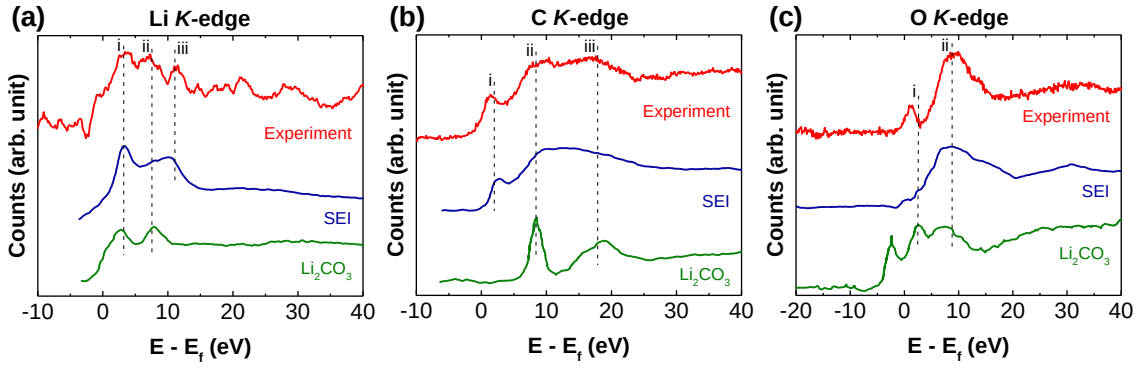

Figure 29. Electron energy loss spectroscopy (EELS) for **(a)** Lithium, **(b)** Carbon, and **(c)** Oxygen *K*-edges from the anode surface.

EELS measurements of the discharged cathode material were carried out on the same aberration-corrected JOEL JEM-ARM200CF. Similarly, an acceleration voltage of 80 kV was used for both imaging and EELS to reduce beam induced damage and contamination. Figure 30 shows a Li *K*-edge from the cathode, indicating the presence of lithium after discharge.

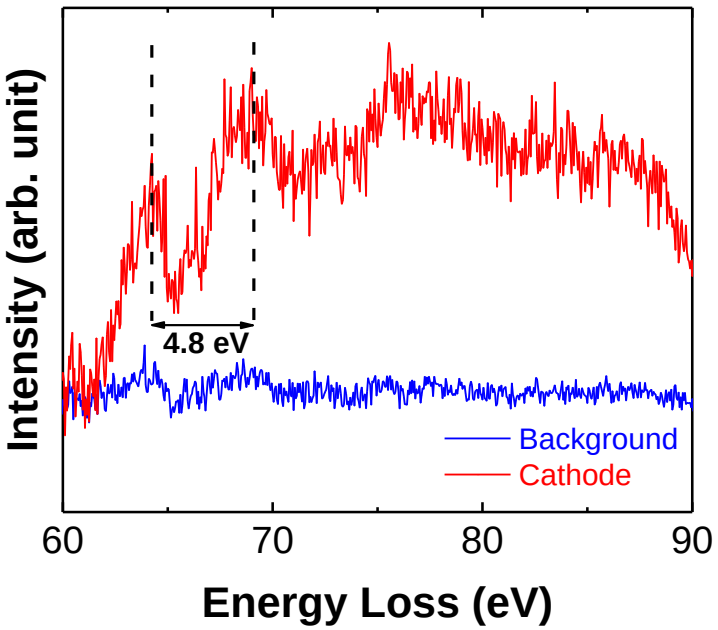

Figure 30. Electron energy loss spectroscopy (EELS) for Lithium *K*-edge from the discharged cathode.

5. RESULTS AND DISCUSSION

Thus far, the research on the Li-air battery has been mainly limited to pure oxygen environment (Li-O_2 batteries) [116], [137], [157], [159] suffering from short cycle life. The major issues with the existing Li-O_2 systems are degradation of the anode electrode, poisoning of the cathode active sites, clogging of the cathode, side reactions involving undesirable products, and electrolyte instability [15], [16], [98], [137], [160]–[162].

Another problem with Li-O_2 systems is that volumetric energy density, due to the necessity of the storing of oxygen, may be too small for practical transportation applications [163]. In the presence of actual components of air such as nitrogen, carbon dioxide, and moisture, these issues become even more complex since a small concentration of such reagents can lead to additional side reactions resulting in undesirable products (i.e., LiOH and Li_2CO_3) at the cathode [16], [19]. LiOH and Li_2CO_3 require higher overpotentials for decomposition [15], [20], [139], [140] compared to pure Li_2O_2, which will adversely affect the cyclability and energy efficiency of Li-air batteries. The issue with the anode is also challenging due to the high reactivity of the lithium anode with the actual air components e.g., N_2, CO_2 and H_2O, which can result in corrosion of the anode and failure of the cell.

There have been attempts to use ambient air conditions or a realistic concentration of H_2O or CO_2 in Li-air batteries [15], [164]–[167]. Most of these studies have used some type of lithium anode protection membrane or solid state electrolyte [168]–[170]; however, these systems still have problems with limited cycle life, side reactions with CO_2 and H_2O, or are unpractical due to the weight of the membrane. A recent paper was able to get longer cycle life with humidity added to the O_2 using an ionic liquid for the electrolyte, although the product included LiOH [171]. In this thesis, two strategies have employed to limit side reactions and achieve long cycle life for the first time in a Li-air battery: (i) on the anode side, a Li_2CO_3 coating was developed that allows only the Li cation to pass through to the lithium anode to protect it from components in the ambient air system [172], [173]. Li_2CO_3 is an insoluble compound in water with high anhydrous properties. Moreover, in presence of CO_2, the reaction with water to produce bicarbonate is not thermodynamically favorable in the ambient conditions (Section 4.1.1.3). (ii) on the cathode side, a new chemistry based

on molybdenum MoS_2 NFs and a mixture of ionic liquid EMIM-BF_4 and DMSO electrolyte was discovered that work together to prevent the formation of undesirable products from the presence of CO_2 and H_2O.

The Li_2CO_3 as the anode protection layer was synthesized in a custom-made electrochemical cell encapsulated with pure CO_2 and run in a constant current density of 500 mA/g for 10 continuous discharge and charge cycles in a one-hour time-lapse. The scanning electron microscopy (SEM) image of the anode surface (Figure 31a) reveals a dense network of rod-shape structures on the anode surface. Raman spectroscopy shows distinct peaks at 717, 743, 1088, and 1456 cm^{-1} for this coating (Figure 31b), which are characteristic peaks of Li_2CO_3[169]. Moreover, the X-ray Photoelectron Spectroscopy (XPS) results shown in Figure 31c-d Li 1s, C 1s, and O 1s show peaks at 55.2, 289.3, and 531.5 eV, respectively, further confirming the presence of Li_2CO_3[174]. These peaks are consistent with previously reported bulk Li_2CO_3 XPS results[174]. In addition, a peak at 284.8 eV corresponds to C-C bonds due to the presence of adventitious carbon bonds and also C(s) products from Li and CO_2 reaction. In collaboration with Dr. Klie's group at Physics department, UIC, the composition of the synthesized Li_2CO_3 layer was further characterized by electron energy loss spectroscopy (EELS). Li *K*-, O *K*- and C *K*-edges obtained from EELS of platelet-like particles extracted from the anode are presented in Figures 31e. For the C *K*-edge the EELS analysis was performed on the portion of the coating lying within a hole (vacuum) of the holey carbon grid to minimize any contribution from the background C film.

The presence of sharp Li *K*-, O *K*- and C *K*-edge peaks in the spectra implies Li, C, and O bonding similar to that of lithium carbonate, previously reported in the literature [175], thus verifying the presence of Li_2CO_3 as a protective layer on the anode surface. It should be mentioned that it has been found previously that the addition of CO_2 to the propylene carbonate electrolyte of a Li-ion cell with a Li anode helps to prevent dendrite formation with Li_2CO_3 as a protective component on the Li anode surface [176].

To study the lithium retention of the protected Li anode, the cell was run in the air environment for 51 cycles with a protected anode similar to the procedure explained in Section 4.2.3. On the cycled anode, an exhaustive stripping test was done using a current rate of 0.5 mA/cm^2 (Figure 31f). The calculations indicate that the protected anode has an

average of 99.97% lithium retention per cycle. Moreover, the Electrochemical Impedance Spectroscopy (EIS) technique was used to study the charge transfer resistance (R_{ct}) of the protective layer (Section 4.2.2). Results shown in Figure 31g indicate that R_{ct} of the protected anode with 10 cycles is ~550 kohms, which is about 20 times more than unprotected anode (30 kohms) confirming the existence of the electrically insulating protection coating on the anode surface.

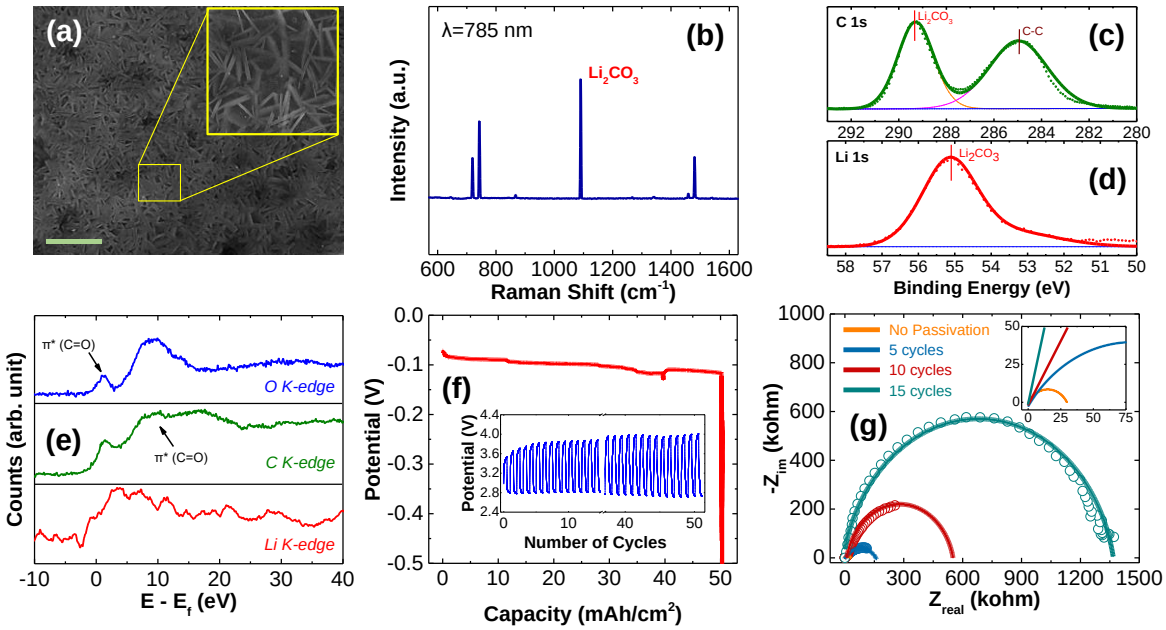

Figure 31. Protected anode. **(a)** Scanning Electron Microscope (SEM) image of the surface of the protected anode (scale bars: 1 µm). **(b)** Raman spectra of the protected anode surface, excited by a 785 nm laser. **(c)** X-ray photoelectron spectroscopy (XPS) spectra of the protected anode surface in Li 1s and **(d)** C 1s regions. **(e)** EELS spectra for Li *K*-, C *K*-, and O *K*-edges of the anode SEI layer consistent with the compound lithium carbonate. The oxygen pre-peak and splitting of the carbon peak are indicative of the double bonds in the CO_3^{-2} ion. **(f)** Exhaustive stripping of protected lithium using current density of 0.5 mA/cm^2. Inset figure shows the cycling test of the protected anode in the air environment under the current rate of 500 mA/g. (**g)** Electrochemical Impedance Spectroscopy (EIS) of passivated anode after 5, 10, and 15 cycles of exposing to pure CO_2 environment compared to the anode without passivation.

Next, a custom-made Swagelok type Li-air battery cell was assembled in an Argon filled glove-box using the MoS_2 NFs cathode, a lithium anode with the protective coating, and ~35 µL of 25% of EMIM-BF_4 and 75% of DMSO electrolyte. This composition of electrolyte provides the maximum oxygen reduction and evolution reactions studied in a three-electrode electrochemical cell. A custom-made air stream consisting of ~79% N_2, ~21% O_2, 500 ppm CO_2, and relative humidity of 45% at 25℃ was used for the battery experiments. Figure 32a shows the long term discharging and charging profiles up to the capacity of 500 mAh/g by applying a constant current density of 500 mA/g. The charge at the first cycle was started at 2.92V, which is very close to the reversible thermodynamic potential of Li_2O_2 formation (2.96V vs Li/Li^+)[4] and reaches the potential of 3.75V at the capacity of 500 mAh/g. The potential gap for the first cycle of the Li-air system is 0.88V, which increases to 1.3V after 50 cycles followed by a gradual increase to 1.62V after 550 cycles. The increase in the potential gap during cycling may be due to slow degradation of the anode protection coating and/or the MoS_2 cathode. No failure of the battery was observed tested up to 700 cycles (Section 4.1.4). Figure 32b demonstrates the dependence of the number of Li-air cycles on the number of cycles used to make the protective coating for the anode. The results indicate a dramatic increase in the number of Li-air cycles when the coating is included compared to when no coating is used. With no coating, the Li-air cell fails after 11 cycles. With the addition of the protective coating (10 deposition cycles) the Li-air cell can cycle up to 700 cycles. This is attributed to a good trade-off between electronic and ionic conductivities of the protection layer at 10 cycles of deposition.

Raman spectroscopy and XPS were performed on the cathode surface to study the discharge products and cell chemistry from different cycles. The Raman results (Figure 32c) show the presence of only a Li_2O_2 peak at 788 cm^{-1}. No peaks were detected related to LiOH (485 cm^{-1}), Li_2CO_3 (1088 cm^{-1}), or LiO_2 (1125 cm^{-1}) in the Raman spectra suggesting that Li_2O_2 is the only product during the discharging process [137], [177]–[179]. On the other hand, the Li_2O_2 peaks disappeared in the charged samples meaning that the majority of accumulated products on the cathode surface were decomposed during the charging processes. To study the possibility of any chemical reactions of the electrolyte with Li_2O_2, a 50-cycle discharged cathode sample was aged in the electrolyte for 200 hours. Raman spectroscopy results after 200 hrs of ageing did not show any evidence of other side

products due to chemical reactions. To further confirm the presence of Li_2O_2 as the product of discharge reaction, XPS analysis were performed on the cathode surface after 1, 100, and 250 cycles (Section 4.3.4.1). Figure 32d-f show the results for the Li 1s, C 1s, and O 1s spectra of the discharged cathode after 250 cycles. The Li 1s and O 1s peaks of Li_2O_2 at 55.07 and 531.12 eV, respectively, are in agreement with previously reported in-situ ambient pressure XPS studies on Li_2O_2 formed in a Li-O_2 cell [180], [181]. The C 1s spectra shows the reference C-C bond of carbon at 284.8 eV and some other carbon peaks at 286.6 and 288.5 eV, which are likely due to the gas diffusion layer. Figure 32d-f further confirm the absence of Li_2CO_3 and LiOH products during discharge process, because of the lack of peaks from them in the XPS spectra.

The charge reaction was further studied by in-situ monitoring of evolved gasses during the first cycle using differential electrochemical mass spectrometry (DEMS) [116], [137], [156]. The charge experiment was performed up to the capacity of 500 mAh/g using a current density of 2500 mA/g for accurate measurements of evolved gasses (Figure 32g). The DEMS results indicate an average of 1.24×10^{-9} mol/s O_2 evolution rate resulting in an e^-/O_2 ratio of 2.07 during the charge reaction. There is no evidence of evolved CO_2 and H_2O during the charge reaction indicating the absence of side products such as Li_2CO_3 and LiOH. Moreover, DEMS analysis was performed before and after the discharge reaction using the current density of 500 mA/g to quantify the molar amounts of consumed gasses. Our results show the consumption of 9.15×10^{-7} moles of O_2 during discharge process up to 500 mAh/g capacity, which is corresponds to a 2.04 e^-/O_2 ratio. These results provide strong evidence for the reversible formation and decomposition of Li_2O_2 as the main product through a $2e^-$ transfer process without any side products.

The ex-situ and in-situ characterizations indicating that CO_2 and H_2O do not cause any detrimental reactions, are further confirmed with Swagelok experiments. For this purpose, the discharging-charging experiment in pure oxygen environment was carried out and its potential gap was compared with that of the Li-air battery (Section 4.1.4). The results shown in Figure 32h clearly demonstrate similar results for both systems, suggesting that the discharge and charge chemistries of our Li-air battery are the same as that of the Li-O_2 system.

To examine the stability of the EMIM-BF_4/DMSO electrolyte in the air system, ^{1}H and ^{13}C nuclear magnetic resonance (NMR) spectroscopy were performed for the fresh and used electrolytes after 550 cycles of cell operation [116]. These results shown in Section 4.3.7 present similar peaks in both electrolytes verifying the stability of the electrolyte during the cell operation tested up to 550 cycles.

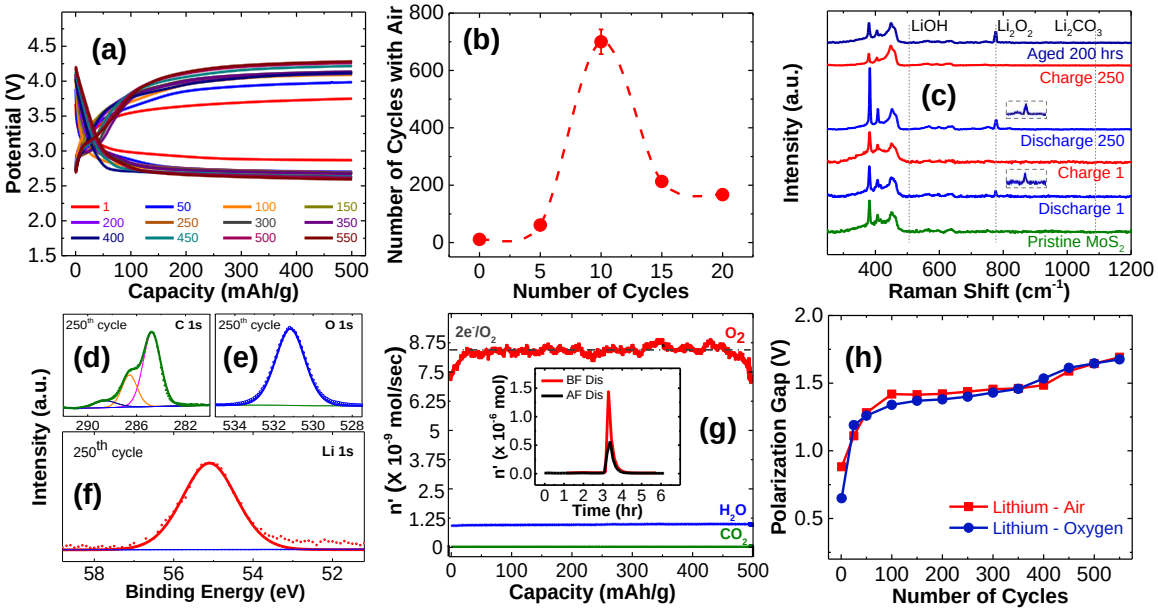

Figure 32. Performance of the Cathode in Lithium-air Battery system (~21% O_2, ~79% N_2, ~500ppm CO_2, 45% RH) using carbon free MoS_2 NFs and mixture electrolyte (IL/DMSO) saturated with 0.1M LiTFSI as the Li salt with protected lithium anode. **(a)** Discharging and charging voltage profile of the Li-air battery after 550 cycles. **(b)** The effect of the anode protection cycling length on the life cycle of the Lithium-air battery. **(c)** Raman spectra of the cathode surface after discharge and charge of the 1st and 250th cycles compared to pristine MoS_2 and the aged sample. **(d)** X-ray photoelectron spectroscopy (XPS) spectra of the cathode surface in C 1s region, **(e)** O 1s, and **(f)** Li 1s after discharge of the 250th cycle. **(g)** Differential Electrochemical Mass Spectrometry (DEMS) profiles of the cell during the 1st charging process after the cell was discharged up to 500 mAh/g. The DEMS experiment shows a 2 e^-/O_2 ratio in the system. (inset: O_2 number of moles detected by DEMS before and after of discharge experiment in 1st cycle.) **(h)** Polarization gap (V) of the Li-air battery compared to Li-O_2 battery with the same operating condition as a function of the number of cycles.

Finally, the morphology of the discharge product was studied by several techniques. First, SEM images of the cathodes after the 1st and 250th cycles shown in Figure 33a-d indicate a film-like morphology of the discharge products on the cathode surface that largely disappears after charging. A similar trend was also observed for samples after 100th cycles. These results confirm the reversibility of product formation on the cathode surface, which is attributed to formation of Li_2O_2 as the main discharge product. Moreover, X-ray diffraction (XRD) experiment performed on the discharge products after 550 cycles reveals the presence of crystalline (100) and (101) facets of Li_2O_2 due to distinct peaks at 32° and 34° (Section 4.3.5) [137], [157]. Also, in collaboration with Dr. Klie's group at Physics department, UIC, TEM images and diffraction patterns captured from the cathode (Figure 33e-f) show the discharge product to be highly crystalline, with the diffraction pattern corresponding to Li_2O_2 viewed alone a c-axis direction. EELS spectra of discharge cathode sample also show a Li *K*-edge fine-structure as evidence of Li_2O_2 formation (Section 4.3.8).

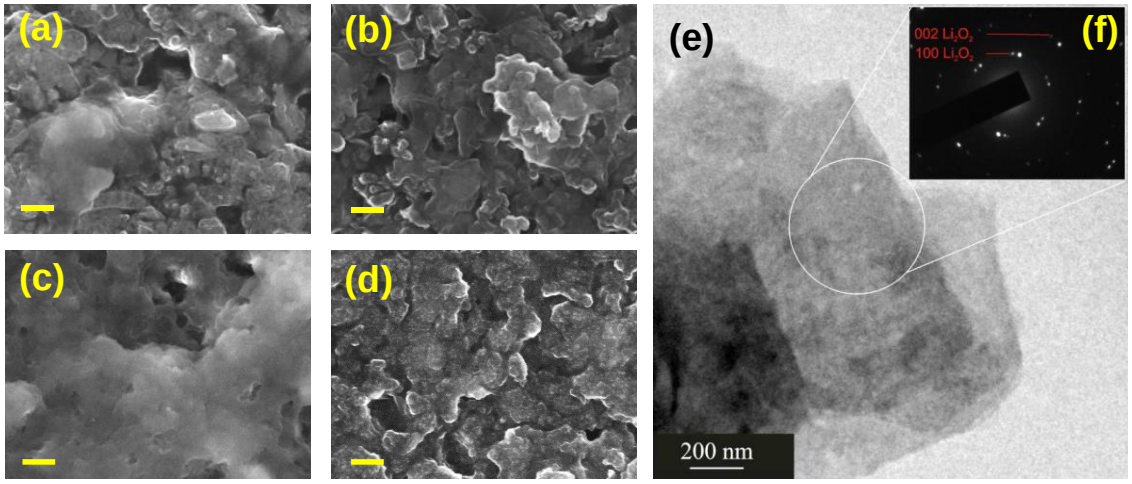

Figure 33. Scanning Electron Microscope (SEM) and Transmission Electron Microscopy (TEM) results of the cathode surface. The SEM images of Li-air battery cathodes are shown after **(a)** The 1st discharge. **(b)** The 1st charge. **(c)** The 250th discharge. **(d)** The 250th charge. (Scale bars: 200 nm.) **(e)** TEM image of a discharge cathode sample. **(f)** Diffraction pattern showing the crystallinity of the particles corresponding to monoclinic lithium peroxide (Li_2O_2).

In collaboration with Dr. Curtiss at Argonne National Laboratory, Density Functional Theory (DFT) calculations were carried out to: (i) provide insight into how the Li_2CO_3 coating delivers protection against degradation of the lithium anode from side reactions and (ii) provide an understanding of why the Li-air cell prevents detrimental cathode reactions involving the N_2, CO_2, and H_2O components existing in the air. First, to explain the protected anode role in the Li-air system, the Li_2CO_3/Li interface was constructed from a (100) surface of Li and three terminations (carbon, oxygen, and lithium) of a (001) Li_2CO_3 surface. The lattice matches of these interfaces was found to be very and upon relaxation the most stable interface was the one with the carbon termination and, therefore, is carbon rich at the interface. The relaxed Li_2CO_3/Li interface with carbon termination is shown in Figure 34a. While thermodynamically Li and Li_2CO_3 are unstable with respect to Li_2O and C[182], the interface appears to be kinetically stable based on investigation of the barrier for O migration from a C-O bond to Li. As shown in Figure 34b a barrier of 1.1 eV is found for this reaction pathway. The stability of the interface is consistent with the long cycle life afforded by the Li_2CO_3 coating in the Li-air cell testing reported here. In addition, it was investigated whether N_2 and O_2 were likely to migrate through the Li_2CO_3 coating by placing the two molecules in the (010) channel of Li_2CO_3 as shown in Figure 34c for O_2 and calculating the energy for the relaxed structure relative to the Li_2CO_3 and the free molecules. The energies were found to be much higher (1.2-3.2 eV) indicating that Li_2CO_3 should provide a good barrier for preventing N_2 and O_2 from reaching the Li anode, assuming no cracks. Since the H_2O and CO_2 molecules are larger than N_2 and O_2, their energies should also be endothermic. Based on previously reported DFT calculations for Li ion batteries [173], [183] it has been shown that Li diffusion through Li_2CO_3 should be quite facile, unlike the results for N_2 and O_2. These results are consistent with the dramatic increase from 11 discharge/charge cycles for the Li-air cell, with no coating, to up to about 700 cycles with a protective coating as shown in Figure 32b.

DFT calculations were also carried out to provide an understanding of why our Li-air cell does not show evidence of any detrimental reactions involving the N_2, CO_2, and H_2O components found in air. Since the main reaction of N_2 will be with the Li anode [161], the discussion of the Li_2CO_3 coating given above provides an explanation for why N_2 is not an apparent problem in the Li-air cell, i.e., the coating prevents the N_2 from reaching the Li

anode. Likewise, the Li_2CO_3 coating on the Li anode prevents any O_2 crossover effect, which causes well-known oxidation of the lithium anode and limits cycle life[161]. The most likely reactions involving CO_2 and H_2O that could limit the cycle life involve reactions with the Li_2O_2 discharge product, the latter being shown to be present from Raman, XPS, and XRD studies. In addition, SEM and TEM indicate that the Li_2O_2 is likely to have a film-like morphology. Thus, calculations of H_2O and CO_2 adsorbed on various relaxed Li_2O_2 surfaces were carried out[184]. The most stable adsorption structures are shown in Figure 34d-e. The strongest adsorption energies for CO_2 and H_2O on the Li_2O_2 surfaces are 0.27 and 0.77 eV, respectively. Neither H_2O nor CO_2 decompose when adsorbed on the Li_2O_2 surfaces. However, based our calculations they could decompose on some defect sites on Li_2O_2 surfaces, if they were present.

In addition, DFT calculations were carried out on the solvation energies of H_2O and CO_2 in the IL/DMSO electrolyte to see how they compare to the adsorption energies on a Li_2O_2 surface. Cluster calculations involving these species with the IL and DMSO indicate that there is quite strong binding (~0.8 eV for both H_2O and CO_2) in the IL. Thus, the solvation energies in solution are at least as strong or stronger than those on the Li_2O_2 surface. *Ab-initio* molecular dynamics calculations were also carried out including both the electrolyte and the Li_2O_2 surface. These simulations with the electrolyte/Li_2O_2 interface did not show any specific preference for the CO_2 or H_2O to adsorb on the surface or stay in the electrolyte; furthermore, the adsorbed species at the interface do not react with the Li_2O_2 surface. Before formation of the Li_2O_2 film on the MoS_2 surface after charging, the H_2O and CO_2 could react either chemically or electrochemically with MoS_2. However, this is not likely to affect the Li_2O_2 film growth significantly due to their low concentrations compared to O_2 and their interactions should not be stronger than that of H_2O. These results are consistent with the lack of evidence for decomposition products such as Li_2CO_3 or LiOH in any of the characterization studies.

Moreover, the classical molecular dynamics simulations with a much larger number of solvent molecules (~32,000) also shows an interaction of CO_2 and H_2O molecules with the IL/DMSO liquid, consistent with the other simulations. The diffusion rates of CO_2 and H_2O in IL/DMSO mixtures at realistic concentrations are approximately one order of magnitude lower than their free or self-diffusion rates [185]–[188]. The peaks in the radial distribution

function (RDF) shown in Figure 34f of solvent around water molecules show interaction of water with BF_4 and DMSO. Further analysis of hydrogen bonds between these species show that approximately 72% of the water molecules participate in small clusters of BF_4, DMSO and H_2O all connected through hydrogen bonds. A representative of such clusters is shown in inset of Figure 34f. The reactions of solvated H_2O molecules in the IL/DMSO electrolyte with either LiO_2 or Li_2O_2 species in the electrolyte are unlikely due to unfavorable thermodynamics and low concentration of H_2O clusters. The reactions of CO_2 with LiO_2 or Li_2O_2 species are unlikely due to the very low concentration of CO_2 clusters in the electrolyte required for the reactions.

As mentioned above, the morphology of the discharge product is film-like. This is important as it should not have as many defect sites as other morphologies such as nanoparticles or toroids, which could cause decomposition reactions involving CO_2 and H_2O. The film-like Li_2O_2 discharge product is consistent with the postulated formation mechanism in our previous paper on a MoS_2 cathode material for a Li-O_2 cell [137]. This was based on a through-solution nucleation and growth mechanism in which solvated LiO_2 forms in the electrolyte after O_2 reduction at the Mo edges of the MoS_2 nanoflakes. The LiO_2 then forms dimers or some other species in the electrolyte that disproportionate to Li_2O_2 and O_2. The Li_2O_2 is very insoluble and then will nucleate and grow on the MoS_2 surface. DFT calculations shown in Figure 34g indicate that the Li_2O_2 has significant interaction energies on the basal plane of a MoS_2 nanoflake that could provide numerous nucleation sites. The high dielectric of the IL/DMSO electrolyte provides enough LiO_2 solubility to be consistent with a solution growth mechanism[189]. Finally, the high charge rate used in the cell means that there will be high nucleation rates and film formation [190], [191] as opposed to toroid or nanoparticle formation for low charge rates. The film formation is consistent with the evidence from the characterization studies.

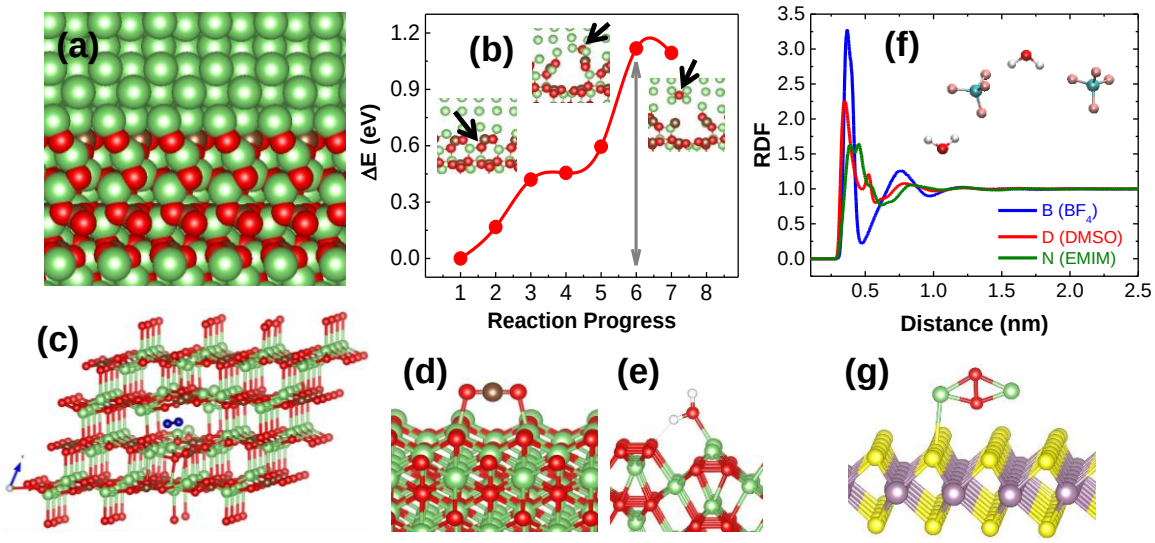

Figure 34. (a) DFT relaxed interface between (001) Li_2CO_3 and (100) Li with carbon termination of the Li_2CO_3 surfaces (results for other interfaces are given in SI file), **(b)** DFT reaction profile of breaking a C-O bond of Li_2CO_3 at the Li(001)/Li_2CO_3(001) interface and migration of O to Li bulk with a barrier of 1.1 eV (structure shown for initial, transition, and final states with black arrow indicating O^- positions) **(c)** DFT relaxed structure of O_2 in Li_2CO_3 channel, which is endothermic by 3.1 eV. **(d)** DFT relaxed structures of CO_2 on the (100) surface of Li_2O_2 with binding energy of 0.27 eV, and **(e)** DFT relaxed structure of H_2O on the (100) surface of Li_2O_2 with binding energies of 0.77 eV. **(f)** Radial distribution function with H_2O as the reference calculated from classical MD trajectory of 2 mol% system. **(g)** DFT relaxed structures of Li_2O_2 on a MoS_2 nanoflake basal plane with binding energy of 0.83 eV.

6. CONCLUSION AND FUTURE WORK

In conclusion in this thesis, an integrated Lithium-air battery system was developed consisting of a protected anode based on lithium carbonate, a bi-functional air cathode based on Molybdenum disulfide catalyst, and ionic liquid/dimethyl sulfoxide mixture electrolyte working in presence of the real air components (Nitrogen, Oxygen, Carbon dioxide, and moisture). This system shows a high cyclability up to 700 cycles with the capacity of 500 mAh/g and under the current density of 500 mA/g. The lithium retention after each cycle in this system is %99.97 which means %17 total lithium loss in the system after 700 cycles continuous operation in the air environment.

Different characterizations including differential electrochemical mass spectroscopy (DEMS), X-ray photoelectron spectroscopy (XPS), and Raman spectroscopy on the cathode reveal that the only discharge product in our system is lithium peroxide (Li_2O_2) without any evidence of side products e.g., lithium hydroxide (LiOH) and lithium carbonate (Li_2CO_3). Nuclear magnetic resonance (NMR) results also show the stability of the electrolyte after 550 cycles. DFT calculations show that there is no reaction involving other species such as CO_2 and H_2O due to the combination of MoS_2 cathode and mixture electrolyte which make the system kinetically favorable for Li_2O_2 formation.

The Lithium-air system studied here is a key step toward the development of next generation of lithium batteries with higher energy density.

For the future of this work, it is suggested to work more in three main components; cathode, electrolyte, and anode; to enhance the cyclability and stability of this system and decrease the overpotential and energy loss in the system. In cathode side, alloyed/dopped materials can be a promising alternative to develop a highly effective catalyst material in order to deliver a system with high power density without compromising the intrinsic energy density. In anode side, the protection layer can be optimized and be implemented in other metal-air and metal-ion systems. Moreover, on part of electrolyte, more investigation is needed to explore the large family of ionic liquids and other inorganic solvents coupled with salts as an alternative to this system to improve the stability of electrolyte while increase the oxygen diffusion and solubility in the system.

CITED LITERATURE

[1] F. Group, *Electrochemical Energy*. 2016.

[2] M. Balaish, A. Kraytsberg, and Y. Ein-Eli, "A critical review on lithium-air battery electrolytes," *Phys. Chem. Chem. Phys.*, vol. 16, no. 7, pp. 2801–2822, 2014.

[3] R. Sahoo, A. Pal, and T. Pal, "2D materials for renewable energy storage devices: Outlook and challenges," *Chem. Commun.*, vol. 52, no. 93, pp. 13528–13542, 2016.

[4] N. Imanishi, A. C. Luntz, and P. Bruce, *The lithium air battery: Fundamentals*. 2014.

[5] Y. Shao, S. Park, J. Xiao, J. Zhang, Y. Wang, and J. Liu, "Electrocatalysts for Nonaqueous Lithium − Air Batteries : Status , Challenges , and Perspective," no. 3, 2012.

[6] M. Zackrisson, L. Avellán, and J. Orlenius, "Life cycle assessment of lithium-ion batteries for plug-in hybrid electric vehicles – Critical issues," *J. Clean. Prod.*, vol. 18, no. 15, pp. 1519–1529, 2010.

[7] P. Nelson, K. Amine, A. Rousseau, and H. Yomoto, "Advanced Lithium-Ion Batteries for Plug-in Hybrid-Electric Vehicles," *Evs23*, 2007.

[8] L. Lu, X. Han, J. Li, J. Hua, and M. Ouyang, "A review on the key issues for lithium-ion battery management in electric vehicles," *Journal of Power Sources*, vol. 226. pp. 272–288, 2013.

[9] J. Lu and K. Amine, "Recent research progress on non-aqueous lithium-air batteries from Argonne National Laboratory," *Energies*, vol. 6, no. 11, pp. 6016–6044, 2013.

[10] H. Lim *et al.*, "Toward a lithium- ' air ' battery : The effect of CO2 on the chemistry of a lithium-oxygen cell Toward a lithium- ' air ' battery : The effect of CO 2 on the chem- istry of a lithium-oxygen cell," vol. 742, 2013.

[11] R. Mohtadi and F. Mizuno, "Magnesium batteries : Current state of the art , issues and future perspectives," pp. 1291–1311, 2014.

[12] J.-S. Lee *et al.*, "Metal-Air Batteries with High Energy Density: Li-Air versus Zn-

Air," *Adv. Energy Mater.*, vol. 1, no. 1, pp. 34–50, Jan. 2011.

[13] H. Yadegari, Q. Sun, and X. Sun, "Sodium-Oxygen Batteries: A Comparative Review from Chemical and Electrochemical Fundamentals to Future Perspective," *Adv. Mater.*, 2016.

[14] A. Eftekhari, Z. Jian, and X. Ji, "Potassium Secondary Batteries," *ACS Appl. Mater. Interfaces*, 2016.

[15] D. Geng *et al.*, "From Lithium-Oxygen to Lithium-Air Batteries: Challenges and Opportunities," *Adv. Energy Mater.*, vol. 201502164, pp. 1–14, 2016.

[16] G. Girishkumar, B. McCloskey, A. C. Luntz, S. Swanson, and W. Wilcke, "Lithium-air battery: Promise and challenges," *J. Phys. Chem. Lett.*, vol. 1, no. 14, pp. 2193–2203, 2010.

[17] K. M. Abraham, "A Polymer Electrolyte-Based Rechargeable Lithium/Oxygen Battery," *J. Electrochem. Soc.*, vol. 143, no. 1, p. 1, 1996.

[18] A. D?bart, A. Paterson, J. Bao, and P. Bruce, "?-MnO2 Nanowires: A Catalyst for the O2 Electrode in Rechargeable Lithium Batteries," *Angew. Chemie Int. Ed.*, vol. 47, no. 24, pp. 4521–4524, Jun. 2008.

[19] Y. Li, X. Wang, S. Dong, X. Chen, and G. Cui, "Recent Advances in Non-Aqueous Electrolyte for Rechargeable Li-O2 Batteries," *Adv. Energy Mater.*, no. 1, pp. 1–26, 2016.

[20] Y.-C. Lu *et al.*, "Lithium-oxygen batteries: bridging mechanistic understanding and battery performance," *Energy Environ. Sci.*, vol. 6, no. 3, pp. 750–768, 2013.

[21] T. Ogasawara, A. D?bart, M. Holzapfel, P. Nov?k, and P. G. Bruce, "Rechargeable Li 2 O 2 Electrode for Lithium Batteries," *J. Am. Chem. Soc.*, vol. 128, no. 4, pp. 1390–1393, Feb. 2006.

[22] Y. Wang and H. Zhou, "A lithium-air battery with a potential to continuously reduce O2 from air for delivering energy," *J. Power Sources*, vol. 195, no. 1, pp. 358–361, Jan. 2010.

[23] G. M. Ehrlich, *Handbook of Batteries*. 2002.

[24] W. Xu *et al.*, "Lithium metal anodes for rechargeable batteries," *Energy Environ. Sci.*, vol. 7, no. 2, pp. 513–537, 2014.

[25] B. D. McCloskey, D. S. Bethune, R. M. Shelby, G. Girishkumar, and A. C. Luntz, "Solvents? Critical Role in Nonaqueous Lithium?Oxygen Battery Electrochemistry," *J. Phys. Chem. Lett.*, vol. 2, no. 10, pp. 1161–1166, May 2011.

[26] S. A. Freunberger *et al.*, "Reactions in the Rechargeable Lithium?O 2 Battery with Alkyl Carbonate Electrolytes," *J. Am. Chem. Soc.*, vol. 133, no. 20, pp. 8040–8047, May 2011.

[27] B. M. Gallant *et al.*, "Chemical and Morphological Changes of Li?O 2 Battery Electrodes upon Cycling," *J. Phys. Chem. C*, vol. 116, no. 39, pp. 20800–20805, Oct. 2012.

[28] C. O. Laoire, S. Mukerjee, E. J. Plichta, M. A. Hendrickson, and K. M. Abraham, "Rechargeable Lithium/TEGDME-LiPF[sub 6]/O[sub 2] Battery," *J. Electrochem. Soc.*, vol. 158, no. 3, p. A302, Mar. 2011.

[29] B. D. McCloskey *et al.*, "Twin Problems of Interfacial Carbonate Formation in Nonaqueous Li–O 2 Batteries," *J. Phys. Chem. Lett.*, vol. 3, no. 8, pp. 997–1001, Apr. 2012.

[30] D. Aurbach, B. D. McCloskey, L. F. Nazar, and P. G. Bruce, "Advances in understanding mechanisms underpinning lithium–air batteries," *Nat. Energy*, vol. 1, no. 9, p. 16128, 2016.

[31] Z. Peng, S. A. Freunberger, Y. Chen, and P. G. Bruce, "A Reversible and Higher-Rate Li-O2 Battery," *Science (80-.).*, vol. 337, no. 6094, pp. 563–566, Aug. 2012.

[32] M. M. Ottakam Thotiyl, S. A. Freunberger, Z. Peng, Y. Chen, Z. Liu, and P. G. Bruce, "A stable cathode for the aprotic Li?O2?battery," *Nat. Mater.*, vol. 12, no. 11, pp. 1050–1056, Sep. 2013.

[33] M. M. Ottakam Thotiyl, S. A. Freunberger, Z. Peng, and P. G. Bruce, "The Carbon Electrode in Nonaqueous Li–O 2 Cells," *J. Am. Chem. Soc.*, vol. 135, no. 1, pp. 494–

500, Jan. 2013.

[34] T. Kuboki, T. Okuyama, T. Ohsaki, and N. Takami, “Lithium-air batteries using hydrophobic room temperature ionic liquid electrolyte,” *J. Power Sources*, vol. 146, no. 1–2, pp. 766–769, Aug. 2005.

[35] Y. Shao *et al.*, “Making Li-Air Batteries Rechargeable: Material Challenges,” *Adv. Funct. Mater.*, vol. 23, no. 8, pp. 987–1004, Feb. 2013.

[36] G. M. Veith, J. Nanda, L. H. Delmau, and N. J. Dudney, “Influence of Lithium Salts on the Discharge Chemistry of Li–Air Cells,” *J. Phys. Chem. Lett.*, vol. 3, no. 10, pp. 1242–1247, May 2012.

[37] W. Xu *et al.*, “The stability of organic solvents and carbon electrode in nonaqueous Li-O2 batteries,” *J. Power Sources*, vol. 215, pp. 240–247, Oct. 2012.

[38] R. Younesi, M. Hahlin, F. Bj?refors, P. Johansson, and K. Edstr?m, “Li?O 2 Battery Degradation by Lithium Peroxide (Li 2 O 2): A Model Study,” *Chem. Mater.*, vol. 25, no. 1, pp. 77–84, Jan. 2013.

[39] H. Zhang, “Ultrathin Two-Dimensional Nanomaterials,” *ACS Nano*, no. Xx, pp. 9451–9469, 2015.

[40] K. R. Paton *et al.*, “Scalable production of large quantities of defect-free few-layer graphene by shear exfoliation in liquids,” *Nat. Mater.*, vol. 13, no. 6, pp. 624–630, 2014.

[41] A. Reina *et al.*, “Large area, few-layer graphene films on arbitrary substrates by chemical vapor deposition,” *Nano Lett.*, vol. 9, no. 1, pp. 30–35, 2009.

[42] Z. Ma, X. Huang, S. Dou, J. Wu, and S. Wang, “One-Pot Synthesis of Fe 2 O 3 Nanoparticles on Nitrogen-Doped Graphene as Advanced Supercapacitor Electrode Materials,” *J. Phys. Chem. C*, vol. 118, no. 31, pp. 17231–17239, 2014.

[43] W. Park *et al.*, “composites Electrical and thermal conductivities of reduced graphene oxide / polystyrene composites,” vol. 113101, pp. 1–13, 2014.

[44] J.-C. Lei, X. Zhang, and Z. Zhou, “Recent advances in MXene: Preparation,

properties, and applications," *Front. Phys.*, vol. 10, no. 3, pp. 276–286, Jun. 2015.

[45] M. Naguib *et al.*, "Two-dimensional transition metal carbides," *ACS Nano*, vol. 6, no. 2, pp. 1322–1331, 2012.

[46] Y. Zhong, X. Xia, F. Shi, J. Zhan, J. Tu, and H. J. Fan, "Transition Metal Carbides and Nitrides in Energy Storage and Conversion," *Adv. Sci.*, vol. 3, pp. 1500286–1500313, 2016.

[47] M. R. Lukatskaya *et al.*, "Cation Intercalation and High Volumetric Capacitance of Two-Dimensional Titanium Carbide," *Science (80-.).*, vol. 341, no. 6153, pp. 1502–1505, Sep. 2013.

[48] M. Ghidiu, M. R. Lukatskaya, M.-Q. Zhao, Y. Gogotsi, and M. W. Barsoum, "Conductive two-dimensional titanium carbide 'clay' with high volumetric capacitance," *Nature*, Nov. 2014.

[49] Z. Li *et al.*, "Hollow hemisphere-shaped macroporous graphene/tungsten carbide/platinum nanocomposite as an efficient electrocatalyst for the oxygen reduction reaction," *Electrochim. Acta*, vol. 221, pp. 31–40, 2016.

[50] Z. Liu, P. Li, F. Zhai, Q. Wan, A. A. Volinsky, and X. Qu, "Amorphous carbon modified nano-sized tungsten carbide as a gas diffusion electrode catalyst for the oxygen reduction reaction," *RSC Adv.*, vol. 5, no. 87, pp. 70743–70748, 2015.

[51] B. Aïssa, A. Ali, K. A. Mahmoud, T. Haddad, and M. Nedil, "Transport properties of a highly conductive 2D Ti 3 C 2 T x MXene/graphene composite," *Appl. Phys. Lett.*, vol. 109, no. 4, p. 43109, Jul. 2016.

[52] A. Miranda, J. Halim, A. Lorke, and M. W. Barsoum, "Rendering Ti 3 C 2 T x (MXene) monolayers visible," *Mater. Res. Lett.*, pp. 1–7, Feb. 2017.

[53] X. Liang, A. Garsuch, and L. F. Nazar, "Sulfur Cathodes Based on Conductive MXene Nanosheets for High-Performance Lithium-Sulfur Batteries," *Angew. Chemie Int. Ed.*, vol. 54, no. 13, pp. 3907–3911, Mar. 2015.

[54] J. Luo *et al.*, "Sn 4+ Ion Decorated Highly Conductive Ti 3 C 2 MXene: Promising Lithium-Ion Anodes with Enhanced Volumetric Capacity and Cyclic Performance,"

ACS Nano, vol. 10, no. 2, pp. 2491–2499, Feb. 2016.

[55] M. Naguib *et al.*, "New Two-Dimensional Niobium and Vanadium Carbides as Promising Materials for Li-Ion Batteries," *J. Am. Chem. Soc.*, vol. 135, no. 43, pp. 15966–15969, Oct. 2013.

[56] M. Boota, B. Anasori, C. Voigt, M.-Q. Zhao, M. W. Barsoum, and Y. Gogotsi, "Pseudocapacitive Electrodes Produced by Oxidant-Free Polymerization of Pyrrole between the Layers of 2D Titanium Carbide (MXene)," *Adv. Mater.*, vol. 28, no. 7, pp. 1517–1522, Feb. 2016.

[57] M.-Q. Zhao *et al.*, "Flexible MXene/Carbon Nanotube Composite Paper with High Volumetric Capacitance," *Adv. Mater.*, vol. 27, no. 2, pp. 339–345, Jan. 2015.

[58] G. Cassabois, P. Valvin, and B. Gil, "Hexagonal boron nitride is an indirect bandgap semiconductor," *Nat. Photonics*, vol. 10, no. 4, pp. 262–267, 2016.

[59] T. Li, Y. Zuo, X. Lei, N. Li, J. Liu, and H. Han, "Regulating the oxidation degree of nickel foam: a smart strategy to controllably synthesize active Ni 3 S 2 nanorod/nanowire arrays for high-performance supercapacitors," *J. Mater. Chem. A*, vol. 4, no. 21, pp. 8029–8040, 2016.

[60] B. Mendoza-Sánchez and Y. Gogotsi, "Synthesis of Two-Dimensional Materials for Capacitive Energy Storage," *Adv. Mater.*, vol. 28, no. 29, pp. 6104–6135, Aug. 2016.

[61] R. Wang, J. Lang, Y. Liu, Z. Lin, and X. Yan, "Ultra-small, size-controlled Ni(OH)2 nanoparticles: elucidating the relationship between particle size and electrochemical performance for advanced energy storage devices," *NPG Asia Mater.*, vol. 7, no. 6, p. e183, Jun. 2015.

[62] S. Gao *et al.*, "Ultrahigh Energy Density Realized by a Single-Layer β-Co(OH) 2 All-Solid-State Asymmetric Supercapacitor," *Angew. Chemie Int. Ed.*, vol. 53, no. 47, pp. 12789–12793, Nov. 2014.

[63] S. Li, J. Wen, T. Chen, L. Xiong, J. Wang, and G. Fang, "In situ synthesis of 3D CoS nanoflake/Ni(OH) 2 nanosheet nanocomposite structure as a candidate

supercapacitor electrode," *Nanotechnology*, vol. 27, no. 14, p. 145401, Apr. 2016.

[64] Y. Zhu, C. Cao, S. Tao, W. Chu, Z. Wu, and Y. Li, "Ultrathin Nickel Hydroxide and Oxide Nanosheets: Synthesis, Characterizations and Excellent Supercapacitor Performances," *Sci. Rep.*, vol. 4, p. 5787, Aug. 2014.

[65] Z. Huang *et al.*, "Wall-like hierarchical metal oxide nanosheet arrays grown on carbon cloth for excellent supercapacitor electrodes," *Nanoscale*, vol. 8, no. 27, pp. 13273–13279, 2016.

[66] Q. Yang, Z. Lu, X. Sun, and J. Liu, "Ultrathin Co3O4 nanosheet arrays with high supercapacitive performance," *Sci. Rep.*, vol. 3, Dec. 2013.

[67] L. Ye, L. Zhao, H. Zhang, B. Zhang, and H. Wang, "One-pot formation of ultra-thin Ni/Co hydroxides with a sheet-like structure for enhanced asymmetric supercapacitors," *J. Mater. Chem. A*, vol. 4, no. 23, pp. 9160–9168, 2016.

[68] L. Wang, C. Lin, F. Zhang, and J. Jin, "Phase Transformation Guided Single-Layer β-Co(OH) 2 Nanosheets for Pseudocapacitive Electrodes," *ACS Nano*, vol. 8, no. 4, pp. 3724–3734, Apr. 2014.

[69] K. F. Mak, C. Lee, J. Hone, J. Shan, and T. F. Heinz, "Atomically Thin MoS2 : A New Direct-Gap Semiconductor," *Phys. Rev. Lett.*, vol. 105, no. 13, p. 136805, Sep. 2010.

[70] C.-C. Shen, Y.-T. Hsu, L.-J. Li, and H.-L. Liu, "Charge Dynamics and Electronic Structures of Monolayer MoS 2 Films Grown by Chemical Vapor Deposition," *Appl. Phys. Express*, vol. 6, no. 12, p. 125801, Dec. 2013.

[71] C. N. R. Rao, H. S. S. Ramakrishna Matte, and U. Maitra, "Graphene Analogues of Inorganic Layered Materials," *Angew. Chemie Int. Ed.*, vol. 52, no. 50, pp. 13162–13185, Dec. 2013.

[72] Z. Yu *et al.*, "Realization of Room-Temperature Phonon-Limited Carrier Transport in Monolayer MoS 2 by Dielectric and Carrier Screening," *Adv. Mater.*, vol. 28, no. 3, pp. 547–552, Jan. 2016.

[73] L. Li *et al.*, "Three-dimensional MoS $_x$ (1 < x < 2) nanosheets decorated

graphene aerogel for lithium–oxygen batteries," *J. Mater. Chem. A*, pp. 10986–10991, 2016.

[74] A. Arunchander, S. G. Peera, and A. K. Sahu, "Synthesis of flower-like molybdenum sulfide/graphene hybrid as an efficient oxygen reduction electrocatalyst for anion exchange membrane fuel cells," *J. Power Sources*, vol. 353, pp. 104–114, Jun. 2017.

[75] L. Hao *et al.*, "Nitrogen-doped MoS2/carbon as highly oxygen-permeable and stable catalysts for oxygen reduction reaction in microbial fuel cells," *J. Power Sources*, vol. 339, pp. 68–79, Jan. 2017.

[76] X. Wang *et al.*, "Uniform Deposition of Co 3 O 4 Nanosheets on Exfoliated MoS 2 Nanosheets as Advanced Catalysts for Water Splitting," *Electrochim. Acta*, vol. 212, pp. 890–897, Sep. 2016.

[77] D. Chen *et al.*, "In situ nitrogenated graphene–few-layer WS2 composites for fast and reversible Li+ storage," *Nanoscale*, vol. 5, no. 17, p. 7890, 2013.

[78] F. Clerici *et al.*, "In situ MoS 2 Decoration of Laser-Induced Graphene as Flexible Supercapacitor Electrodes," *ACS Appl. Mater. Interfaces*, vol. 8, no. 16, pp. 10459–10465, Apr. 2016.

[79] M. Acerce, D. Voiry, and M. Chhowalla, "Metallic 1T phase MoS2 nanosheets as supercapacitor electrode materials," *Nat. Nanotechnol.*, vol. 10, no. 4, pp. 313–318, Mar. 2015.

[80] J. Feng *et al.*, "Metallic Few-Layered VS 2 Ultrathin Nanosheets: High Two-Dimensional Conductivity for In-Plane Supercapacitors," *J. Am. Chem. Soc.*, vol. 133, no. 44, pp. 17832–17838, Nov. 2011.

[81] L. Ma, L. Xu, X. Zhou, X. Xu, and L. Zhang, "Synthesis of a hierarchical MoSe 2 /C hybrid with enhanced electrochemical performance for supercapacitors," *RSC Adv.*, vol. 6, no. 94, pp. 91621–91628, 2016.

[82] S. K. Balasingam, A. Thirumurugan, J. S. Lee, and Y. Jun, "Amorphous MoS x thin-film-coated carbon fiber paper as a 3D electrode for long cycle life symmetric

supercapacitors," *Nanoscale*, vol. 8, no. 23, pp. 11787–11791, 2016.

[83] G. A. Muller, J. B. Cook, H.-S. Kim, S. H. Tolbert, and B. Dunn, "High Performance Pseudocapacitor Based on 2D Layered Metal Chalcogenide Nanocrystals," *Nano Lett.*, vol. 15, no. 3, pp. 1911–1917, Mar. 2015.

[84] K. Chang and W. Chen, "In situ synthesis of MoS2/graphene nanosheet composites with extraordinarily high electrochemical performance for lithium ion batteries," *Chem. Commun.*, vol. 47, no. 14, p. 4252, 2011.

[85] H. Jiang *et al.*, "2D Monolayer MoS 2 -Carbon Interoverlapped Superstructure: Engineering Ideal Atomic Interface for Lithium Ion Storage," *Adv. Mater.*, vol. 27, no. 24, pp. 3687–3695, Jun. 2015.

[86] C. Zhu, X. Mu, P. A. van Aken, Y. Yu, and J. Maier, "Single-Layered Ultrasmall Nanoplates of MoS 2 Embedded in Carbon Nanofibers with Excellent Electrochemical Performance for Lithium and Sodium Storage," *Angew. Chemie Int. Ed.*, vol. 53, no. 8, pp. 2152–2156, Feb. 2014.

[87] X. Xiong *et al.*, "Flexible Membranes of MoS2/C Nanofibers by Electrospinning as Binder-Free Anodes for High-Performance Sodium-Ion Batteries," *Sci. Rep.*, vol. 5, no. 1, p. 9254, Aug. 2015.

[88] Y. Shi *et al.*, "Self-assembly of hierarchical MoSx/CNT nanocomposites (2<x<3): towards high performance anode materials for lithium ion batteries," *Sci. Rep.*, vol. 3, Jul. 2013.

[89] D. Kong *et al.*, "Rational design of MoS 2 @graphene nanocables: towards high performance electrode materials for lithium ion batteries," *Energy Environ. Sci.*, vol. 7, no. 10, pp. 3320–3325, Aug. 2014.

[90] Y. Chen, J. Lu, S. Wen, L. Lu, and J. Xue, "Synthesis of SnO 2 /MoS 2 composites with different component ratios and their applications as lithium ion battery anodes," *J. Mater. Chem. A*, vol. 2, no. 42, pp. 17857–17866, Sep. 2014.

[91] A. Chaudhari *et al.*, "Fabrication of MoS 2 Nanowire Arrays and Layered Structures via the Self-Assembly of Block Copolymers," *Adv. Mater. Interfaces*, vol. 3, no. 11,

p. 1500596, Jun. 2016.

[92] S. Qin, W. Lei, D. Liu, and Y. Chen, “Advanced N-doped mesoporous molybdenum disulfide nanosheets and the enhanced lithium-ion storage performance,” *J. Mater. Chem. A*, vol. 4, no. 4, pp. 1440–1445, 2016.

[93] S. R. Marri, S. Ratha, C. S. Rout, and J. N. Behera, “3D cuboidal vanadium diselenide embedded reduced graphene oxide hybrid structures with enhanced supercapacitor properties,” *Chem. Commun.*, vol. 53, no. 1, pp. 228–231, 2017.

[94] C. Wang, W. Wan, Y. Huang, J. Chen, H. H. Zhou, and X. X. Zhang, “Hierarchical MoS2 nanosheet/active carbon fiber cloth as a binder-free and free-standing anode for lithium-ion batteries,” *Nanoscale*, 2014.

[95] G. Chen *et al.*, “Facile synthesis of hierarchical MoS 2 –carbon microspheres as a robust anode for lithium ion batteries,” *J. Mater. Chem. A*, vol. 4, no. 24, pp. 9653–9660, 2016.

[96] Z.-L. Wang, D. Xu, J.-J. Xu, and X.-B. Zhang, “Oxygen electrocatalysts in metal-air batteries: from aqueous to nonaqueous electrolytes.,” *Chem. Soc. Rev.*, vol. 43, p. 10.1039/c3cs60248f, 2013.

[97] F. Li *et al.*, “The water catalysis at oxygen cathodes of lithium-oxygen cells.,” *Nat. Commun.*, vol. 6, p. 7843, 2015.

[98] J. Christensen *et al.*, “A Critical Review of Li/Air Batteries,” *J. Electrochem. Soc.*, vol. 159, no. 2, p. R1, 2012.

[99] H. Yadegari *et al.*, “On Rechargeability and Reaction Kinetics of Sodium-Air Batteries,” *Energy Environ. Sci.*, vol. 7, pp. 3747–3757, 2014.

[100] B. M. Gallant *et al.*, “The Kinetics and Product Characteristics of Oxygen Reduction and Evolution in Li-O 2 Batteries,” pp. 14–16.

[101] C. Xia, M. Waletzko, L. Chen, K. Peppler, P. J. Klar, and J. Janek, “Evolution of Li2O2 growth and its effect on kinetics of Li-O2 batteries,” *ACS Appl. Mater. Interfaces*, vol. 6, no. 15, pp. 12083–12092, 2014.

[102] S. Meini *et al.*, "solution : implications for cycle-life of Li – air cells †," pp. 11478–11493, 2013.

[103] J. Xiao *et al.*, "Optimization of Air Electrode for Li/Air Batteries," *J. Electrochem. Soc.*, vol. 157, no. 4, p. A487, 2010.

[104] H. Ohkuma, I. Uechi, M. Matsui, Y. Takeda, O. Yamamoto, and N. Imanishi, "Stability of carbon electrodes for aqueous lithium-air secondary batteries," *J. Power Sources*, vol. 245, pp. 947–952, 2014.

[105] E. Yoo and H. Zhou, "Li-air rechargeable battery based on metal-free graphene nanosheet catalysts," *ACS Nano*, vol. 5, no. 4, pp. 3020–3026, 2011.

[106] B. Sun, X. Huang, S. Chen, P. Munroe, and G. Wang, "Porous graphene nanoarchitectures: An efficient catalyst for low charge-overpotential, long life, and high capacity lithium-oxygen batteries," *Nano Lett.*, vol. 14, no. 6, pp. 3145–3152, 2014.

[107] S. Zhang, Z. Wen, K. Rui, C. Shen, Y. Lu, and J. Yang, "Graphene nanosheets loaded with Pt nanoparticles with enhanced electrochemical performance for sodium–oxygen batteries," *J. Mater. Chem. A*, vol. 3, no. 6, pp. 2568–2571, 2015.

[108] J. Xiao *et al.*, "Hierarchically Porous Graphene as a Lithium–Air Battery Electrode," *Nano Lett.*, vol. 11, no. 11, pp. 5071–5078, Nov. 2011.

[109] Y. Li *et al.*, "Nitrogen-doped graphene nanosheets as cathode materials with excellent electrocatalytic activity for high capacity lithium-oxygen batteries," *Electrochem. commun.*, vol. 18, pp. 12–15, Jan. 2012.

[110] G. Wu *et al.*, "Nitrogen-Doped Graphene-Rich Catalysts Derived from Heteroatom Polymers for Oxygen Reduction in Nonaqueous Lithium–O 2 Battery Cathodes," *ACS Nano*, vol. 6, no. 11, pp. 9764–9776, Nov. 2012.

[111] Y. Li *et al.*, "Discharge product morphology and increased charge performance of lithium–oxygen batteries with graphene nanosheet electrodes: the effect of sulphur doping," *J. Mater. Chem.*, vol. 22, no. 38, p. 20170, 2012.

[112] T. Liu *et al.*, "Cycling Li-O2 batteries via LiOH formation and decomposition,"

Science (80-.)., vol. 350, no. 6260, pp. 530–533, 2015.

[113] Q. Li, R. Cao, J. Cho, and G. Wu, "Nanostructured carbon-based cathode catalysts for nonaqueous lithium-oxygen batteries.," *Phys. Chem. Chem. Phys.*, vol. 16, no. 27, pp. 13568–82, 2014.

[114] V. Viswanathan, V. Pande, K. M. Abraham, A. C. Luntz, B. D. McCloskey, and D. Addison, "Comment on 'Cycling Li-O2 batteries via LiOH formation and decomposition,'" *Science (80-.).*, vol. 352, no. 6286, pp. 667–667, May 2016.

[115] T. Liu, G. Kim, J. Carretero-González, E. Castillo-Martínez, and C. P. Grey, "Response to Comment on 'Cycling Li-O_2 batteries via LiOH formation and decomposition'.," *Science*, vol. 352, no. 6286, p. 667, 2016.

[116] J. Lu *et al.*, "A lithium–oxygen battery based on lithium superoxide," *Nature*, vol. 529, no. 7586, pp. 1–7, Jan. 2016.

[117] D. Zhai *et al.*, "Raman evidence for late stage disproportionation in a Li-O2 battery," *J. Phys. Chem. Lett.*, vol. 5, no. 15, pp. 2705–2710, 2014.

[118] W. H. Ryu, F. S. Gittleson, M. Schwab, T. Goh, and A. D. Taylor, "A mesoporous catalytic membrane architecture for lithium-oxygen battery systems," *Nano Lett.*, vol. 15, no. 1, pp. 434–441, 2015.

[119] D. Zhai *et al.*, "Disproportionation in Li–O 2 Batteries Based on a Large Surface Area Carbon Cathode," *J. Am. Chem. Soc.*, vol. 135, no. 41, pp. 15364–15372, 2013.

[120] F. S. Gittleson, W. H. Ryu, and A. D. Taylor, "Operando observation of the gold-electrolyte interface in Li-O2 batteries," *ACS Appl. Mater. Interfaces*, vol. 6, no. 21, pp. 19017–19025, 2014.

[121] M. Olivares-Marín, A. Sorrentino, R.-C. Lee, E. Pereiro, N.-L. Wu, and D. Tonti, "Spatial Distributions of Discharged Products of Lithium–Oxygen Batteries Revealed by Synchrotron X-ray Transmission Microscopy," *Nano Lett.*, vol. 15, no. 10, pp. 6932–6938, Oct. 2015.

[122] W. L. Bowden, "Transition Metal Polysulfides as Battery Cathodes," *J. Electrochem. Soc.*, vol. 135, no. 1, p. 1, 1988.

[123] G. D. Park, J. S. Cho, and Y. C. Kang, “Sodium-ion storage properties of nickel sulfide hollow nanospheres/reduced graphene oxide composite powders prepared by a spray drying process and the nanoscale Kirkendall effect,” *Nanoscale*, vol. 7, no. 40, pp. 16781–16788, 2015.

[124] T. M. Masikhwa *et al.*, “High performance asymmetric supercapacitor based on CoAl-LDH/GF and activated carbon from expanded graphite,” *RSC Adv.*, vol. 6, no. 52, pp. 46723–46732, 2016.

[125] Z. Li, X. Yu, A. Gu, H. Tang, L. Wang, and Z. Lou, “Anion exchange strategy to synthesis of porous NiS hexagonal nanoplates for supercapacitors,” *Nanotechnology*, vol. 28, no. 6, p. 65406, Feb. 2017.

[126] Y. Tang *et al.*, “Synthesis of Capsule-like Porous Hollow Nanonickel Cobalt Sulfides via Cation Exchange Based on the Kirkendall Effect for High-Performance Supercapacitors,” *ACS Appl. Mater. Interfaces*, vol. 8, no. 15, pp. 9721–9732, Apr. 2016.

[127] M. Kristl, B. Dojer, S. Gyergyek, and J. Kristl, “Synthesis of nickel and cobalt sulfide nanoparticles using a low cost sonochemical method,” *Heliyon*, vol. 3, no. 3, p. e00273, Mar. 2017.

[128] W. Wei, L. Mi, Y. Gao, Z. Zheng, W. Chen, and X. Guan, “Partial Ion-Exchange of Nickel-Sulfide-Derived Electrodes for High Performance Supercapacitors,” *Chem. Mater.*, vol. 26, no. 11, pp. 3418–3426, Jun. 2014.

[129] Y. Li, S. Liu, W. Chen, S. Li, L. Shi, and Y. Zhao, “Facile synthesis of flower-like cobalt sulfide hierarchitectures with superior electrode performance for supercapacitors,” *J. Alloys Compd.*, vol. 712, pp. 139–146, Jul. 2017.

[130] J. Xu *et al.*, “Flexible Asymmetric Supercapacitors Based upon Co 9 S 8 Nanorod//Co 3 O 4 @RuO 2 Nanosheet Arrays on Carbon Cloth,” *ACS Nano*, vol. 7, no. 6, pp. 5453–5462, Jun. 2013.

[131] Z. Ma *et al.*, “Novel Flower-like Nickel Sulfide as an Efficient Electrocatalyst for Non-aqueous Lithium-Air Batteries,” *Sci. Rep.*, vol. 5, no. January 2016, p. 18199,

2015.

[132] Z. Lu, Y. Zhou, Z. Liang, Z. Liu, S. Chu, and Y. Cui, “Ultrathin Two-Dimensional Atomic Crystals as Stable Interfacial Layer for Improvement of Lithium Metal Anode,” 2014.

[133] K. Liao, X. Wang, Y. Sun, D. Tang, M. Han, and P. He, “An oxygen cathode with stable full discharge-charge capability based on 2D conducting oxide,” *Carbon N. Y.*, vol. 8, no. 1, pp. 1–9, 2015.

[134] S. Tong *et al.*, “Mesoporous NiO with a single-crystalline structure utilized as a noble metal-free catalyst for non-aqueous Li–O 2 batteries,” *J. Mater. Chem. A*, vol. 3, no. 31, pp. 16177–16182, 2015.

[135] C. Shen, Z. Wen, F. Wang, T. Wu, and X. Wu, “Cobalt-Metal-Based Cathode for Lithium-Oxygen Battery with Improved Electrochemical Performance,” *ACS Catal.*, vol. 6, no. 7, pp. 4149–4153, 2016.

[136] P. Zhang *et al.*, “MoS 2 nanosheets decorated with gold nanoparticles for rechargeable Li–O 2 batteries,” *J. Mater. Chem. A*, vol. 3, no. 28, pp. 14562–14566, 2015.

[137] M. Asadi *et al.*, “Cathode Based on Molybdenum Disulfide Nanoflakes for Lithium-Oxygen Batteries.,” *ACS Nano*, vol. 10, no. 2, pp. 2167–75, Feb. 2016.

[138] C. Ling, R. Zhang, K. Takechi, and F. Mizuno, “Intrinsic Barrier to Electrochemically Decompose Li 2 CO 3 and LiOH,” 2014.

[139] M. Park, H. Sun, H. Lee, J. Lee, and J. Cho, “Lithium-air batteries: Survey on the current status and perspectives towards automotive applications from a Battery Industry Standpoint,” *Adv. Energy Mater.*, vol. 2, no. 7, pp. 780–800, 2012.

[140] D. Capsoni, M. Bini, S. Ferrari, E. Quartarone, and P. Mustarelli, “Recent advances in the development of Li-air batteries,” *J. Power Sources*, vol. 220, pp. 253–263, 2012.

[141] J. Xiao *et al.*, “From Lithium-Oxygen to Lithium-Air Batteries: Challenges and Opportunities,” *J. Power Sources*, vol. 49, no. 13, pp. 5071–5078, 2013.

[142] S. R. Gowda, A. Brunet, and B. D. Mccloskey, “Implications of CO 2 Contamination in Rechargeable Nonaqueous Li −,” pp. 2–5, 2013.

[143] A. L. O. Co, K. Takechi, T. Shiga, and T. Asaoka, “ChemComm COMMUNICATION,” pp. 3463–3465, 2011.

[144] V. A. Online, “Environmental Science battery †,” pp. 677–681, 2014.

[145] J. Zhang, Z. Zhao, Z. Xia, and L. Dai, “A metal-free bifunctional electrocatalyst for oxygen reduction and oxygen evolution reactions,” *Nat. Nanotechnol.*, vol. 10, no. 5, pp. 444–452, 2015.

[146] J. Snyder, T. Fujita, M. W. Chen, and J. Erlebacher, “Oxygen reduction in nanoporous metal–ionic liquid composite electrocatalysts,” *Nat. Mater.*, vol. 9, no. 11, pp. 904–907, 2010.

[147] X. Cao, C. Jin, F. Lu, Z. Yang, M. Shen, and R. Yang, “Electrochemical Properties of MnCo 2 O 4 Spinel Bifunctional Catalyst for Oxygen Reduction and Evolution Reaction,” vol. 161, no. 5, pp. 296–300, 2014.

[148] H. Jiang *et al.*, “Iron Carbide Nanoparticles Encapsulated in Mesoporous Fe–N-Doped Graphene-Like Carbon Hybrids as Efficient Bifunctional Oxygen Electrocatalysts,” *ACS Appl. Mater. Interfaces*, vol. 7, no. 38, pp. 21511–21520, Sep. 2015.

[149] Y. Liang *et al.*, “Co3O4 nanocrystals on graphene as a synergistic catalyst for oxygen reduction reaction,” *Nat. Mater.*, vol. 10, no. 10, pp. 780–786, Aug. 2011.

[150] T. W. Kim, M. A. Woo, M. Regis, and K.-S. Choi, “Electrochemical Synthesis of Spinel Type ZnCo 2 O 4 Electrodes for Use as Oxygen Evolution Reaction Catalysts,” *J. Phys. Chem. Lett.*, vol. 5, no. 13, pp. 2370–2374, Jul. 2014.

[151] Y. Zhao *et al.*, “Hierarchical mesoporous perovskite La0.5Sr0.5CoO2.91 nanowires with ultrahigh capacity for Li-air batteries,” *Proc. Natl. Acad. Sci.*, vol. 109, no. 48, pp. 19569–19574, Nov. 2012.

[152] J. Shui, Y. Lin, J. W. Connell, J. Xu, X. Fan, and L. Dai, “Nitrogen-Doped Holey Graphene for High-Performance Rechargeable Li–O 2 Batteries,” *ACS Energy Lett.*,

vol. 1, no. 1, pp. 260–265, Jul. 2016.

[153] Y.-C. Lu, H. A. Gasteiger, and Y. Shao-Horn, “Catalytic Activity Trends of Oxygen Reduction Reaction for Nonaqueous Li-Air Batteries,” *J. Am. Chem. Soc.*, vol. 133, no. 47, pp. 19048–19051, Nov. 2011.

[154] Q. Li *et al.*, “One-step synthesis of Mn3O4/reduced graphene oxide nanocomposites for oxygen reduction in nonaqueous Li–O2 batteries,” *Chem. Commun.*, vol. 49, no. 92, p. 10838, 2013.

[155] Y. Duan, B. Zhang, D. C. Sorescu, J. Karl Johnson, E. H. Majzoub, and D. R. Luebke, “Density functional theory studies on the electronic, structural, phonon dynamical and thermo-stability properties of bicarbonates MHCO 3 , M = Li, Na, K,” *J. Phys. Condens. Matter*, vol. 24, no. 32, p. 325501, Aug. 2012.

[156] B. D. McCloskey, D. S. Bethune, R. M. Shelby, G. Girishkumar, and A. C. Luntz, “Solvents ’ Critical Role in Nonaqueous Lithium À Oxygen Battery,” *J. Phys. Chem. Lett.*, vol. 2, pp. 1161–1166, 2011.

[157] H.-G. Jung, J. Hassoun, J.-B. Park, Y.-K. Sun, and B. Scrosati, “An improved high-performance lithium–air battery,” *Nat. Chem.*, vol. 4, no. 7, pp. 579–585, 2012.

[158] Y. Liu, Y. Zhao, L. Jiao, and J. Chen, “A graphene-like MoS2/graphene nanocomposite as a highperformance anode for lithium ion batteries,” *J. Mater. Chem. A*, vol. 2, no. 32, pp. 13109–13115, 2014.

[159] M. M. Ottakam Thotiyl, S. a Freunberger, Z. Peng, Y. Chen, Z. Liu, and P. G. Bruce, “A stable cathode for the aprotic Li-O2 battery.,” *Nat. Mater.*, vol. 12, no. September, pp. 1050–6, 2013.

[160] J. Lu *et al.*, “A nanostructured cathode architecture for low charge overpotential in lithium-oxygen batteries.,” *Nat. Commun.*, vol. 4, p. 2383, Aug. 2013.

[161] R. S. Assary *et al.*, “The Effect of Oxygen Crossover on the Anode of a Li-O 2 Battery using an Ether-Based Solvent: Insights from Experimental and Computational Studies,” *ChemSusChem*, vol. 6, no. 1, pp. 51–55, Jan. 2013.

[162] N. Garcia-Araez and P. Novák, “Critical aspects in the development of lithium-air

batteries," *J. Solid State Electrochem.*, vol. 17, no. 7, pp. 1793–1807, 2013.

[163] K. G. Gallagher *et al.*, "Quantifying the promise of lithium–air batteries for electric vehicles," *Energy Environ. Sci.*, vol. 7, p. 1555, 2014.

[164] J. Xiao *et al.*, "Hierarchically Porous Graphene as a Lithium À Air Battery Electrode," *Nano Lett.*, vol. 11, pp. 5071–5078, 2011.

[165] J. G. Zhang, D. Wang, W. Xu, J. Xiao, and R. E. Williford, "Ambient operation of Li/Air batteries," *J. Power Sources*, vol. 195, no. 13, pp. 4332–4337, 2010.

[166] Z. Guo, X. Dong, S. Yuan, Y. Wang, and Y. Xia, "Humidity effect on electrochemical performance of Li–O2 batteries," *J. Power Sources*, vol. 264, pp. 1–7, Oct. 2014.

[167] D. Zhu, L. Zhang, M. Song, X. Wang, and Y. Chen, "An in situ formed Pd nanolayer as a bifunctional catalyst for Li-air batteries in ambient or simulated air," *Chem. Commun.*, vol. 49, no. 83, p. 9573, 2013.

[168] T. Zhang and H. Zhou, "A reversible long-life lithium-air battery in ambient air.," *Nat. Commun.*, vol. 4, no. May, p. 1817, 2013.

[169] P. Pasierb, S. Komornicki, M. Rokita, and M. Rękas, "Structural properties of Li2CO3-BaCO3 system derived from IR and Raman spectroscopy," *J. Mol. Struct.*, vol. 596, no. 1–3, pp. 151–156, 2001.

[170] S. K. Das, J. Chai, S. Rahman, and A. Sarkar, "Synthesis , Characterization and Performance Evaluation of an Advanced Solid Electrolyte and Air Cathode for Rechargeable Lithium-Air Batteries," *J. Mater. Sci. Chem. Eng.*, vol. 4, no. January, pp. 74–89, 2016.

[171] S. Wu *et al.*, "A Synergistic System for Lithium-Oxygen Batteries in Humid Atmosphere Integrating a Composite Cathode and a Hydrophobic Ionic Liquid-Based Electrolyte," *Adv. Funct. Mater.*, vol. 26, no. 19, pp. 3291–3298, 2016.

[172] X.-B. Cheng, R. Zhang, C.-Z. Zhao, F. Wei, J.-G. Zhang, and Q. Zhang, "A Review of Solid Electrolyte Interphases on Lithium Metal Anode," *Adv. Sci.*, vol. 3, no. 3, p. n/a-n/a, 2016.

[173] H. Iddir and L. A. Curtiss, “Li Ion Diffusion Mechanisms in Bulk Monoclinic Li 2 CO 3 Crystals from Density Functional,” *J. Phys. Chem. C*, vol. 114, pp. 20903–20906, 2010.

[174] Y. Bi *et al.*, “Stability of Li 2 CO 3 in cathode of lithium ion battery and its influence on electrochemical performance,” *RSC Adv.*, vol. 6, no. 23, pp. 19233–19237, 2016.

[175] M. Sina *et al.*, “Investigation of SEI layer formation in conversion iron fluoride cathodes by combined STEM/EELS and XPS,” *J. Phys. Chem. C*, vol. 119, no. 18, pp. 9762–9773, 2015.

[176] D. Aurbach, “In situ FTIR Spectroelectrochemical Studies of Surface Films Formed on Li and Nonactive Electrodes at Low Potentials in Li Salt Solutions Containing CO[sub 2],” *J. Electrochem. Soc.*, vol. 140, no. 11, p. L155, 1993.

[177] D. Zhai *et al.*, “Raman Evidence for Late Stage Disproportionation in a Li–O 2 Battery,” *J. Phys. Chem. Lett.*, vol. 5, no. 15, pp. 2705–2710, Aug. 2014.

[178] Y. Chen, S. A. Freunberger, Z. Peng, O. Fontaine, and P. G. Bruce, “Charging a Li–O2 battery using a redox mediator,” *Nat. Chem.*, vol. 5, no. 6, pp. 489–494, May 2013.

[179] N. B. Aetukuri, B. D. McCloskey, J. M. García, L. E. Krupp, V. Viswanathan, and A. C. Luntz, “Solvating additives drive solution-mediated electrochemistry and enhance toroid growth in non-aqueous Li–O2 batteries,” *Nat. Chem.*, vol. 7, no. 1, pp. 50–56, Dec. 2014.

[180] P. Du *et al.*, “Compatibility of lithium salts with solvent of the non-aqueous electrolyte in Li–O2 batteries,” *Phys. Chem. Chem. Phys.*, vol. 15, no. 15, p. 5572, 2013.

[181] Y.-C. Lu *et al.*, “In situ ambient pressure X-ray photoelectron spectroscopy studies of lithium-oxygen redox reactions.,” *Sci. Rep.*, vol. 2, p. 715, 2012.

[182] K. Leung, F. Soto, K. Hankins, P. B. Balbuena, and K. L. Harrison, “Stability of Solid Electrolyte Interphase Components on Lithium Metal and Reactive Anode Material Surfaces,” *J. Phys. Chem. C*, vol. 120, no. 12, pp. 6302–6313, Mar. 2016.

[183] S. Shi, Y. Qi, H. Li, and L. G. Hector, "Defect Thermodynamics and Diffusion Mechanisms in Li 2 CO 3 and Implications for the Solid Electrolyte Interphase in Li-Ion Batteries," *J. Phys. Chem. C*, vol. 117, no. 17, pp. 8579–8593, May 2013.

[184] K. C. Lau, L. A. Curtiss, and J. Greeley, "Density Functional Investigation of the Thermodynamic Stability of Lithium Oxide Bulk Crystalline Structures as a Function of Oxygen Pressure," *J. Phys. Chem. C*, vol. 115, no. 47, pp. 23625–23633, Dec. 2011.

[185] P. Mark and L. Nilsson, "Structure and dynamics of liquid water with different long-range interaction truncation and temperature control methods in molecular dynamics simulations," *J. Comput. Chem.*, vol. 23, no. 13, pp. 1211–1219, 2002.

[186] P. Mark and L. Nilsson, "Structure and Dynamics of the TIP3P , SPC , and SPC / E Water Models at 298 K," *J. Phys. Chem. A*, vol. 105, no. 43, pp. 9954–9960, 2001.

[187] H. J. C. Berendsen, J. R. Grigera, and T. P. Straatsma, "The Missing Term in Effective Pair Potentials," *J. Phys. Chem.*, vol. 91, no. 24, pp. 6269–6271, 1987.

[188] M. J. W. Frank, J. A. M. Kuipers, W. P. M. Van Swaaij, and W. P. M. van Swaaij, "Diffusion Coefficients and Viscosities of CO2 + H2O, CO2 + CH3OH, NH3 + H2O, and NH3 + CH3OH Liquid Mixtures," *J. Chem. Eng. Data*, vol. 41, no. 2, pp. 297–302, 1996.

[189] L. Johnson *et al.*, "The role of LiO2 solubility in O2 reduction in aprotic solvents and its consequences for Li–O2 batteries," *Nat. Chem.*, vol. 6, no. 12, pp. 1091–1099, Nov. 2014.

[190] M. J. Welland *et al.*, "An atomistically informed mesoscale model for growth and coarsening during discharge in lithium-oxygen batteries," *J. Chem. Phys.*, vol. 143, no. 22, p. 224113, Dec. 2015.

[191] B. D. Adams, C. Radtke, R. Black, M. L. Trudeau, K. Zaghib, and L. F. Nazar, "Current density dependence of peroxide formation in the Li–O2 battery and its effect on charge," *Energy Environ. Sci.*, vol. 6, no. 6, p. 1772, 2013.

VITA

Baharak Sayahpour

Gender: Female **Cell:** (312) 889-2656

Date of Birth: Dec. 06, 1990 **E-mail:** bsayah2@uic.edu

EDUCATION

- **University of Illinois at Chicago, Chicago, IL**
  - M.Sc. in Mechanical Engineering (GPA: 4.0/4.0) 2015 - present
- **University of Tehran, Tehran, Iran**
  - B.Sc. in Chemical Engineering (GPA: 3.35/4.0) 2009 - 2014

RESEARCH EXPERIENCES

- **Nanomaterials and Energy System Laboratory, Collage of Engineering, UIC**

  Research Assistance July 2015 – Present
- **Thermal Processes Technology Institute, Martin-Luther-University, Germany**

  Research Intern July 2014 – August 2014
- **Catalysis and Nano-Structured Materials Research Laboratory, U of Tehran**

  Research Assistant July 2012 - March 2013
- **Process Design and Simulation Research Center, U of Tehran**

  Research Assistant April 2014 - June 2014
- **Iran Polymer and Petrochemical Institute (IPPI)**

  Research Assistant Sep 2014 – Jan 2015

TEACHING EXPERIENCES

- **University of Illinois at Chicago, Chicago, IL**

  Teaching Assistant Spring 2016: Intermediate Thermodynamics (ME325)

  Teaching Assistant Fall 2016: Intermediate Thermodynamics (ME325)

WORK EXPERIENCES

- **Namvaran Consulting Engineers, Tehran**

  Intern in Piping Department April 2015 – June 2015

- **National Iranian Oil Company (NIOC)**

  Summer Intern August 2013 - Sep 2013

- **Oil Turbo Compressor (OTC) Group, Tehran**

  Project Engineer (part-time) April 2012 - Nov 2013

VOLUNTEER EXPERIENCES

- **Materials Research Society (MRS), UIC Chapter, Chicago**

  Vice President May 2017 – Present

- **Mechanical and Industrial Engineering Graduate Association (MIEGA), UIC**

  Treasurer of Central Council Sep 2016 – Present

- **Iranian Association of Chemical Engineering (IAChE), Tehran**

  Main Member of Student Branch Dec 2010 – Oct 2012

- **Scientific Association of Chemical Engineering, University of Tehran**

  Main *Member of Central Council* Nov 2010 – October 2012

- **Environmental Committee, University of Tehran**

  Main Member of Central Council May 2012 – May 2014

HONORS AND AWARDS

- Received DAAD (Deutscher Akademischer Austausch Dienst) Scholarship for Summer Research Internship program 2014
- Received engineering school scholarship for the undergraduate program, University of Tehran, Iran 2009-14
- Ranked among top 0.5% of 400,000 participants in the national universities entrance exam, Iran 2009
- Finalist of the national qualifier competition in Mathematics Olympiad, Iran 2008
- Finalist of the national qualifier competition in Physics Olympiad, Iran 2007

PATENTS AND PUBLICATIONS

Patents:

- Amin Salehi-Khojin, Baharak Sayahpour, Pedram Abbasi, Mohammad Asadi, "Anode Protection for Energy Storage Systems (Metal-Sulfur, Metal-Air, Metal-ion and etc. batteries)" *Provisional Patent Applcation,* Filed on June 2016.

Submitted manuscripts:

- Sayahpour, Baharak, Pedram Abbasi, Mohammad Asadi, Ahn Ngo, Klas Karis, Jacobo Jokisaari, Badri Narayanan, Marc Gerard, Poya Yasaei, Fatemeh Khalili-Araghi, Robert Klie, Larry A. Curtiss, Amin Salehi-Khojin. "Enabling Operation of Lithium-Oxygen Batteries with Long Cycle Life in a Realistic Air Atmosphere." *Nature* (Revision Request).
- Kibum Kim, Mohammad Asadi, Pedram Abbasi, Aditya Venkata Addepalli, Poya Yasaei, Baharak Sayahpour, Amin Salehi-Khojin "Conversion of Carbon Dioxide to Synthesis Gas Using a Solar-Driven Artificial Leaf" *Advanced Energy Materials* (Under Review).

Conference Proceedings:

- B. Sayahpour, M. Asadi, P. Abbasi, L.A. Curtiss, A. Salehi-Khojin, "An Air Breathing Lithium-Oxygen Battery" Oral Accepted at "The American Institute of Chemical Engineers Annual Meeting (AIChE 2017)", Minneapolis, USA.
- B. Sayahpour, P. Abbasi, M. Asadi, L.A. Curtiss, A. Salehi-Khojin, "A High Performance Lithium-Oxygen Battery Working in Real Air Environment" Submitted at "Materials Research Society (MRS 2017)", Boston, USA.
- M. Asadi, B. Sayahpour, A. Salehi-Khojin, "Long Life Cycle Lithium-Oxygen Battery Using Molybdenum Disulfide Nanoflakes" Oral presentation at "The American Institute of Chemical Engineers Annual Meeting (AIChE 2016)", San Francisco, USA.
- P. Abbasi, M. Asadi, B. Sayahpour, A. Salehi-Khojin, "Niobium Doped Molybdenum Disulfide Catalyst for CO_2 Reduction Reaction" Oral presentation at "The American Institute of Chemical Engineers Annual Meeting (AIChE 2016)", San Francisco, USA.
- A. Banisharif, S. Menbari, B.Sayahpour, A. A. Firooz, Y. Mortazavi, A. Khodadadi, "TiO2 Doped with Fe2O3 Photocatalysts for Enhanced Photo-degradation of Gaseous Trichloroethylene (TCE)" Paper presented at "The 4th International Conference on Ultrafine Grained and Nanostructured Materials (UFGNSM 2013)", Tehran, Iran.

Published journal papers:

- Abbasi, Pedram, Mohammad Asadi, Cong Liu, Soroosh Sharifi-Asl, Baharak Sayahpour, Amirhossein Behranginia, Peter Zapol, Reza Shahbazian-Yassar, Larry A. Curtiss, and Amin Salehi-Khojin. "Tailoring the Edge Structure of Molybdenum Disulfide towards Electrocatalytic Reduction of Carbon Dioxide." *ACS nano* (2016).

CERTIFICATES

- "Experimental Working at Center of Thermal Process Technology", MLU, Germany
- "How to Publish a Scientific Journal Article Workshop" Springer and Edanz, 2013
- "PFD and P&ID Course" Novin Parsian Technical Complex, Tehran 2013
- "Introduction to Standard and Standardization" Iran Standard Research Institute
- "Project Planning Course" Training Center of Oil Turbo Compressor (OTC)
- Workshop of "Computational Fluid Dynamics Application in Chemical Engineering"
- "Individual Developing Plan (IDP) Course" Training Center of Oil Turbo Compressor
- "Documentation of Gas Stations Projects" Training Center of Oil Turbo Compressor
- Workshop of "Enhanced Oil Recovery (EOR)", University of Tehran, Fall 2011
- Workshop of "Natural Gas Process Plants Design", University of Tehran, Fall 2010

SKILLS

Extensive Computer Skills: Proficient in working with **Matlab**, **Origin, HYSYS.**

Hands-on experience in **Aspen plus, PDMS, OLGA.**

Characterization Technics: Raman, XRD, XPS, NMR, DLS, EIS.

MEMBERSHIPS

- American Institute of Chemical Engineers (AIChE)
- American Society of Mechanical Engineers (ASME)
- Electrochemical Society (ECS)
- Society of Women Engineers (SWE)